SOME ASPECTS OF SELF-INTERACTING BRANS-DICKE THEORY

By

Amal Majid

A THESIS
SUBMITTED IN PARTIAL FULFILLMENT OF THE
REQUIREMENTS FOR THE DEGREE OF
DOCTOR OF PHILOSOPHY
IN
MATHEMATICS

Supervised By

Prof. Dr. Muhammad Sharif

DEPARTMENT OF MATHEMATICS
UNIVERSITY OF THE PUNJAB
LAHORE-PAKISTAN
JANUARY 2022

CERTIFICATE

I certify that the research work presented in this thesis is the original work of **Ms Amal Majid** D/O **Majid Mehmood** and is carried out under my supervision. I endorse its evaluation for the award of **Ph.D.** degree through the official procedure of **University of the Punjab**.

Prof. Dr. Muhammad Sharif
(**Supervisor**)

DECLARATION

I, **Ms Amal Majid** D/O **Majid Mehmood**, hereby declare that the matter printed in this thesis is my original work. This thesis does not contain any material that has been submitted for the award of any other degree in any university and to the best of my knowledge, neither does this thesis contain any material published or written previously by any other person, except due reference is made in the text of this thesis. Most of the contents have been appeared as my research papers.

Amal Majid

DEDICATED

To

My Loving Parents

and

My Adorable Son

Adil Farhan Butt

Table of Contents

Table of Contents v

List of Tables viii

List of Figures ix

Acknowledgements xiii

Abstract xiv

Abbreviations xvi

Introduction 1

1 Self-interacting Brans-Dick Gravity and Stellar Structures 9

1.1 Scalar-Tensor Theory . . . 9

1.1.1 Brans-Dicke Theory of Gravitation . . . 11

1.1.2 Self-interacting Brans-Dick Theory of Gravitation . . . 12

1.2 Physical Parameters . . . 14

1.3 Cosmology . . . 15

1.4 Self-gravitating Systems . . . 17

1.4.1 White Dwarfs . . . 18

1.4.2 Neutron Stars . . . 19

1.4.3 Quark Stars . . . 20

1.4.4 Black Holes . . . 20

1.4.5 Matching of Interior and Exterior Spacetimes . . . 21

1.5 Equation of State . . . 22

1.6 Complexity of Self-gravitating Systems . . . 25

1.7 Gravitational Decoupling Approach . . . 27

1.8 Embedding Classes 29
1.9 Physical Acceptability of Models 30
1.9.1 Viability Conditions 30
1.9.2 Stability Analysis 32

2 Complexity of Sphere in Self-interacting Brans-Dick Gravity 34
2.1 SBD Field Equations for Static Sphere 35
2.1.1 Structure Scalars 39
2.1.2 Complexity Factor for Static Sphere 41
2.2 SBD Field Equations for Non-static Sphere 46
2.2.1 Structure Scalars 50
2.2.2 Complexity and Evolution of the System 51
2.2.3 Kinematical Variables 53
2.2.4 Stability of $Y_{TF} = 0$ Condition 56

3 Cosmological Solution through Gravitational Decoupling in SBD Gravity 58
3.1 SBD Field Equations for Non-static Sphere with Additional Matter Source 59
3.2 Gravitational Decoupling via MGD Approach 61
3.3 Anisotropic FLRW Solution 63
3.3.1 Massless Scalar Field Dominated Era 66
3.3.2 Radiation-Dominated Era 68
3.3.3 Matter-Dominated Era 71
3.3.4 Vacuum Energy Dominated Era 71

4 Extended Gravitational Decoupled Solutions in SBD Theory 74
4.1 EGD Approach and SBD Field Equations for Static Sphere 75
4.1.1 Anisotropic Solutions 78
4.2 Extended Schwarzschild Solutions 95
4.2.1 Traceless Θ^{γ}_{δ} 97
4.2.2 Barotropic Equation of State 100
4.2.3 A Particular Solution 103

5 Anisotropic Strange Stars through Embedding Technique in MBD Gravity 107
5.1 Embedding Class-one Solution via MIT Bag Model 108
5.1.1 Matching Conditions 109
5.2 Physical Features of Compact Stars 111

5.2.1 Energy Conditions 115
5.2.2 Effective Mass, Compactness and Redshift 117
5.2.3 Stability of Stellar System 118

6 Concluding Remarks **121**

Appendix A **128**

Appendix B **129**

Bibliography **132**

List of Tables

5.1 Physical parameters of LMC X-4 with $m_\Psi = 0.001$ for different values of ω_{BD} and $\mathcal{B}$. 112
5.2 Physical parameters of LMC X-4 with $m_\Psi = 0.3$ for different values of ω_{BD} and $\mathcal{B}$. 112

List of Figures

3.1 Behavior of $g(r)$ for $k = 0,\ c_1 = 1$ and $c_2 = 0.0001$. 66
3.2 Plots of $\rho,\ p_r$ and $p_\perp$ of anisotropic FLRW solution with $\varsigma = 1$ for $\varrho = 0.1$ (blue) and 0.5 (green). 67
3.3 Energy conditions with $\varsigma = 1$ for $\varrho = 0.1$ (blue) and 0.5 (green). . . . 67
3.4 Plots of v_r^2 and $v_\perp^2$ with $\varsigma = 1$ for $\varrho = 0.1$ (blue) and 0.5 (green). . . . 68
3.5 Plots of $\rho,\ p_r$ and $p_\perp$ of anisotropic FLRW solution with $\varsigma = 1/3$ for $\varrho = 0.1$ (blue) and 0.5 (green). 69
3.6 Energy conditions with $\varsigma = 1/3$ for $\varrho = 0.1$ (blue) and 0.5 (green). . . 69
3.7 Plots of v_r^2 and $v_\perp^2$ with $\varsigma = 1/3$ for $\varrho = 0.1$ (blue) and 0.5 (green). . . 70
3.8 Plots of $\rho,\ p_r$ and $p_\perp$ of anisotropic FLRW solution with $\varsigma = 0$ for $\varrho = 0.1$ (blue) and 0.5 (green). 70
3.9 Energy conditions with $\varsigma = 0$ for $\varrho = 0.1$ (blue) and 0.5 (green). . . . 71
3.10 Plots of v_r^2 and $v_\perp^2$ with $\varsigma = 0$ for $\varrho = 0.1$ (blue) and 0.5 (green). . . . 72
3.11 Plots of $\rho,\ p_r$ and $p_\perp$ of anisotropic FLRW solution with $\varsigma = -1$ for $\varrho = 0.1$ (blue) and 0.5 (green). 72
3.12 Energy conditions with $\varsigma = -1$ for $\varrho = 0.1$ (blue) and 0.5 (green). . . 73
3.13 Plots of v_r^2 and $v_\perp^2$ with $\varsigma = -1$ for $\varrho = 0.1$ (blue) and 0.5 (green). . . 73

4.1 Plots of matter variables and anisotropy of extended Tolman IV solution for case I. 82
4.2 DEC for anisotropic Tolman IV with case I. 83

4.3 Plots of mass, compactness and redshift parameters corresponding to anisotropic Tolman IV for case I. 84
4.4 Plots of gravitational mass versus radius (left) and baryonic mass versus gravitational mass (right) corresponding to anisotropic Tolman IV with case I. 84
4.5 Plots of radial/tangential velocities and $|v_\perp^2 - v_r^2|$ corresponding to anisotropic Tolman IV for case I. 85
4.6 Matter variables and anisotropy of extended KB solution for case I. . 86
4.7 DEC for extended KB solution with case I. 87
4.8 Plots of mass, compactness and redshift parameters corresponding to extended KB solution for case I. 87
4.9 Plots of gravitational mass versus radius (left) and baryonic mass versus gravitational mass (right) for extended KB solution with case I. . 88
4.10 Plots of radial/tangential velocities and $|v_\perp^2 - v_r^2|$ for extended KB solution with case I. 88
4.11 Plots of matter variables and anisotropy of extended Tolman IV for case II. 91
4.12 DEC for anisotropic Tolman IV with case II. 91
4.13 Plots of mass, compactness and redshift parameters corresponding to anisotropic Tolman IV for case II. 92
4.14 Plots of gravitational mass versus radius (left) and baryonic mass versus gravitational mass (right) corresponding to anisotropic Tolman IV for case II. 92
4.15 Plots of radial/tangential velocities and $|v_\perp^2 - v_r^2|$ corresponding to anisotropic Tolman IV for case II. 92
4.16 Plots of matter variables and anisotropy of extended KB solution for case II. 93
4.17 DEC for extended KB solution with case II. 93

4.18 Plots of mass, compactness and redshift parameters corresponding to extended KB solution for case II. 94
4.19 Plots of gravitational mass versus radius (left) and baryonic mass versus gravitational mass (right) corresponding to extended KB solution for case II. 94
4.20 Plots of radial/tangential velocities and $|v_\perp^2 - v_r^2|$ corresponding to extended KB solution for case II. 94
4.21 Plot of $\mathcal{K}$ for case I. 98
4.22 Plots of matter variables for case I. 98
4.23 Energy conditions for case I. 99
4.24 Metric potentials for case I. 100
4.25 Plot of $\mathcal{K}$ for case II. 101
4.26 Matter variables for case II. 101
4.27 Energy conditions for case II. 102
4.28 Metric potentials for case II. 102
4.29 Plot of $\mathcal{K}$ for case III. 104
4.30 Matter variables for case III. 104
4.31 Energy conditions for case III. 105
4.32 Metric potentials for case III. 105

5.1 Plots of metric potentials for massive scalar field versus radial coordinate. 113
5.2 Effective energy density, effective radial/transverse pressure as functions of r with $m_\Psi = 0.001$. 113
5.3 Effective energy density, effective radial/transverse pressure as functions of r with $m_\Psi = 0.3$. 114
5.4 Variation of effective anisotropy as a function of r. 115
5.5 DEC plotted against the radial coordinate. 116
5.6 Plots of relation between mass, compactness factor and redshift against radial coordinate. 117

5.7 Variation of radial velocity, tangential velocity and $|v_\perp^2 - v_r^2|$ with respect to radial coordinate with $m_\Psi = 0.001$. 119
5.8 Variation of radial velocity, tangential velocity and $|v_\perp^2 - v_r^2|$ with respect to radial coordinate with $m_\Psi = 0.3$. 119
5.9 Plots of adiabatic index versus r. 120

Acknowledgements

Thanks to **Allah Almighty**, the most beneficent and the most merciful, Who gave me this life and blessed me with the ability to learn and observe. Special praises to the **Prophet Muhammad (Peace Be Upon Him)**, Whose teachings not only helped me surface above the lows of my life but also proved a guiding light through the highs.

There is no argument that I could not have accomplished this demanding task without the guidance, insight and constructive comments offered by my esteemed supervisor **Prof. Dr. Muhammad Sharif**. I am also grateful to the faculty members for imparting knowledge and wisdom throughout my studies. I would also express my thanks to the members of *The Group of Gravitation and Cosmology* especially **Dr. Arfa** and **Dr. Qanitah** for valuable suggestions and friendly support. Thanks to the Higher Education Commission, Islamabad for its financial assistance through the *Indigenous Fellowship Program Phase-II, Batch-VI.*

This acknowledgement would be incomplete without mentioning my **parents**. Without their never ending support and unwavering belief in me, this goal would have been nothing but a dream. I can never thank them enough for helping me out in looking after my son. I am also thankful to my sister **Nada** for her undying love and care. I highly appreciate the moral support provided by my caring **parents in law**. A special thanks to my husband **Farhan** and son **Adil** for adjusting to my tough routine and patiently dealing with my roller coaster of emotions. May Allah bless them all!

Lahore **Amal Majid**

August, 2021

Abstract

This thesis focuses on the study of various cosmological and astrophysical aspects in the framework of self-interacting Brans-Dicke gravity. Firstly, we explore the physical attributes of a static as well as a dynamical source that induce complexity within the fluid. We orthogonally split the Riemann tensor to obtain structure scalars relating to comoving congruence and Tolman mass. We define the complexity factor with the help of these scalars to demonstrate the complex nature of the system. Moreover, the vanishing complexity condition is used to obtain solutions. The factors that induce complexity in an initially complexity-free dynamical system are also examined.

Secondly, we extend isotropic non-static spherical spacetime to anisotropic domain by means of minimal geometric deformation. This deformation decouples the system of field equations into two sets, one describing the isotropic matter field and the other governed by anisotropic source. The former array is evaluated by assuming the metric potentials of Friedmann-Lemaître-Robertson-Walker spacetime. We construct the anisotropic extension corresponding to power-law forms of scalar field and scale factor. Moreover, a linear equation of state links density and pressure of the configuration. We investigate physical behavior of the anisotorpic version for different values of the equation of state parameter.

Thirdly, we adopt extended gravitational decoupling method to extend known static spherical solutions. Deformations in radial as well as temporal metric components disintegrate the system of field equations into two arrays. We employ the metric functions of Tolman IV, Krori-Barua and Schwarzschild metrics to specify the set related to the seed source. In order to construct a suitable solution of the second

system, constraints are applied on the additional source and metric potentials. The impact of the massive scalar field as well as the decoupling parameter on the salient characteristics of the extended solutions is analyzed graphically.

Finally, we generate an anisotropic solution for a static sphere filled with quark matter. The system of field equations is derived for specific form of potential function by employing the MIT bag model. The unknown metric tensors are evaluated through a well-behaved function along with the condition for class-one embedding. The unknown constants are specified in terms of mass and radius of the configuration with the help of junction conditions. We estimate the radius of LMC X-4 for different values of the bag constant by employing the star's observed mass. We also discuss the physical viability and stability of the model through various tests.

Abbreviations

In this thesis, the metric signatures $(+,-,-,-)$ will be used, unless otherwise specified. Greek indices will vary from 0 to 3. Also, the following list of abbreviations will be used.

BD:	Brans-Dicke
BH:	Black Hole
CMBR:	Cosmic Microwave Background Radiation
DEC:	Dominant Energy Condition
EoS:	Equation of State
EGD:	Extended Geometric Deformation
FLRW:	Friedmann-Lemaître-Robertson-Walker
GR:	General Relativity
KB:	Krori-Barua
MBD:	Massive Brans-Dicke
MGD:	Minimal Geometric Deformation
MIT:	Massachusetts Institute of Technology
NEC:	Null Energy Condition
SEC:	Strong Energy Condition
SBD:	Self-interacting Brans-Dicke
SQM:	Strange Quark Matter
WEC:	Weak Energy Condition

Introduction

The study of large scale structures such as stars, galaxies and their clusters provide insights into the dynamics of the universe. The intricate nature of these stellar structures massively depends upon the interdependent physical variables such as energy density, pressure and heat flux. To determine the characteristics of celestial objects, it is necessary to gain complete or maximum information to compute the complexity factor for the considered system. Such a factor specifies the degree of complexity found within the system and provides a measure for comparing different self-gravitating structures. The problem of measuring the complexity of cosmic structures is not new and numerous attempts have been made to define such a factor [1]. In spite of these works, a consensus on a definition of complexity factor has not been achieved.

Among the proposed definitions, the concepts of order or arrangement of atoms and entropy of a system have been taken into account. However, dense stellar systems have tightly packed particles in their interior. This arrangement restricts the movement of nuclear matter in the radial direction. Consequently, radial pressure is less than the force in the transverse direction leading to anisotropy in pressure. Thus, anisotropy plays a significant role in determining the viability and stability of self-gravitating systems. Recently, Herrera [2] devised a new complexity factor for static sphere in the context of GR by assuming that the complexity-free system is

isotropic as well as homogeneous. The distinguishing feature of Herrera's technique is the integration of the system's active gravitational mass, inhomogeneous energy density and anisotropic pressure in the definition of complexity. He obtained structure scalars through the orthogonal splitting of Riemann tensor to generate the complexity factor.

Herrera's definition of complexity has also been extended for a non-static radiating sphere by minimizing complexity in the mode of evolution [3]. Sharif and Butt computed the complexity factor based on Herrera's approach for a static cylindrically symmetric self-gravitating system [4]. They also investigated the effect of electromagnetic field on the complexity factor of static spherical [5] as well as cylindrical [6] structures and concluded that complexity increases in the presence of charge. Herrera and his collaborators [7] formulated three complexity factors for an axially symmetric system and examined a possible relation between symmetry and complexity of the setup. They also employed this notion to establish a hierarchy from the simplest (Minkowski) to more complex (radiating) systems [8]. The complexity of a charged non-static spherical system has also been explored [9]. Recently, Herrera et al. determined the conditions under which a quasi-homologous system is complexity free [10].

The study of cosmos has led to the discovery of astounding phenomena that have governed the evolution of the universe since its beginning. The cosmological principle suggests that the universe is isotropic and homogeneous at scales larger than $300h^{-1}Mpc$ [11]. In accordance with this principle, FLRW metric is often employed to examine the expanding cosmos. However, cosmological probes (other than CMBR) in the last decade suggest deviations from the isotropic structure, e.g., the study of

inhomogeneous Supernova Ia detected slight departure from isotropy [12]. Other tools that have been used to determine the possible inconsistencies include the distribution of infrared galaxies [13] and radio sources [14], gamma-ray bursts [15], etc. Although some of the results indicated the presence of anisotropy, they were of little statistical importance. Recently, Migkas and Reiprich [16] used the directional behavior of X-rays from galactic clusters as a cosmic probe to test the isotropy of the cosmos. This technique was applied to different galactic clusters and the results showed anisotropic behavior in the cosmic region [17]. Therefore, in order to discuss the history and fate of the universe, it is necessary to generate anisotropic cosmological solutions of the field equations.

Gravitational collapse leads to stellar death which results in the formation of compact structures (white dwarf, neutron star and BH). Black hole is one of the self-gravitating systems with a singularity hidden behind the event horizon. These cosmic objects have a strong gravitational field and serve as excellent laboratories to test relativistic theories in the strong-field regime. The existence of BHs has been strengthened due to the recent detection of gravitational waves [18]. Schwarzschild obtained the first BH solution for a vacuum spacetime [19]. General relativity formulates surprisingly simple solutions for BHs in accordance with the no-hair conjecture (BH solutions cannot carry additional charges [20]) with three prominent features: mass, charge and angular momentum [21]. The validity of no-hair theorem is now being tested with improved studies and observations of BH systems. In fact, different setups have been constructed to evade the no-hair theorem [22]. Recent studies suggest that BHs, as sources of extreme gravity, can possess soft quantum hair [23].

However, the derivation of new solutions representing BHs is hindered by the non-linearity as well as high degree of freedom in the field equations.

Over the years, researchers have devised new techniques to obtain viable models of stellar structures. Recently, Ovalle [24] proposed the method of MGD to extend a seed source (vacuum or isotropic) to complex fluid distributions. This technique was first implemented in the framework of Randall-Sundrum braneworld to derive consistent spherically symmetric solutions. In this approach, an additional source is incorporated in the seed distribution on the condition that the two sources interact gravitationally only. A geometric deformation in the radial metric component decouples the system of field equations into two sets with lesser degrees of freedom as compared to the original system. The two systems are solved independently and their respective solutions are combined to obtain a solution of the complete model.

Following the procedure of MGD, Ovalle et al. [25] employed this technique to incorporate the effects of anisotropy in perfect fluid configuration and generated three anisotropic models from the Tolman IV solution. Different anisotropic BH solutions were obtained by applying this approach to a vacuum Schwarzschild solution [26]. Estrada and Tello-Ortiz [27] adopted the MGD approach to construct two physically acceptable anisotropic solutions from Heintzmann solution. Sharif and Sadiq [28] applied this method to KB solution and explored the impact of charge on the extended anisotropic system. Geometric deformations on Tolman VII metric potentials have also been applied to construct a physically viable anisotropic solution [29]. Sharif and Ama-Tul-Mughani [30] decoupled the field equations representing a cloud of strings and obtained corresponding anisotropic extensions.

The approach of gravitational decoupling through MGD has proved highly beneficial in obtaining physically relevant anisotropic solutions. However, this method applies to the scenario in which the considered sources do not exchange energy. Recently, Ovalle [31] introduced decoupling through deforming both (radial/temporal) metric potentials. Decoupling through EGD disintegrates the system without restricting the type of matter distribution. Contreras and Bargueño [32] applied this method to vacuum BTZ solution in 2+1-dimensions. The EGD scheme has also been applied to evaluate anisotropic versions of Tolman IV [33] and KB [34] solutions. Recently, Ovalle et al. [35] formulated hairy BHs by extending Schwarzschild spacetime through the EGD technique. There are also some attempts [36] to obtain anisotropic solutions in modified theories through MGD as well as EGD schemes.

Apart from the three outcomes of collapse, another compact stellar structure is also hypothesized as an end state of inward fall of a neutron star. It is believed that such a cosmic object is composed of strange quark matter which is a favorable state of baryon matter. A strange quark star is an intermediate stage between BH and neutron star which has too much mass at its core for the neutrons to hold their individuality but still evades collapse into a BH. Recent observational estimates of masses and radii of some stars (Her X-1, 4U 1820-30, LMC X-4, etc.) are not consistent with neutron star prototype. Instead they can be treated as suitable candidates for strange quark stars. The MIT Bag model [37] has been determined as the best approximation for the EoS to formulate solutions representing quark stars.

In 1937, Dirac [38] hypothesized that all large numbers obtained by the combinations of fundamental atomic constants are related to cosmological parameters. Subsequently, the gravitational constant (G) must be a function of cosmic time. In

1961, Brans and Dicke [39] modified GR by incorporating Dirac observations in a scalar-tensor theory and formulated a spherical vacuum solution. Brans-Dicke gravity incorporates a massless scalar field $\varphi = \frac{1}{G(t)}$ to discuss the evolution of the cosmos. A tunable parameter (ω_{BD}) couples the scalar field to the matter distribution. As the role of scalar field is enhanced during the inflationary era, the values of the coupling parameter must be small to explain this scenario [40]. On the other hand, the solar system tests are satisfied for $\omega_{BD} > 40,000$ [41]. This issue is resolved by the SBD theory which assigns a mass to the scalar field through a potential function $V(\Psi)$ (where Ψ is a massive scalar field) [42]. In SBD theory, if the mass of the scalar field is greater than $2 \times 10^{-25} GeV$, the solar system observations cannot constrain ω_{BD} and its values greater than $-\frac{3}{2}$ are allowed [43].

Solutions representing cosmological as well as astrophysical scenarios have been formulated in BD theory. Santos and Gregory [44] examined the cosmos in SBD theory and showed that the radiation dominated universe is 2-dimensional while vacuum or dust-filled cosmos is 3-dimensional. Sen et al. [45] studied the late-time acceleration of the cosmos through a dissipative fluid. Mak and Harko [46] derived three solutions for a flat FLRW geometry in SBD theory and checked them for consistency with Supernova Ia observations. Chakraborty and Debnath [47] investigated cosmic acceleration by taking power-law forms of the scale factor and scalar field in the presence of a self-interacting potential. Sharif and Waheed [48] explored the values of the SBD coupling parameter in different eras and found accelerated expansion corresponding to higher values of the parameter.

Thorne and Dykla [49] studied BHs in three dimensions and concluded that 3-dimensional BD BHs are identical to their counterparts in GR. Hawking [50] showed

that a stationary BH metric satisfies the BD field equations if and only if it is also a solution of GR. Geroch method [51] was employed by Sneddon and McIntosh [52] to discuss vacuum models. Bruckman and Kazes [53] considered a perfect matter source with a linear EoS to formulate solutions for a spherically symmetric spacetime. Riazi and Askari [54] used numerical techniques to approximate solution for an empty sphere and studied the trend of rotation curves. Campanelli and Lousto [55] studied a family of BD solutions and determined the range of parameters yielding BH solutions different from GR. Sharif and Manzoor formulated structure scalars to study the evolution of dynamical spheres [56] and cylinders [57] in SBD theory. Complexity factors for axially symmetric structure were computed to investigate the effect of massive scalar field on the complexity of compact systems [58]. Solutions constructed via decoupling as well as MIT bag model were checked for viable behavior [59].

This thesis focuses on the formulation of the complexity factors and spherical solutions in the background of SBD gravity. We investigate essential features and behavior of extended cosmological as well as astrophysical spacetimes. We also determine the viability and stability of stellar solutions corresponding to the MIT bag model. The thesis is compiled according to the following framework.

- Chapter **One** includes some primary notions and definitions to comprehend the work presented in this thesis.

- Chapter **Two** explores the complexity of static as well as dynamical anisotropic spheres.

- Chapter **Three** examines the anisotropic extension of flat FLRW model obtained via MGD scheme.

- Chapter **Four** provides the anisotropic versions of Tolman IV, KB and Schwarzschild ansatz formulated through EGD decoupling
- Chapter **Five** investigates the structural features and stability of strange quark star model governed by the MIT bag EoS.
- Chapter **Six** presents a summary of the major results obtained in this thesis alongside some fascinating problems for future research.

Chapter 1

Self-interacting Brans-Dick Gravity and Stellar Structures

The mechanism and evolution of the vast universe massively depend on the large scale structures such as stars and their collapsed remnants. Thus, the study of these components is vital to gain a better understanding of the cosmos and its origin. In this chapter, we discuss a scalar-tensor modification of GR alongside some fundamental notions related to cosmic as well as stellar evolution.

1.1 Scalar-Tensor Theory

The revolutionary proposition that the geometry of the universe is interlinked with the matter distribution led to the theory of GR described by the Einstein-Hilbert action as

$$\mathcal{S} = \int \sqrt{-g} \left(\frac{\mathcal{R}}{2\kappa^2} + L_m \right) d^4x, \tag{1.1.1}$$

where g, $\mathcal{R}$ and L_m represent the determinant of the metric tensor ($g_{\gamma\delta}$), Ricci scalar and matter Lagrangian, respectively. Moreover, $\kappa^2 = \frac{8\pi G}{c^4}$ is the coupling constant

with c symbolizing the speed of light. The action of a theory encompasses the necessary elements describing a physical system and its motion. The addition of an extra degree of freedom in the form of a scalar, vector or tensor field modifies the action (1.1.1) and yields alternative theories of gravity. Different approaches (such as the inclusion of non-Christoffel connection, higher-order terms of curvature, etc.) have generated extensions of GR. Another method to construct a modified version of GR is the incorporation of a scalar field (represented by spin-0 particle) leading to a scalar-tensor theory [60]. However, the first scalar-tensor theory was proposed even before Einstein introduced the theory of GR. Nordström, the pioneer of scalar-tensor theories, described gravity through a scalar field in a flat spacetime by considering the gravitational constant as a Lorentz scalar. Although this theory yields the equivalence of inertial and gravitational masses, its application was limited to conformally flat spacetimes only.

In 1937, Dirac [38] found that the comparison of gravitational and electrical forces existing between the sub-atomic particles (electron and proton) leads to a large dimensionless number of order 10^{40}. Similarly, the age (t_c) of the cosmos estimated in terms of units of atomic constant has approximately the same order of magnitude, i.e.,

$$t_c \sim \frac{q_e^2}{G m_e m_p},$$

where q_e denotes the charge of electron. Moreover, m_e and m_p are the masses of electron and proton, respectively. This coincidence led to the formulation of the *Large Number Hypothesis* which stated that the *physical constants occurring in nature must be connected via a mathematical relation.* Based on his findings, Dirac proposed that the constant measuring the strength of gravity varies inversely with cosmic time.

In 1955, Jordan employed Dirac's hypothesis to build a scalar-tensor theory via non-minimal coupling between tensor and scalar fields in the modified Einstein-Hilbert action. The main criticism against this theory was the non-conservation of energy and momentum due to the creation of new matter.

Another principle that significantly contributed to the formulation of scalar-tensor gravitational framework was presented by Mach. He claimed that the matter distribution in the universe determined the inertia of an object. In other words, the inertia of a cosmic structure vanishes in the background of an empty cosmos. Although the principle is not supported by any empirical data, it has certainly provided a foundation for different theories of relativity. Einstein referred to the Machian principle in his book "*The Meaning of Relativity*" as an important source of motivation during the development of GR.

1.1.1 Brans-Dicke Theory of Gravitation

In 1961, Brans and Dicke [39] discussed Mach principle in relation to the equivalence principle (the effects of gravity and acceleration are indistinguishable) and formulated a scalar-tensor theory of gravity known as BD gravity. In order to encompass Dirac hypothesis, they included a massless scalar field that described the effects of a dynamical gravitational constant. The action of BD theory with $8\pi G_0 = c = 1$ (G_0 is the present day value of gravitational constant), is written as

$$\mathcal{S} = \int \sqrt{-g}\left(\varphi\mathcal{R} - \frac{\omega_{BD}}{\varphi}\nabla_\gamma\varphi\nabla^\gamma\varphi + L_m\right)d^4x, \tag{1.1.2}$$

which contains a minimal coupling between scalar field and matter content. Varying the action (1.1.2) with respect to $g_{\gamma\delta}$ and φ respectively, yields BD field and wave

equations as

$$G_{\gamma\delta} = \varphi\left(\mathcal{R}_{\gamma\delta} - \frac{1}{2}g_{\gamma\delta}\mathcal{R}\right) = T^{(m)}_{\gamma\delta} + T^{\varphi}_{\gamma\delta}, \tag{1.1.3}$$

$$\Box\varphi = \varphi^{,\gamma}{}_{;\gamma} = \frac{T^{(m)}}{3+2\omega_{BD}}, \tag{1.1.4}$$

where $\mathcal{R}_{\gamma\delta}$ and $T^{(m)}_{\gamma\delta}$ symbolize the Ricci tensor and energy-momentum tensor corresponding to the matter source with $T^{(m)} = g_{\gamma\delta}T^{\gamma\delta(m)}$. Moreover, the contribution of the scalar field in the energy of the system is described as

$$T^{\varphi}_{\gamma\delta} = \varphi_{,\gamma;\delta} - g_{\gamma\delta}\Box\varphi + \frac{\omega_{BD}}{\varphi}(\varphi_{,\gamma}\varphi_{,\delta} - \frac{g_{\gamma\delta}\varphi_{,\alpha}\varphi^{,\alpha}}{2}), \tag{1.1.5}$$

where ";" represents covariant derivative and $\Box$ is the D'Almbertian operator. Brans-Dicke gravity is the prototype of a scalar-tensor alternative to GR that has been extended to a wider family of scalar-tensor theories [61].

1.1.2 Self-interacting Brans-Dick Theory of Gravitation

In cosmology, the inflationary model was proposed to overcome the flatness and horizon problems in the early cosmos. However, according to this model, the rapidly expanding universe fails to transition from the period of inflation into the next cosmological era. Although BD gravity has significant implications in the field of cosmology, it fails to successfully solve this problem (termed as the *graceful exit problem*). The BD coupling parameter must be less than 25 [40] to adequately describe the inflationary era which disagrees with the statistical data [62]. Moreover, in BD theory, the effect of scalar field reduces corresponding to large values of the coupling parameter. Thus, cosmological issues are discussed for small values of ω_{BD} while large and positive values of the coupling parameter are required to satisfy the weak field

tests. In order to establish a standard domain of the parameter, a potential function is introduced. This function adjusts the values by assigning a mass to the scalar field which leads to an extension of BD gravity known as SBD (or MBD) theory. The action (1.1.2) is modified as

$$\mathcal{S} = \int \sqrt{-g}\left(\Psi\mathcal{R} - \frac{\omega_{BD}}{\Psi}\nabla_\gamma\Psi\nabla^\gamma\Psi - V(\Psi) + L_m\right)d^4x, \tag{1.1.6}$$

which leads to the following SBD equations

$$G_{\gamma\delta} = T^{(\text{eff})}_{\gamma\delta} = \frac{1}{\Psi}(T^{(m)}_{\gamma\delta} + T^{\Psi}_{\gamma\delta}), \tag{1.1.7}$$

$$\Box\Psi = \frac{T^{(m)}}{3+2\omega_{BD}} + \frac{1}{3+2\omega_{BD}}(\Psi\frac{dV(\Psi)}{d\Psi} - 2V(\Psi)), \tag{1.1.8}$$

with

$$T^{\Psi}_{\gamma\delta} = \Psi_{,\gamma;\delta} - g_{\gamma\delta}\Box\Psi + \frac{\omega_{BD}}{\Psi}(\Psi_{,\gamma}\Psi_{,\delta} - \frac{g_{\gamma\delta}\Psi_{,\alpha}\Psi^{,\alpha}}{2}) - \frac{V(\Psi)g_{\gamma\delta}}{2}. \tag{1.1.9}$$

Various cosmological and astrophysical models have been developed corresponding to different forms of self-interacting potentials [63]. The specific form of potential is unknown but it has been assumed that at high temperatures the potential is proportional to Ψ^2 [44]. Furthermore, Quiros [64] showed that the de Sitter solution in GR arises in the SBD theory for the quadratic potential ($V(\Psi) = m^2\Psi^2$, where m is coupled to the mass of the scalar field) only. The most common form of potential function considered for different cosmic scenarios [44, 65] is

$$V(\Psi) = \frac{1}{2}m_\Psi^2\Psi^2,$$

where m_Ψ is the mass of the scalar field. Note that the combination $(\Psi\frac{dV(\Psi)}{d\Psi} - 2V(\Psi))$ in Eq.(1.1.8) vanishes for the chosen potential function which simplifies the mathematical calculations.

1.2 Physical Parameters

Different physical parameters are required to effectively describe self-gravitating systems which are briefly discussed in this section.

- **Mass**

  The measure of matter contained within a cosmic system corresponds to its mass which determines the motion of the object. Mass is classified into inertial and gravitational masses which gauge the resistance to change in the system's motion and the influence of gravitational forces, respectively. The total mass within a sphere of radius r is computed through the Misner-Sharp formula as [66]

  $$m = \frac{R}{2}(1 - g^{\gamma\delta} R_{,\gamma} R_{,\delta}), \tag{1.2.1}$$

  where R denotes the radius of the sphere. Tolman [67] presented an alternate definition for computing the total mass of the spherical system with volume V as

  $$m_T = \int_V \sqrt{-g}(T_0^0 - T_1^1 - T_2^2 - T_3^3)dV. \tag{1.2.2}$$

  The mass obtained using Tolman's formula coincides with the Misner-Sharp mass at the boundary but varies within the sphere (except in the special case of homogeneous distribution and isotropic pressures). The Misner-Sharp formula has been used extensively in numerical computations of stellar collapse [68] but Tolman mass gives a better estimate in case of anisotropic fluids.

- **Four Acceleration**

  The change in four velocity (v^γ) of a body induces acceleration defined as

  $$a_\gamma = v_{\gamma;\delta} v^\delta. \tag{1.2.3}$$

The path followed by the particles of fluid is geodesic when four acceleration is zero.

- **Expansion Parameter**

  It is a scalar quantity which measures the rate of change in the volume of an object with respect to time, i.e., it indicates whether the particles of the fluid move closer or away from each other. The expansion scalar is defined as

$$\vartheta = v^{\gamma}_{;\gamma}. \tag{1.2.4}$$

- **Shear Tensor**

  This second rank tensor calculates the distortion in the shape of an object as

$$\sigma_{\gamma\delta} = v_{(\gamma;\delta)} + a_{(\gamma}v_{\delta)} - \frac{1}{3}\vartheta h_{\gamma\delta}, \tag{1.2.5}$$

  where $v_{(\gamma;\delta)} = \frac{1}{2}(v_{\gamma;\delta} + v_{\delta;\gamma})$ and $h_{\gamma\delta} = g_{\gamma\delta} + v_{\gamma}v_{\delta}$ denotes the projection tensor.

1.3 Cosmology

The field of cosmology combines astronomy and physics to create cosmic models that effectively discuss the evolution of the universe from its genesis to the current epoch. On the basis of suitable models, cosmologists predict the future and ultimately the end of the cosmos. The big bang theory is one of the leading propositions regarding the origin of the universe. According to this theory, the universe exponentially inflated from an ultra-dense hot state around 13.8 billion years ago. After the inflation stopped, the cooling universe (with a temperature of 10 billion degrees) was dominated by photons and neutrinos moving relativistically to each other. This era,

dubbed as radiation-dominated epoch, was taken over by the matter or dust era in which atoms began to form which ultimately resulted in the birth of stellar and galactic structures. In 1929, Hubble measured the velocity and distance of galactic structures and discovered that the universe is undergoing expansion. Moreover, cosmological data compiled from different astrophysical observations (like redshift-luminosity relation of Supernova Ia [69], X-rays emission of galaxies [70], WMAP [71], etc.) confirm that the cosmos is currently expanding at an increasing rate. The positive acceleration is attributed to a mysterious repulsive force termed dark energy which exhibits itself as an intrinsic property of the vacuum, i.e., the effects of dark energy enhance in a larger volume of space.

It is believed that the universe is composed of elementary building blocks. However, the definition of the fundamental unit of the cosmos has changed over time to preserve the definition of isotropy and homogeneity of the universe. Initially, stars were considered as the basic units, i.e., the number of stars present in a fixed volume determined the density of matter within that region. Later, Hubble treated galaxies as the elementary units to measure the rate of cosmic expansion. However, the discovery that galaxies and their clusters occupy the edges of huge regions of almost empty space (known as voids) led to the belief that voids serve as the best elementary unit [72]. Although the isotropy and homogeneity of the universe has not been verified observationally, this assumption helped in the construction of the FLRW cosmic model given as

$$ds^2 = dt^2 - a^2(t)(\frac{dr^2}{1-kr^2} + r^2 d\theta^2 + r^2 \sin^2 d\phi^2), \tag{1.3.1}$$

where $a(t)$ denotes the scale factor which measures the change in distance between different points as the universe expands. Moreover, the values of curvature parameter

$k = -1, 0, 1$ refer to open, flat and closed universe models, respectively. The elegant feature of this model is the equivalence of all positions in the universe.

1.4 Self-gravitating Systems

The individual components of a self-gravitating structure are bound together under the influence of combined gravity of the whole system. In astrophysics, self-gravitation plays a significant role in the formation of stars as well as stellar and galactic clusters. Numerous astrophysical experiments (Sloan Digital Sky Survey, Large Synoptic Survey Telescope, Two-degree Field Galaxy Redshift Survey) have proved that the study of these components is vital to gain a better understanding of the cosmos and its origin. The study of these systems has revealed that the presence of interacting nuclear matter in extremely dense celestial structures generates anisotropy, i.e., their physical properties change in different directions [73]. Anisotropy arises from pion condensation [74], phase transition [75] and super-fluid [76]. Thus, anisotropy is one of the salient features governing the geometry and evolution of cosmic structures. Self-gravitating bodies are intricate cosmic objects whose physical properties may undergo a fundamental change due to a slight fluctuation in the interior.

Stellar structures are the most commonly found self-gravitating systems in the cosmos. They are born when the residue material from a cosmic event infiltrates a dormant *nebula* composed of dust and hydrogen gas. The colliding particles, within the huge cloud, clump together and eventually turn into a *protostar*. When the protostar achieves a temperature of approximately 10 million Kelvin, the hydrogen atoms fuse to form helium. At this stage (*main-sequence phase*), the compression of gas at the core initiates nuclear reactions releasing a great deal of energy and pressure.

Although the outward pressure from the fusion reactions balances the inward pull of gravity, the collapse of a star is imminent. With the passage of time, fuel for nuclear reactions diminishes leading to stellar collapse. The life span of a less massive star is longer as compared to that of a massive star as fusion reactions inside the massive object speed up to provide essential pressure against increased gravity. The collapse of the star is followed by smaller but dense remnants known as compact objects. The family of compact objects is different from burning stars as the necessary outward pressure is supplied by *degenerate matter* instead of nuclear reactions. As the particles of the extremely dense degenerate matter follow the Pauli exclusion principle (two identical fermions must occupy different energy levels), they produce sufficient degeneracy pressure to halt the contraction of the compact stellar object. The stellar remnants are smaller in size as compared to their parents but they possess stronger gravitational and magnetic fields [77].

1.4.1 White Dwarfs

The color of the star is an indicator of its surface temperature and energy distribution. Most of the visible light radiated by the hottest stars (having a surface temperature of around 25,000 Kelvin) is dominated by blue color whereas the electromagnetic spectrum of the coolest stars (with a temperature of 3000 Kelvin) comprises mostly of light energy at red wavelengths. Stellar objects with a temperature of approximately 10,000 Kelvin release white light. The end products of less massive stars ($M < 8M_{\odot}$, $M_{\odot}$ represents solar mass) cool down as they radiate the residual energy and shine with a white light thus, giving them the name *white dwarfs*. They are dense objects which pack one solar mass in a radius comparable to that of the earth [77]. In 1930,

Chandrasekhar [78] constructed white dwarf models corresponding to the EoS of degenerate electrons and discovered that white dwarfs can attain a maximum mass of $1.4M_{\odot}$. Beyond this limit, the white dwarf will continue to collapse under the effect of self-gravity. These stellar remnants counterbalance the force of inward gravity via the degeneracy pressure of electrons.

1.4.2 Neutron Stars

The gravitational collapse of massive stars ends in a luminous explosion known as a supernova. If the mass of the star (before collapse) lies in the interval of 8 to $20M_{\odot}$, the extreme conditions in the interior of the core combine electrons and protons to form neutrons leading to the birth of *neutron stars*. These stars are extremely dense compact objects with more mass than white dwarfs accumulated in a smaller radius. They have a core of 1.4 to $3M_{\odot}$ which resists further collapse by resisting the inward pull of gravity through degeneracy pressure of newly generated neutrons [79]. These celestial bodies either exist individually or have a companion to form binary systems. The discovery of neutrons led to the prediction of neutron stars in 1934 [80] but observational evidence came later. This is because neutron stars do not emit enough radiation and are mostly undetectable. Generally, they are spotted as rapidly rotating pulsars which emit radiation at regular intervals ranging from milliseconds to seconds. The first pulsar was discovered in 1967 pulsating for 0.3 seconds after every 1.37 seconds [81]. Some stellar candidates of pulsars include 4U 1820-30, Her X-1, PSR J1903+327, etc.

1.4.3 Quark Stars

Quarks, the fundamental sub-atomic particles of matter, are classified into six flavors based on their mass and charge. The six types of quarks (up, down, bottom, top, strange and charm) occur in nature as a combination with other quarks or antiquarks. In order to discuss the strong forces between these elementary particles, they have been allotted red, green and blue colors while the corresponding antiquarks are assigned the respective anticolors. The sub-atomic particles, protons and neutrons, are composed of up and down quarks whereas the remaining four types are produced in high energy cosmic events. Researchers believe that there is a possibility that neutrons fail to endure the extreme temperature and pressure in the interior region of neutron stars. As a consequence they break down into their constituent particles known as quarks. Witten [82] conjectured that matter consisting of comparable numbers of up, down and strange quarks, is more stable than hadronic matter. Furthermore, the existence of strange stars can also explain the outflow of a huge amount of radiation and energy in extremely luminous supernovae [83]. Quark stars are ultra-dense structures with smaller radii than neutron stars. Some pulsars are classified as quark stars since their observational data do not meet the physical description of neutron stars.

1.4.4 Black Holes

Highly massive stars (with a mass of more than $20M_{\odot}$) explode in a supernova leaving behind completely collapsed objects known as *BHs*. The composite matter of the entire star is forced into a tiny space giving rise to a *spacetime singularity* with an extremely strong gravitational field. An object can only escape the BH's gravitational pull if it is traveling at a speed greater than that of light. Black holes

are categorized on the basis of their mass as supermassive, stellar, intermediate and miniature. These compact objects may continue to grow in size by absorbing dust and gas from its surrounding. The most prominent feature of these fascinating structures is the *event horizon* which marks the boundary of the area around the singularity which traps all objects, even light.

1.4.5 Matching of Interior and Exterior Spacetimes

The boundary (Σ) of an astrophysical object divides the spacetime into two different regions, interior and exterior. The vacuum exterior of a static uncharged celestial object is defined via Schwarzschild metric given as

$$ds^2 = \frac{r-2M}{r}dt^2 - \frac{r}{r-2M}dr^2 - r^2 d\theta^2 - r^2 \sin^2\theta d\phi^2, \tag{1.4.1}$$

where M is the total mass of the compact structure. To ensure smoothness and continuity of geometry at the boundary surface, the following conditions must be satisfied at the hypersurface ($\hat{h} = r - R = 0,\ R$ is the constant radius) [84]

$$(ds^2_-)_\Sigma = (ds^2_+)_\Sigma, \quad (K_{ij_-})_\Sigma = (K_{ij_+})_\Sigma, \tag{1.4.2}$$

Here, K_{ij} denotes curvature whereas subscripts $-$ and $+$ represent interior and exterior spacetimes, respectively. The continuity of the first fundamental form ($[ds^2]_\Sigma = 0$) leads to

$$[H]_\Sigma \equiv H(r \to R^+) - H(r \to R^-) \equiv H^+_R - H^-_R,$$

for any function $H(r)$. The above condition yields $g^-_{00}(R) = g^+_{00}(R)$. On the other hand, the continuity of the second fundamental form (K_{ij}) is equivalent to the O'Brien and Synge [85] junction conditions, given as

$$[G_{\gamma\delta}\mathfrak{n}^\gamma \mathfrak{n}^\delta]_\Sigma = 0,$$

where $\mathfrak{n}_\gamma$ is a unit normal. Using the above equation alongside the field equations implies $[T_{\gamma\delta}\mathfrak{n}^\gamma\mathfrak{n}^\delta]_\Sigma = 0$. In the presence of the massive scalar field, two additional conditions that must be satisfied at the boundary are

$$(\Psi(r)_-)_\Sigma = (\Psi(r)_+)_\Sigma, \quad (\Psi'(r)_-)_\Sigma = (\Psi'(r)_+)_\Sigma, \tag{1.4.3}$$

where prime denotes differentiation with respect to the radial co-ordinate.

1.5 Equation of State

The structure and evolution of the cosmos as well as the interior of self-gravitating systems depend on a large number of state variables such as pressure, energy density, temperature, etc. However, not all factors have the same impact on the mechanism of the celestial system. Consequently, the dominant factors in a given scenario are often related through an EoS which helps in the discussion of cosmological as well as astrophysical setups. Barotropic EoS has been frequently used in literature to devise different solutions. It defines a simple relationship between density (ρ) and pressure (p) as

$$p = \varsigma\rho, \tag{1.5.1}$$

where ς is the EoS parameter. The values of $\varsigma = 1,\ 1/3,\ 0,\ -1$ correspond to a stiff fluid, radiation-dominated phase, dust and vacuum energy dominated cosmos, respectively.

Lane and Emden provided a polytropic EoS that relates density and pressure of matter configuration as

$$p = K\rho^\gamma = K\rho^{\frac{n+1}{n}},$$

where K, n and γ denote polytropic constant, polytropic index and polytropic exponent, respectively. This EoS has aided in developing the mechanical structure of stellar systems in equilibrium via the introduction of dimensionless variables in hydrostatic and Poisson's equations. It is used to model degenerate gasses in relativistic (for $\gamma = \frac{4}{3}$) as well as non-relativistic limits (for $\gamma = \frac{5}{3}$) when K is determined via natural constants [86]. For instance, highly massive white dwarfs are represented by polytropes corresponding to $n = 3$. On the other hand, when K is a free parameter the polytropic EoS describes the matter distribution of convective stars ($n = 1.5$) or isothermal spheres ($n \to \infty$). In the case of anisotropic fluid, the polytropic EoS takes the form

$$p_r = K\rho^{\gamma} = K\rho^{\frac{n+1}{n}}, \tag{1.5.2}$$

where p_r denotes radial pressure.

The investigation of essential features of neutron and quark stars also requires a suitable EoS. However, despite the existence of several models, researchers have not agreed upon one EoS. The quark star is composed of SQM (general Wittens conjecture [82]) made of an equal number of up, down and strange quarks and is assumed to be the true ground state for the confined hadrons [87]. Interestingly, the neutron star EoS failed to explain the compactness of the compact stellar objects like 4U 1820-30, SAX J 1808.4-3658, 4U 1728-34, Her X-1, RXJ 185635-3754 and PSR 0943+10, etc., whereas SQM EoS (MIT Bag model) has satisfactorily explained the compactness of the stellar candidates [88]. Recent observations of gravitational waves from binary neutron stars collision (GW170817 [89] and GW190425 [90]), have made it possible to estimate the range of masses and thus constrain the mass of neutron and quark stars. These estimates are consistent with the approximations made by employing the MIT

bag model. Thus, in the absence of a best fit, the MIT bag model is considered as the best approximation for SQM EoS.

The MIT bag model EoS is developed by considering three types of quark matter: strange (s), up (u) and down (d) [91]. The quarks exist in a region of spacetime with vacuum energy density $\mathcal{B}$. For massless and non-interacting quarks, the quark pressure, corresponding to anisotropic fluid, is $p_r^{\mathcal{F}} = \frac{\rho^{\mathcal{F}}}{3}$ ($\mathcal{F} = u,\ d,\ s$). The total quark pressure and density are, respectively, stated as

$$p_r = \sum_{\mathcal{F}} p^{\mathcal{F}} - \mathcal{B}, \quad \rho = \sum_{\mathcal{F}} \rho^{\mathcal{F}} + \mathcal{B}.$$

The EoS for SQM is

$$p_r = \frac{1}{3}(\rho - 4\mathcal{B}), \tag{1.5.3}$$

which has been utilized to construct viable models of strange stars corresponding to different values of the bag constant. The interval for massless strange quarks is $58.9MeV/fm^3 \leq \mathcal{B} \leq 91.5MeV/fm^3$ [92] whereas the massive quarks correspond to the range $56MeV/fm^3 \leq \mathcal{B} \leq 78MeV/fm^3$ [93]. The bag constant ($\mathcal{B}$) appearing in the EoS evaluates the difference between energy density of true (global minimum of energy with stable configuration) and false (local minimum of energy with unstable configuration) vacuum. Moreover, increasing the bag constant lowers the quark pressure ultimately affecting the stellar structure. Many people have considered the MIT bag model as an EoS for predicting the interior distribution of quarks in strange stars [94].

1.6 Complexity of Self-gravitating Systems

A system is considered complex if it is composed of interconnected components and a single formalism cannot adequately describe its essential physical properties. The nature and degree of the relationship between different parts of the complex system are not completely known. Consequently, a disturbance in the parameters may lead to an unpredictable change in physical behavior. Therefore, formulating a complexity factor that assesses the role of each parameter and relates them through a mathematical expression proves helpful. This factor not only provides a yardstick to compare the complexity of different systems but also establishes a criterion for the stability of the system. The concept of complexity in physics stems from the comparison of two systems, ideal gas and a perfect crystal. The atoms of ideal gas are randomly arranged obeying no rules of symmetry. Hence, all its accessible states have the same probability requiring maximum information for the description of distances and symmetries of its cell. On the other hand, low information content is needed to describe a perfect crystal as its probability distribution of accessible states is centered around its symmetric structure. However, the interesting fact is that complexity of these two contrasting structures vanishes. Earlier efforts of defining complexity were based on the idea of arrangement of atoms, information contained in a small piece and disequilibrium (how various probabilistic states differ from the equiprobable distribution) of the system. Obviously, under this definition, the two physical models were treated differently in terms of complexity.

Lopez-Ruiz et al. [95] built upon the previous definitions by including the product of system disequilibrium and information. The new definition allocated the same complexity to, both, the ideal gas and the perfect crystal. A complexity factor for

self-gravitating systems has already been developed on the basis of the definition proposed by Lopez-Ruiz et al. by interpreting probability distribution as energy density. Moreover, the complexity of compact stars (neutron stars and white dwarfs) has been evaluated using this definition [6]. However, this definition only includes the energy density of the fluid and neglects other important features (pressure, dissipation, temperature, etc.) which play a significant role in structure formation. Recently, a new technique was adopted to compute complexity for a static sphere in terms of pressure anisotropy and density inhomogeneity in the framework of GR [2]. Moreover, the devised factor vanished for a homogeneous and isotropic fluid. Structure scalars play a significant role in determining the complexity factor according to the new criterion.

In order to incorporate the characteristics of the comoving congruence, invariants via orthogonal splitting of the Riemann tensor ($\mathcal{R}_{\gamma\beta\delta\alpha}$) are obtained. These invariants are known as structure scalars. For this purpose, the elements of splitting are introduced as [96]

$$Y_{\gamma\delta} = \mathcal{R}_{\gamma\beta\delta\alpha}v^{\beta}v^{\alpha}, \tag{1.6.1}$$

$$Z_{\gamma\delta} =^{*} \mathcal{R}_{\gamma\beta\delta\alpha}v^{\beta}v^{\alpha} = \frac{1}{2}\eta_{\gamma\beta\mu\epsilon}\mathcal{R}^{\mu\epsilon}_{\delta\alpha}v^{\beta}v^{\alpha}, \tag{1.6.2}$$

$$X_{\gamma\delta} =^{*} \mathcal{R}^{*}_{\gamma\beta\delta\alpha}v^{\beta}v^{\alpha} = \frac{1}{2}\eta^{\mu\epsilon}_{\gamma\beta}R^{*}_{\mu\epsilon\delta\alpha}v^{\beta}v^{\alpha}, \tag{1.6.3}$$

where $\mathcal{R}^{*}_{\gamma\beta\delta\alpha} = \frac{1}{2}\eta_{\gamma\beta\mu\epsilon}\mathcal{R}^{\mu\epsilon}_{\delta\alpha}$ is the dual tensor and $\eta_{\gamma\beta\mu\epsilon} = v_{\gamma}\epsilon_{\beta\mu\epsilon}$ is the Levi-Civita tensor (with $\epsilon_{\nu\alpha\beta}$ representing the permutation symbol). The structure scalars are derived by decomposing the tensors $X_{\gamma\delta}$, $Y_{\gamma\delta}$ and $Z_{\gamma\delta}$ into their trace ($X_T = X^{\gamma}_{\gamma}$, $Y_T =$

Y^{γ}_{γ}) and trace-free parts ($X_{TF},\ Y_{TF}$) as

$$X_{\gamma\delta} = \frac{X_T}{3}h_{\gamma\delta} + X_{<\gamma\delta>}, \tag{1.6.4}$$

$$Y_{\gamma\delta} = \frac{Y_T}{3}h_{\gamma\delta} + Y_{<\gamma\delta>}, \tag{1.6.5}$$

$$Z = \sqrt{Z_{\gamma\delta}Z^{\gamma\delta}}, \tag{1.6.6}$$

where

$$X_{<\gamma\delta>} = h^{\beta}_{\gamma}h^{\alpha}_{\delta}\left(X_{\alpha\beta} - \frac{X_T}{3}h_{\alpha\beta}\right), \tag{1.6.7}$$

$$Y_{<\gamma\delta>} = h^{\beta}_{\gamma}h^{\alpha}_{\delta}\left(Y_{\alpha\beta} - \frac{Y_T}{3}h_{\alpha\beta}\right). \tag{1.6.8}$$

These structure scalars contain important information regarding different aspects of the fluid distribution. Thus, they play a key role in determining the complexity of any physical setup.

1.7 Gravitational Decoupling Approach

In order to explore the complex nature of the cosmos as well as self-gravitating systems, analytical solutions of the field equations are required. Hence, the task of constructing well-behaved solutions which adequately describe cosmic scenarios has attracted the attention of many researchers. Ovalle [24] developed a technique that not only simplifies the extraction of solutions from non-linear field equations but also generates anisotropic solutions. This approach is applied in accordance with the following steps.

- The domain of a simple seed source (vacuum, dust or isotropic fluid) is extended by adding a scalar, vector or tensor source ($\Theta_{\gamma\delta}$) as

$$T^{(m)}_{\gamma\delta} + \varrho\Theta_{\gamma\delta}, \tag{1.7.1}$$

where the dimensionless parameter ϱ tracks the strength of the coupling between the two matter sources.

- The addition of a new source increases the degrees of freedom. In order to reduce the number of unknowns, the decoupling technique is applied to disintegrate the system of field equations into two sets. For this purpose, either of the following two schemes can be adopted.

  1. **MGD Method**

     The two matter sources are separated by linearly transforming the radial metric component only. The fluid distributions affect each other gravitationally only which leads to the conservation of individual sources.

  2. **EGD Method**

     The decomposition of field equations is achieved by applying transformations on g_{00} and g_{11}. In this scenario, the fluids exchange energy and are not conserved individually. However, the overall system obeys the principle of conservation of matter and energy.

  In both cases, each set of equations incorporates the effect of only one source.

- The array corresponding to the seed source is determined with the help of a well-behaved solution which reduces the number of unknown parameters. On the other hand, constraints on the additional source are applied to obtain a solution of the Θ-sector. A combination of both solutions generates a new solution of the field equations.

Thus, the method of decoupling transforms a simple seed source into intricate matter distributions by successively incorporating complex sources. Moreover, applying the

above method in reverse order yields simplified analogs of complex solutions [97].

1.8 Embedding Classes

In four-dimensional spacetime, the Riemann tensor describes the geometry of the gravitational source. An n-dimensional manifold V_2 embeds an m-dimensional manifold V_1 ($m < n$), if the injective continuous mapping $f : V_1 \to V_2$ provides a homeomorphism between V_1 and $f(V_1)$. Moreover, the manifold V_1 belongs to embedding class-w, if it can be embedded in a flat space of $m+w$ dimensions (where $m+w$ is the lowest dimension in which V_1 can be embedded). In 1948, Karmarkar [98] showed that a four-dimensional sphere S can generally be immersed in six-dimensional Euclidean space, i.e., it belongs to embedding class-two. Further, he built on Eisenhart's [99] work and derived a condition for the embedding of S in five-dimensional flat spacetime.

Eisenhart showed that if there exists a tensor $W_{\gamma\delta}$ (with $W_{\gamma\delta} = W_{\delta\gamma}$) that satisfies the Gauss-Codazi equations

$$\mathcal{R}_{\alpha\delta\beta\upsilon} = 2eW_{\alpha[\beta}W_{\upsilon]\delta} \quad \text{and} \quad W_{\alpha[\delta;\beta]} - \Gamma^{\lambda}_{\delta\beta}W_{\alpha\lambda} + \Gamma^{\lambda}_{\alpha[\delta}W_{\beta]\lambda} = 0,$$

then it is possible to embed an m-dimensional space in a pseudo-Euclidean space with $(m+1)$ dimensions. Here the coefficients of the second differential form are denoted by $W_{\alpha\delta}$ whereas $e = \pm 1$. Karmarkar derived a constraint that allows the embedding of four-dimensional spherical spacetime in a five-dimensional flat space as

$$\mathcal{R}_{1212}\mathcal{R}_{0303} + \mathcal{R}_{1202}\mathcal{R}_{1303} - \mathcal{R}_{2323}\mathcal{R}_{0101} = 0. \tag{1.8.1}$$

However, a spacetime with $\mathcal{R}_{2323} = 0$ fails to adhere to Karmarkar's condition. An

example of such a line element is the conformally flat fluid configuration with zero density.

1.9 Physical Acceptability of Models

The solution of the field equations must fulfil certain conditions to be physically relevant. As the matter inside a stellar model is concentrated in the core, the density and pressure of a well-behaved solution must be maximum at the center with a monotonically decreasing trend towards the surface of the star. Moreover, the solution must be consistent with the viability and stability conditions discussed below.

1.9.1 Viability Conditions

The universe is a well-structured yet incomprehensible system composed of heavenly bodies and other mysterious components. The key to understanding the evolution of the vast cosmos lies in the study of the arrangement as well as the physical behavior of celestial objects. In this regard, the concept of relativity played a remarkable role in providing elementary insights into the mechanism governing the interior of astronomical bodies. The solutions of the non-linear field equations describe the intricate nature of cosmic objects. However, the non-linear differential equations may yield physically irrelevant solutions as well. It is necessary for the study of cosmic structures that their interior consists of normal matter, i.e., energy and momentum must be well-defined at every point inside. For this purpose, constraints on the energy-momentum tensor, termed as energy conditions, are imposed.

The energy bounds emerge from the Raychaudhuri equation when the attractive

nature of gravity and non-negativity of energy density are taken into account. The Raychaudhuri equation is used to explain the evolution of the expansion scalar with time corresponding to the congruence of timelike and null geodesics respectively, as

$$\frac{d\vartheta}{d\tau}=-\frac{\vartheta^2}{3}+w_{\gamma\delta}w^{\gamma\delta}-\sigma_{\gamma\delta}\sigma^{\gamma\delta}-\mathcal{R}_{\gamma\delta}v^{\gamma}v^{\delta}, \tag{1.9.1}$$

$$\frac{d\vartheta}{d\tau}=-\frac{\vartheta^2}{2}+w_{\gamma\delta}w^{\gamma\delta}-\sigma_{\gamma\delta}\sigma^{\gamma\delta}-\mathcal{R}_{\gamma\delta}l^{\gamma}l^{\delta}, \tag{1.9.2}$$

where the rotation of the curves is described by the vorticity tensor $w_{\gamma\delta}$ and l_{γ} represents the vector field describing null geodesics. The congruence of geodesics diverges if $\frac{d\vartheta}{d\tau}>0$ and converges if $\frac{d\vartheta}{d\tau}$ is negative. As gravity compels the geodesics to converge, therefore $\frac{d\vartheta}{d\tau}<0$. Assuming that $w_{\gamma\delta}=0$ and neglecting the quadratic terms involving the shear tensor (as $\sigma_{\gamma\delta}\sigma^{\gamma\delta}\geq 0$), Eqs.(1.9.1) and (1.9.2) lead to $\vartheta=-\tau\mathcal{R}_{\gamma\delta}v^{\gamma}v^{\delta}$ and $\vartheta=-\tau\mathcal{R}_{\gamma\delta}l^{\gamma}l^{\delta}$, respectively. Thus, the following constraints are imposed on Ricci tensor

$$\mathcal{R}_{\gamma\delta}v^{\gamma}v^{\delta}\geq 0,\quad \mathcal{R}_{\gamma\delta}l^{\gamma}l^{\delta}\geq 0. \tag{1.9.3}$$

Since the curvature of spacetime is linked to the matter distribution via field equations, therefore the above inequalities yield

$$(T_{\gamma\delta}-\frac{g_{\gamma\delta}T}{2})v^{\gamma}v^{\delta}\geq 0,\quad (T_{\gamma\delta}-\frac{g_{\gamma\delta}T}{2})l^{\gamma}l^{\delta}\geq 0.$$

For anisotropic configuration, these conditions are classified into four categories given below

$$\text{NEC:}\quad \rho+p_r\geq 0,\quad \rho+p_{\perp}\geq 0, \tag{1.9.4}$$

$$\text{WEC:}\quad \rho\geq 0,\quad \rho+p_r\geq 0,\quad \rho+p_{\perp}\geq 0, \tag{1.9.5}$$

$$\text{SEC:}\quad \rho+p_r\geq 0,\quad \rho+p_{\perp}\geq 0,\quad \rho+p_r+2p_{\perp}\geq 0, \tag{1.9.6}$$

$$\text{DEC:}\quad \rho\pm p_r\geq 0,\quad \rho\pm p_{\perp}\geq 0. \tag{1.9.7}$$

The incompatibility of a physical model with the NEC means that the model disobeys all energy conditions which indicates the presence of exotic matter.

1.9.2 Stability Analysis

A stable object can restore its equilibrium after perturbations caused by external forces. In astrophysics, stability analysis of stellar structure is of great importance as it determines the evolution of the physical models. For instance, the formation of compact stars is possible only when the collapsing object achieves a new equilibrium position that can sustain the influence of external fluctuations and irregularities. Thus, it is essential to inspect the solutions representing self-gravitating systems for stability. Different criteria have been developed to inspect the stability of an astrophysical setup.

Speed of sound helps to determine the stability of anisotropic stellar models. The sound wave propagates through different media at different rates. However, its speed never exceeds that of light. This phenomenon is incorporated in the causality condition as $0 < v_r^2 < 1$ and $0 < v_\perp^2 < 1$, where $v_r^2 = \frac{dp_r}{d\rho}$ and $v_\perp^2 = \frac{dp_\perp}{d\rho}$ represent radial and tangential velocities, respectively and $p_\perp$ is the tangential pressure [100]. Abreu et al. [101] used Herrera's cracking approach and proposed another criterion which states that a system free from cracking is potentially stable. A system cracks when the inward directed radial forces are unable to maintain their direction under external perturbations. A mathematical expression for this approach reads

$$0 < |v_\perp^2 - v_r^2| < 1.$$

Another commonly used tool to examine the stability of relativistic spherical systems is the adiabatic index. This indicates stiffness of the EoS for a specific energy

density by connecting the EoS with the internal structure of the sphere. Chandrasekhar [102] studied the dynamical stability of relativistic stars against infinitesimal radial adiabatic perturbation. Heintzmann and Hillebrandt [103] found that an anisotropic compact object will achieve stability if the adiabatic index is greater than $\frac{4}{3}$ everywhere inside the configuration. The expression for the adiabatic index for an anisotropic system is given by [103]

$$\Gamma = \frac{p_r + \rho}{p_r}\frac{dp_r}{d\rho} = \frac{p_r + \rho}{p_r}v_r^2.$$

Chapter 2

Complexity of Sphere in Self-interacting Brans-Dick Gravity

This chapter aims to derive a definition of complexity for a static as well as a dynamic spherical system in the background of SBD gravity. We measure complexity of the structure in terms of inhomogeneous energy density, anisotropic pressure and massive scalar field. For this purpose, we formulate structure scalars by orthogonally splitting the Riemann tensor. We also evaluate the vanishing complexity condition to obtain solutions for two static stellar models. Moreover, we show that self-gravitating models collapsing homologously follow the simplest mode of evolution. Furthermore, we demonstrate the effect of scalar field on the complexity and evolution of non-dissipative as well as dissipative systems. The criteria under which the system deviates from the initial state of zero complexity is also discussed.

The chapter is arranged as follows. We formulate the complexity condition for a static sphere through structure scalars in the next section. In section **2.2**, the dynamics of a spherical self-gravitating system is incorporated in the definition of complexity corresponding to the sign convention $(-,+,+,+)$. The results of this chapter have been published [104, 105].

2.1 SBD Field Equations for Static Sphere

We consider a static sphere bounded by a hypersurface defined by

$$ds^2 = e^{\lambda(r)}dt^2 - e^{\chi(r)}dr^2 - r^2(d\theta^2 + \sin^2\theta d\phi^2). \tag{2.1.1}$$

The interior of the sphere is filled with anisotropic fluid described by

$$T_\delta^{\gamma(m)} = \rho v^\gamma v_\delta - P h_\delta^\gamma + \Pi_\delta^\gamma, \tag{2.1.2}$$

where the anisotropy in pressure is represented by P and Π_δ^γ which satisfy the following relations

$$\Pi_\delta^\gamma = \Pi(\mathfrak{s}^\gamma \mathfrak{s}_\delta + \frac{h_\delta^\gamma}{3}), \quad P = \frac{1}{3}(p_r + 2p_\perp), \quad \Pi = p_r - p_\perp = -\Delta,$$

where $\mathfrak{s}^\gamma$is a radial four vector. Moreover, $v^\gamma = (e^{\frac{-\lambda}{2}}, 0, 0, 0)$ and $\mathfrak{s}^\gamma = (0, e^{\frac{-\chi}{2}}, 0, 0)$ satisfy the following conditions

$$\mathfrak{s}^\gamma v_\gamma = 0, \quad \mathfrak{s}^\gamma \mathfrak{s}_\gamma = -1.$$

Using Eqs.(1.1.6)-(1.1.9) and (2.1.1), the field equations are obtained as

$$\frac{1}{r^2} - e^{-\chi}\left(\frac{1}{r^2} - \frac{\chi'}{r}\right) = \frac{1}{\Psi}\left(\rho + T_0^{0\Psi}\right), \tag{2.1.3}$$

$$-\frac{1}{r^2} + e^{-\chi}\left(\frac{1}{r^2} + \frac{\lambda'}{r}\right) = \frac{1}{\Psi}\left(p_r - T_1^{1\Psi}\right), \tag{2.1.4}$$

$$\frac{e^{-\chi}}{4}\left(2\lambda'' + \lambda'^2 - \chi'\lambda' + 2\frac{\lambda' - \chi'}{r}\right) = \frac{1}{\Psi}\left(p_\perp - T_2^{2\Psi}\right), \tag{2.1.5}$$

where

$$T_0^{0\Psi} = e^{-\chi}\left[\Psi'' + \left(\frac{2}{r} - \frac{\chi'}{2}\right)\Psi' + \frac{\omega_{BD}}{2\Psi}\Psi'^2 - e^{\chi}\frac{V(\Psi)}{2}\right], \tag{2.1.6}$$

$$T_1^{1\Psi} = e^{-\chi}\left[\left(\frac{2}{r} + \frac{\lambda'}{2}\right)\Psi' - \frac{\omega_{BD}}{2\Psi}\Psi'^2 - e^{\chi}\frac{V(\Psi)}{2})\right], \tag{2.1.7}$$

$$T_2^{2\Psi} = e^{-\chi}\left[\Psi'' + \left(\frac{1}{r} - \frac{\chi'}{2} + \frac{\lambda'}{2}\right)\Psi' + \frac{\omega_{BD}}{2\Psi}\Psi'^2 - e^{\chi}\frac{V(\Psi)}{2}\right]. \quad (2.1.8)$$

The wave equation (1.1.8) takes the form

$$\begin{aligned}\Box\Psi &= -e^{-\chi}\left[\left(\frac{2}{r} - \frac{\chi'}{2} + \frac{\lambda'}{2}\right)\Psi' + \Psi''\right] \\ &= \frac{1}{3+2\omega_{BD}}\left[\rho - 3P + \left(\Psi\frac{dV(\Psi)}{d\Psi} - 2V(\Psi)\right)\right]. \quad (2.1.9)\end{aligned}$$

The spacetime is divided by the hypersurface into two different regions, interior and exterior. The exterior region is taken to be the Schwarzschild spacetime. To ensure smoothness and continuity of geometry at the boundary surface ($r = r_\Sigma =$ constant), the following conditions must be satisfied

$$\begin{aligned}(e^{\lambda})_\Sigma &= (1 - \frac{2M}{r})_\Sigma, \\ (e^{-\chi})_\Sigma &= (1 - \frac{2M}{r})_\Sigma, \\ (p_r)_\Sigma &= 0.\end{aligned}$$

The total energy within a sphere of radius r is computed through the Misner-Sharp formula which yields

$$m = \frac{r}{2}\mathcal{R}^3_{232} = \frac{r}{2}(1 - e^{-\chi}) = \frac{1}{2}\int r^2 T_0^{0(\text{eff})} dr. \quad (2.1.10)$$

The Tolman-Oppenheimer-Volkoff equation is obtained through the field equations and mass function as

$$T_1^{1'(\text{eff})} = \frac{2m - r^3 T_1^{1(\text{eff})}}{2r(r-2m)}(T_0^{0(\text{eff})} - T_1^{1(\text{eff})}) + \frac{2}{r}(T_2^{2(\text{eff})} - T_1^{1(\text{eff})}). \quad (2.1.11)$$

The mass function can be expressed in terms of the Weyl tensor which evaluates the effect of tidal forces and appears as the traceless part in the splitting of Riemann tensor as

$$\mathcal{R}^{\gamma}_{\alpha\beta\sigma} = C^{\gamma}_{\alpha\beta\sigma} + \frac{\mathcal{R}^{\gamma}_{\beta}}{2}g_{\alpha\sigma} - \frac{\mathcal{R}_{\alpha\beta}}{2}\delta^{\gamma}_{\sigma} + \frac{\mathcal{R}_{\alpha\sigma}}{2}\delta^{\gamma}_{\beta} - \frac{\mathcal{R}^{\gamma}_{\sigma}}{2}g_{\alpha\beta} - \frac{1}{6}(\delta^{\gamma}_{\beta}g_{\alpha\sigma} - g_{\alpha\beta}\delta^{\gamma}_{\sigma}), \quad (2.1.12)$$

where $C^{\gamma}_{\alpha\beta\sigma}$ is the Weyl tensor.

The Weyl tensor is decomposed into trace-free electric ($E_{\alpha\beta}$) and magnetic ($H_{\alpha\beta}$) parts by using the four velocity of the observer. In the case of spherical symmetry, these tensors reduce to

$$E_{\gamma\delta} = C_{\gamma\alpha\delta\sigma}v^{\alpha}v^{\sigma}, \tag{2.1.13}$$

$$H_{\gamma\delta} = 0, \tag{2.1.14}$$

where

$$\begin{aligned} C_{\gamma\nu\kappa\sigma} &= (g_{\gamma\nu\alpha\beta}g_{\kappa\sigma\delta\gamma} - \eta_{\gamma\nu\alpha\beta}\eta_{\kappa\sigma\delta\gamma})v^{\alpha}v^{\delta}E^{\beta\gamma}, \\ g_{\gamma\nu\alpha\beta} &= g_{\gamma\alpha}g_{\nu\beta} - g_{\gamma\beta}g_{\nu\alpha}. \end{aligned} \tag{2.1.15}$$

Substituting the Weyl tensor in Eq.(2.1.13), it follows that

$$E_{\gamma\delta} = \varepsilon(\mathfrak{s}_{\gamma}\mathfrak{s}_{\delta} + \frac{h_{\gamma\delta}}{3}), \tag{2.1.16}$$

with

$$\begin{aligned} &\varepsilon = \frac{e^{-\chi}}{4}\left(-\lambda'' - \frac{\lambda'^2 - \chi'\lambda'}{2} + \frac{\lambda' - \chi'}{r} + 2\frac{1-e^{\chi}}{r^2}\right), \\ &E^{\gamma}_{\gamma} = 0 = E_{\gamma\delta}v^{\delta}. \end{aligned} \tag{2.1.17}$$

Through Eqs.(1.1.7) and (2.1.10), we obtain the relation

$$m = \frac{r^3}{6}(T_0^{0(\mathrm{eff})} - T_2^{2(\mathrm{eff})} + T_1^{1(\mathrm{eff})}) + \frac{\varepsilon r^3}{3}, \tag{2.1.18}$$

leading to a definition for ε given by

$$\varepsilon = -\frac{1}{2r^3}\int_0^r r^3 T_0^{0'(\mathrm{eff})}dr + \frac{1}{2}(T_2^{2(\mathrm{eff})} - T_1^{1(\mathrm{eff})}). \tag{2.1.19}$$

This demonstrates the relationship between the Weyl tensor, inhomogeneous energy density and anisotropic pressure in the presence of scalar field. Substituting the above equation in (2.1.18), the mass function can be rewritten as

$$m(r)=\frac{r^3}{6}T_0^{0(\text{eff})}-\frac{1}{6}\int_0^r r^3T_0^{0'(\text{eff})}dr. \tag{2.1.20}$$

It is observed that the first term on the right side gives the value of mass function when the energy density is homogeneous whereas the second term exhibits the change induced by the inhomogeneous energy density. We now find the total mass of the spherical system enclosed within the boundary r_Σ using an alternate definition proposed by Tolman as

$$m_T=\frac{1}{2}\int_0^r r^2e^{\frac{\lambda+\chi}{2}}(T_0^{0(\text{eff})}-T_1^{1(\text{eff})}-2T_2^{2(\text{eff})})dr. \tag{2.1.21}$$

Inserting field Eqs.(2.1.3)-(2.1.5) in (2.1.21), the Tolman mass reduces to

$$m_T=e^{\frac{\lambda-\chi}{2}}\lambda'\frac{r^2}{2}. \tag{2.1.22}$$

Using the above equation with (2.1.4), the final expression for Tolman mass turns out to be

$$m_T=e^{\frac{\lambda+\chi}{2}}(m-\frac{r^3}{2}T_1^{1(\text{eff})}). \tag{2.1.23}$$

The gravitational acceleration is calculated by using four acceleration as

$$a=-\mathfrak{s}^\gamma a_\gamma=\frac{e^{-\frac{\chi}{2}}\lambda'}{2},$$

which, in accordance with Eq.(2.1.23), leads to

$$a=\frac{e^{-\frac{\lambda}{2}}m_T}{r^2}.$$

This shows that the Tolman mass can also be treated as the active gravitational mass. After simplifications [106], the Tolman mass can be re-expressed as

$$m_T=(m_T)_\Sigma(\frac{r}{r_\Sigma})^3-r^3\int_r^{r_\Sigma}e^{\frac{\lambda+\chi}{2}}\left[\frac{1}{r}(T_1^{1(\text{eff})}-T_2^{2(\text{eff})})+\frac{1}{2r^4}\int_0^r r^3T_0^{0'(\text{eff})}dr\right]dr, \tag{2.1.24}$$

or equivalently

$$m_T=(m_T)_\Sigma(\frac{r}{r_\Sigma})^3-r^3\int_r^{r_\Sigma}\frac{e^{\frac{\lambda+\chi}{2}}}{r}\left(\frac{T_1^{1(\text{eff})}-T_2^{2(\text{eff})}}{2}-\varepsilon\right)dr. \tag{2.1.25}$$

2.1.1 Structure Scalars

Using the field equations in Eq.(2.1.12), the Riemann tensor takes the form

$$\mathcal{R}^{\alpha\delta}_{\beta\gamma}=C^{\alpha\delta}_{\beta\gamma}+2T^{(\text{eff})[\alpha}_{[\beta}\delta^{\delta]}_{\gamma]}+T^{(\text{eff})}\left(\frac{1}{3}\delta^\alpha_{[\beta}\delta^\delta_{\gamma]}-\delta^{[\alpha}_{[\beta}\delta^{\delta]}_{\gamma]}\right), \tag{2.1.26}$$

which is split using Eqs.(1.1.9), (2.1.2) and (2.1.15) as

$$\mathcal{R}^{\alpha\delta}_{\beta\gamma}=\mathcal{R}^{\alpha\delta}_{(I)\beta\gamma}+\mathcal{R}^{\alpha\delta}_{(II)\beta\gamma}+\mathcal{R}^{\alpha\delta}_{(III)\beta\gamma}+\mathcal{R}^{\alpha\delta}_{(IV)\beta\gamma}+\mathcal{R}^{\alpha\delta}_{(V)\beta\gamma}, \tag{2.1.27}$$

where

$$\mathcal{R}^{\alpha\delta}_{(I)\beta\gamma} = \frac{2}{\Psi}\left[\rho v^{[\alpha}v_{[\beta}\delta^{\delta]}_{\gamma]}-Ph^{[\alpha}_{[\beta}\delta^{\delta]}_{\gamma]}+(\rho-3P)(\frac{1}{3}\delta^\alpha_{[\beta}\delta^\delta_{\gamma]}-\delta^{[\alpha}_{[\beta}\delta^{\delta]}_{\gamma]})\right], \tag{2.1.28}$$

$$\mathcal{R}^{\alpha\delta}_{(II)\beta\gamma} = \frac{2}{\Psi}\Pi^{[\alpha}_{[\beta}\delta^{\delta]}_{\gamma]}, \tag{2.1.29}$$

$$\mathcal{R}^{\alpha\delta}_{(III)\beta\gamma} = 4v^{[\alpha}v_{[\beta}E^{\delta]}_{\gamma]}-\epsilon^{\alpha\delta}_\gamma\epsilon_{\beta\gamma\lambda}E^{\gamma\lambda}, \tag{2.1.30}$$

$$\begin{aligned}\mathcal{R}^{\alpha\delta}_{(IV)\beta\gamma} &= \frac{2}{\Psi}\left[\Psi^{[,\alpha}_{[;\beta}\delta^{\delta]}_{\gamma]}+\frac{\omega_{BD}}{\Psi}\Psi^{,[\alpha}\Psi_{,[\beta}\delta^{\delta]}_{\gamma]}-\left(\Box\Psi+\frac{\omega_{BD}}{2\Psi}\Psi_{,\gamma}\Psi^{,\gamma}+\frac{V(\Psi)}{2}\right)\right.\\ &\times \left.\delta^{[\alpha}_{[\beta}\delta^{\delta]}_{\gamma]}\right],\end{aligned} \tag{2.1.31}$$

$$\mathcal{R}^{\alpha\delta}_{(V)\beta\gamma} = \frac{1}{\Psi}\left[\left(-\frac{\omega_{BD}}{\Psi}\Psi_{,\gamma}\Psi^{,\gamma}-2V(\Psi)-3\Box\Psi\right)\left(\frac{1}{3}\delta^\alpha_{[\beta}\delta^\delta_{\gamma]}-\delta^{[\alpha}_{[\beta}\delta^{\delta]}_{\gamma]}\right)\right]. \tag{2.1.32}$$

The three tensors $X_{\alpha\beta},\ Y_{\alpha\beta}$ and $Z_{\alpha\beta}$ (expressed in Eqs.(1.6.1)-(1.6.3)) are evaluated using the above definition of the Riemann tensor as

$$\begin{aligned}
X_{\gamma\delta} &= \frac{1}{\Psi}\left(\frac{\rho h_{\gamma\delta}}{3}+\frac{\Pi_{\gamma\delta}}{2}\right)-E_{\gamma\delta}-\frac{1}{4\Psi}(\Psi^{,\sigma}_{;\sigma}h_{\gamma\delta}-2\Psi_{,\gamma;\sigma}v_{\delta}v^{\sigma} \\
&- \frac{\omega_{BD}}{4\Psi^2}\Psi_{,\gamma}\Psi_{,\delta}+\frac{5h_{\gamma\delta}}{12\Psi}V(\Psi), \qquad (2.1.33)\\
Y_{\gamma\delta} &= \frac{1}{\Psi}\left(\frac{(\rho+3P)h_{\gamma\delta}}{6}+\frac{\Pi_{\gamma\delta}}{2}\right)+E_{\gamma\delta}+\frac{1}{2\Psi}(\Psi_{,\gamma;\delta}-\Psi_{,\gamma;\sigma}v_{\delta}v^{\sigma} \\
&- \Psi_{,\sigma;\delta}v_{\gamma}v^{\sigma}+\Psi_{,\sigma;\sigma}v_{\sigma}v^{\sigma}g_{\gamma\delta})+\frac{\omega_{BD}}{2\Psi^2}\Psi_{,\gamma}\Psi_{,\delta}-\frac{h_{\gamma\delta}}{6\Psi}\left(\frac{\omega_{BD}}{\Psi}\Psi_{,\sigma}\Psi^{,\sigma}\right. \\
&- V(\Psi)\big), \qquad (2.1.34)\\
Z_{\gamma\delta} &= \frac{1}{4\Psi}(\eta_{\gamma\alpha\delta\beta}\Psi^{,\beta}_{;\sigma}v^{\alpha}v^{\sigma}). \qquad (2.1.35)
\end{aligned}$$

Now, the structure scalars [96] are derived by employing Eqs.(1.6.4)-(1.6.8) as

$$\begin{aligned}
X_T &= X^m_T+X^{\Psi}_T=\frac{1}{4\Psi}(\rho)-\frac{1}{4\Psi}\left(5\Box\Psi-2\Psi_{,\gamma;\delta}v^{\gamma}v^{\delta}-\frac{\omega_{BD}}{\Psi}\Psi_{,\alpha}\Psi^{,\alpha}\right. \\
&+ 5V(\Psi)\big), \qquad (2.1.36)\\
X_{TF} &= X^m_{TF}+X^{\Psi}_{TF}=\frac{1}{\Psi}(\frac{\Pi}{2}-\varepsilon\Psi)+\frac{1}{2\Psi}\left(\Box\Psi-\frac{\omega_{BD}}{\Psi}\Psi_{,\alpha}\Psi^{,\alpha}\right. \\
&- \Psi_{,\gamma;\delta}v^{\gamma}v^{\delta}\big), \qquad (2.1.37)\\
Y_T &= Y^m_T+Y^{\Psi}_T=\frac{1}{2\Psi}(\rho+3p_r-2\Pi)+\frac{1}{2\Psi}\left(\Box\Psi+2\Psi_{,\gamma;\delta}v^{\gamma}v^{\delta}\right. \\
&+ V(\Psi)\big), \qquad (2.1.38)\\
Y_{TF} &= Y^m_{TF}+Y^{\Psi}_{TF}=\frac{1}{\Psi}(\frac{\Pi}{2}+\varepsilon\Psi)+\frac{1}{2\Psi}\left(\Box\Psi+\frac{\omega_{BD}}{\Psi}\Psi_{,\alpha}\Psi^{,\alpha}\right. \\
&- \Psi_{,\gamma;\delta}v^{\gamma}v^{\delta}\big). \qquad (2.1.39)
\end{aligned}$$

It follows from the above equations that under the influence of scalar field, the total energy density within the system is determined by X_T whereas the scalar Y_T describes the effects of principal stresses produced by inhomogeneous energy density. Using

Eqs.(2.1.37) and (2.1.39), we have

$$X^m_{TF}+Y^m_{TF}=\frac{2\Pi}{\Psi}\text{ and }Y^{\Psi}_{TF}-X^{\Psi}_{TF}=\frac{\omega_{BD}}{\Psi^2}\Psi_{,\alpha}\Psi^{,\alpha},$$

which shows that local anisotropy in pressure is found by X^m_{TF} and Y^m_{TF} whereas the coupling parameter is determined by X^{Ψ}_{TF} and Y^{Ψ}_{TF}. From Eqs.(2.1.25) and (2.1.39), it is observed that Y_{TF} appears in the expression for Tolman mass as

$$m_T=(m_T)_{\Sigma}\left(\frac{r}{r_{\Sigma}}\right)+r^3\int_r^{r_{\Sigma}}\frac{e^{\frac{\lambda+\chi}{2}}}{r}(-Y^m_{TF}+Y^{\Psi}_{TF})+\frac{e^{\frac{\lambda-\chi}{2}}\Psi'}{2r\Psi}dr. \tag{2.1.40}$$

This indicates that Y_{TF} gauges the impact of anisotropic pressure and inhomogeneous density on the active gravitational mass.

2.1.2 Complexity Factor for Static Sphere

In this section, we formulate the complexity factor which is governed by the physical features such as energy density, pressure, heat flux. In general, a system is said to be least complex if its physical structure is completely described by a small number of factors. For example, a spherical object filled with dust fluid has only one necessary ingredient which is the energy density of the fluid whereas, the inclusion of isotropic pressure to dust fluid leads to a slightly more complex system known as a perfect fluid. In GR, the complexity factor depends on the inhomogeneous and anisotropic distribution [2]. However, in our work, the complexity is determined by the scalar field and self-interacting scalar potential in addition to inhomogeneous energy density and anisotropic pressure. The complexity of this system can, therefore, be completely described by the structure scalar Y_{TF}, since it is not only a relation between the sources of complexity but also a measure of how they affect the Tolman mass. Setting

$Y_{TF}=0$ leads to vanishing complexity factor condition which establishes the following relation among the physical variables

$$\frac{\Pi}{\Psi}=\frac{1}{2r^3}\int_0^r r^3 T_0^{0'(\text{eff})}dr+\frac{e^{-\chi}\Psi'}{2r\Psi}. \tag{2.1.41}$$

It must be noted that the complexity factor vanishes for isotropic and homogeneous matter distribution in GR. However, in the context of SBD gravity, an additional condition $\frac{e^{-\chi}\Psi'}{2r\Psi}=0$ is required to obtain a complexity-free structure. Equation (2.1.41) can be used as a restraint for formulating solution of the field equations.

Gokhroo and Mehra [107] obtained a physically reasonable interior solution for an anisotropic sphere with variable energy density to explain the larger red-shifts of quasi-stellar objects. Using their assumptions, we illustrate the behavior of self-gravitating system for the condition of vanishing complexity. The assumed energy density (maximum at the center and decreasing along the radius) is given by

$$\rho=\rho_0(1-\frac{r^2}{r_\Sigma^2}), \tag{2.1.42}$$

which leads to the mass function

$$m(r)=\frac{1}{2}\left[\frac{\rho_0 r^3}{3\Psi}\left(1-\frac{3k_1r^2}{5r_\Sigma^2}\right)+\int_0^r\frac{r^2}{\Psi}T_0^{0\Psi}dr\right]. \tag{2.1.43}$$

Substituting the above equation in (2.1.10), the expression for the metric function turns out to be

$$e^{-\chi}=\frac{1}{\Psi}\left(1-\beta r^2+\frac{3k_1\beta r^4}{5r_\Sigma^2}\right)-\int_0^r\frac{r^2}{\Psi}T_0^{0\Psi}dr, \tag{2.1.44}$$

where $k_1\in(0,1)$ and $\beta=\frac{\rho_0}{3}$. Using Eqs.(2.1.4) and (2.1.5), it follows that

$$\frac{1}{\Psi}\{\Pi+e^{-\chi}[\Psi''+\Psi'(-\frac{\chi'}{2}+\frac{1}{r})+\frac{\omega_{BD}}{\Psi}\Psi'^2]\}=e^{-\chi}[\frac{-\lambda''}{2}-\frac{\lambda'^2}{4}$$

$$+\frac{\lambda'}{2r}+\frac{1}{r^2}+\frac{\chi'}{2}(\frac{\lambda'}{2}+\frac{1}{r})]-\frac{1}{r^2}. \tag{2.1.45}$$

Introducing new variables as

$$e^{\lambda} = e^{\int(2z-\frac{2}{r})dr}, \tag{2.1.46}$$

$$e^{-\chi}=y(r) = \frac{1}{\Psi}\left(1-\beta r^2+\frac{3k_1\beta r^4}{5r_\Sigma^2}\right)-\int_0^r\frac{r^2}{\Psi}T_0^{0\Psi}dr, \tag{2.1.47}$$

such that Eq.(2.1.45) reduces to

$$\begin{aligned}\left(-\frac{2\Psi}{\Psi z+\Psi'}\right)\left(\frac{\Pi}{2\Psi}+\frac{1}{r^2}\right) &= y'+y\left(\frac{2\Psi}{\Psi z+\Psi'}\right)\left[z^2-\frac{3z}{r}+z'+\frac{2}{r^2}\right.\\ &+ \left.\frac{1}{\Psi}\left(\Psi''+\frac{\Psi'}{r}+\frac{\omega_{BD}}{\Psi}\Psi'^2\right)\right],\end{aligned} \tag{2.1.48}$$

with the value of Π provided by Eqs.(2.1.41) and (2.1.42). Hence, the metric can be expressed in terms of the new variables as

$$ds^2=-e^{\int(2z-\frac{2}{r})dr}+\frac{\xi}{\int\left(-\frac{2\Psi}{\Psi z+\Psi'}\right)\left(\frac{\Pi}{2\Psi}+\frac{1}{r^2}\right)\xi dr+C}dr^2+r^2d\theta^2+r^2\sin^2\theta d\phi^2,$$

where C is a constant of integration and

$$\begin{aligned}\xi &= \exp\left\{\int\left(\frac{2\Psi}{\Psi z+\Psi'}\right)\left[z^2-\frac{3z}{r}+z'+\frac{2}{r^2}\right.\right.\\ &+ \left.\left.\frac{1}{\Psi}\left(\Psi''+\frac{\Psi'}{r}+\frac{\omega_{BD}}{\Psi}\Psi'^2\right)\right]dr\right\}.\end{aligned}$$

The energy density, radial and tangential pressure in the presence of scalar field take the form

$$\begin{aligned}\rho &= \frac{2\Psi m'}{r^2}-(1-\frac{2m}{r})\left[\left(\frac{2}{r}+\frac{m'}{(r-2m)}\right)\Psi'+\Psi''-\frac{\omega_{BD}}{2\Psi}\Psi'^2\right]\\ &+ \frac{V(\Psi)}{2},\\ p_r &= \frac{\Psi}{2r^2}\left[-1+\frac{m}{r}+z(r-2m)\right]-(1-\frac{2m}{r})\left[\left(-\frac{1}{r}-z\right)\Psi'+\Psi''\right.\end{aligned}$$

$$+ \quad \frac{\omega_{BD}}{2\Psi}\Psi'^2\Big] - \frac{V(\Psi)}{2},$$

and

$$p_\perp = \frac{\Psi}{2}\left[(\frac{1}{r^2}+z^2+z'-\frac{z}{r})+\frac{z}{2}(\frac{m}{r^2}-\frac{m'}{r})\right]-(1-\frac{2m}{r})$$
$$\times \quad \left[\left(z-\frac{m'}{(r-2m)}\right)\Psi'-\Psi''-\frac{\omega_{BD}}{2\Psi}\Psi'^2\right]-\frac{V(\Psi)}{2}.$$

We now formulate a possible solution with zero complexity by adopting the polytropic EoS (1.5.2). Introducing new variables

$$\alpha=\frac{p_{r0}}{\rho_0},\quad r=\frac{\xi}{A},\quad A^2=\frac{\rho_0}{2\alpha(n+1)},\quad \psi^n=\frac{\rho}{\rho_0},\quad \mu(\xi)=\frac{2m(r)A^3}{\rho_0},$$

lead to the following form of Eqs.(2.1.9)-(2.1.11)

$$\Psi = \frac{-\left[1-\frac{2(n+1)\alpha\mu}{\xi}\right]^{-1}}{(3+2\omega_{BD})}\left\{\int\frac{\rho_0}{(2A\xi)^2}\left[\mu+\frac{\alpha\xi^3\psi^{n+1}}{2\Psi}-\frac{\xi^3T_1^{\Psi1}}{2\rho_0\Psi}\right]\right.$$
$$- \quad \frac{\rho_0\mu}{2(A\xi)^2}\left[1-\frac{2(n+1)\alpha\mu}{\xi}\right]^{-1}d\xi\left[\rho_0\psi^n(1-3K\psi\rho_0^{\frac{1}{n}})+\Psi\frac{dV(\Psi)}{d\Psi}\right.$$
$$\left.\left. - \quad 2V(\Psi)\right]\right\}, \tag{2.1.49}$$

$$\frac{d\mu}{d\xi} = \frac{\xi^2\psi^n}{\Psi}+\frac{\xi^2}{\Psi\rho_0}T_0^{\Psi0}, \tag{2.1.50}$$

$$\frac{d\psi}{d\xi} = \frac{\psi^{-n}}{\alpha(n+1)}\frac{dT_1^{\Psi1}}{d\xi}-\left\{\frac{\xi^2}{2}\left[\frac{1-\frac{2(n+1)\alpha\mu}{\xi}}{1+\alpha\psi}\right]\right\}^{-1}\left[\left(\mu+\frac{\alpha\xi^3\psi^{n+1}}{2\Psi}\right.\right.$$
$$- \quad \left.\frac{\xi^3}{2\rho_0\Psi}T_1^{\Psi1}\right)\left(1+\frac{T_0^{\Psi0}-T_1^{\Psi1}}{\Psi}\right)+\frac{\xi}{n+1}\left(\frac{1-\frac{2(n+1)\alpha\mu}{\xi}}{1-\alpha\psi}\right)$$
$$\left.\times \quad \left(\frac{\psi^{-n}}{p_{r0}}\Pi+\frac{\Upsilon}{\alpha}\right)\right], \tag{2.1.51}$$

where

$$T_0^{\Psi0} = \left[1-\frac{2\mu\alpha(n+1)}{\xi}\right]\left[\Psi''+\frac{\omega_{BD}\Psi'^2}{2\Psi}+\frac{2A\Psi'}{\xi}\right]+\frac{\rho_0\mu\Psi'}{2A\xi^2}+\frac{V(\Psi)}{2},$$
$$T_1^{\Psi1} = \left(\frac{4}{1+r\Psi'}\right)\left\{\frac{\Psi'}{4A\xi^2}\left(\rho_0\mu+\xi^3K\psi^{n+1}\rho_0^\gamma\right)+\left[1-2\frac{\mu\alpha(n+1)}{\xi}\right]\right.$$

$$\times \quad \left(\frac{2A\Psi'}{\xi}-\frac{\omega_{BD}\Psi'^2}{2\Psi}\right)-\frac{V(\Psi)}{2}\Bigg\},$$

$$\Upsilon = \left[1-\frac{2\mu\alpha(n+1)}{\xi}\right]\left[\Psi''+\frac{\omega_{BD}\Psi'^2}{2\Psi}-\frac{A\Psi'}{\xi}\right]+\frac{\rho_0\mu\Psi'}{2A\xi^2}.$$

The subscript 0 indicates the behavior of respective quantities at the center. The vanishing complexity condition in terms of the new variables is

$$\frac{6\Pi}{n\rho_0}+\frac{2\xi}{n\rho_0}\frac{d\Pi}{d\xi} = \xi\psi^{n-1}\frac{d\psi}{d\xi}+\frac{\xi}{n\rho_0}\frac{dT_0^{\Psi 0}}{d\xi}+\frac{\rho_0\mu A^2}{2\Psi\xi}\frac{d\Psi}{d\xi}+\frac{\xi A^2}{\Psi} \tag{2.1.52}$$

$$\times \quad \left[1-\frac{2\mu\alpha(n+1)}{\xi}\right]\left(\frac{d\Psi}{d\xi}+\frac{A}{2}\frac{d^2\Psi}{d\xi^2}\right), \tag{2.1.53}$$

where

$$\frac{dT_0^{\Psi 0}}{d\xi} = \left[\frac{2\mu\alpha(n+1)}{\xi^2}\right]\left(A^2\frac{d^2\Psi}{d\xi^2}+\frac{A\omega_{BD}}{\Psi}\frac{d\Psi}{d\xi}+\frac{2A^2}{\xi}\frac{d\Psi}{d\xi}\right)$$

$$+ \quad \left[1-\frac{2\mu\alpha(n+1)}{\xi}\right]\left[A^3\frac{d^3\Psi}{d\xi^3}+\frac{2\omega_{BD}A^2}{\Psi}\frac{d\Psi}{d\xi}d^2\Psi d\xi^2-\frac{\omega_{BD}A^2}{\Psi^2}\right.$$

$$\times \quad \left.\left(\frac{d\Psi}{d\xi}\right)^2-\frac{2A^2}{\xi^2}\frac{d\Psi}{d\xi}+2A^3\frac{d^2\Psi}{d\xi^2}\right]+\frac{\rho_0\mu}{2\xi^3}\left(\xi\frac{d^2\Psi}{d\xi^2}-\frac{d\Psi}{d\xi}\right)$$

$$+ \quad \frac{\xi}{2n\rho_0}\frac{dV(\Psi)}{d\Psi}\frac{d\Psi}{d\xi}.$$

The system of four equations (2.1.49)-(2.1.53) in five unknowns ($\Pi,\ \mu,\ \psi,\ \Psi,\ V(\Psi)$) gives us the freedom to fix one of the unknowns. Hence, the solutions of the system will vary according to the choice of $V(\Psi)$. Further, the obtained solutions can be checked for viability and stability through energy conditions and Chandrasekhar technique [108], respectively.

2.2 SBD Field Equations for Non-static Sphere

We consider a collapsing sphere bounded by a hypersurface represented in comoving co-ordinates as

$$ds^2 = -A^2(t,r)dt^2 + B^2(t,r)dr^2 + R^2(t,r)(d\theta^2 + \sin^2\theta d\phi^2). \tag{2.2.1}$$

The energy density, radial/transverse pressures and heat flux (q_γ) of the anisotropic collapsing sphere are specified by the following energy-momentum tensor

$$T^{(m)}_{\gamma\delta} = (\rho + p_\perp)v_\gamma v_\delta + p_\perp g_{\gamma\delta} + (p_r - p_\perp)\mathfrak{s}_\gamma\mathfrak{s}_\delta + q_\gamma v_\delta + v_\gamma q_\delta,$$

where $\mathfrak{s}_\gamma = (0, B, 0, 0)$. The four velocity ($v_\gamma = (-A, 0, 0, 0)$) and heat flux ($q_\gamma = (0, qB, 0, 0)$) obey the following relations

$$v^\gamma v_\gamma = -1, \quad v^\gamma q_\gamma = 0.$$

In order to simplify the calculations, we rewrite the energy-momentum tensor as

$$T^{(m)}_{\gamma\delta} = \rho v_\gamma v_\delta + Ph_{\gamma\delta} + \Pi_{\gamma\delta} + q(\mathfrak{s}_\gamma v_\delta + v_\gamma\mathfrak{s}_\delta). \tag{2.2.2}$$

The field equations are obtained as

$$\frac{1}{\Psi}(A^2\rho - T^\Psi_{00}) = \frac{\dot{R}\left(\frac{2\dot{B}}{B} + \frac{\dot{R}}{R}\right)}{R} - \frac{A^2\left(\frac{R'^2}{R^2} - \frac{2B'R'}{BR} - \frac{B^2}{R^2} + \frac{2R''}{R}\right)}{B^2}, \tag{2.2.3}$$

$$\frac{1}{\Psi}(-qAB + T^\Psi_{01}) = -\frac{2A'\dot{R}}{AR} + \frac{2\dot{B}R'}{BR} - \frac{2\dot{R}'}{R}, \tag{2.2.4}$$

$$\frac{1}{\Psi}(B^2p_r + T^\Psi_{11}) = -\frac{B^2\left(\frac{2\ddot{R}}{R} - \frac{\dot{R}\left(\frac{2\dot{A}}{A} - \frac{\dot{R}}{R}\right)}{R}\right)}{A^2} + \frac{R'\left(\frac{2A'}{A} + \frac{R'}{R}\right)}{R} - \frac{B^2}{R^2}, \tag{2.2.5}$$

$$\frac{1}{\Psi}(R^2p_r + T^\Psi_{22}) = -\frac{R^2\left(-\frac{\dot{A}\left(\frac{\dot{B}}{B} + \frac{\dot{R}}{R}\right)}{A} + \frac{\dot{B}\dot{R}}{BR} + \frac{\ddot{B}}{B(t,r)} + \frac{\ddot{R}}{R}\right)}{A^2}$$

$$+ \quad \frac{R^2\left(\frac{R'}{}\frac{\frac{A'}{A}-\frac{B'}{B}}{R}-\frac{A'B'}{AB}+\frac{A''}{A}+\frac{R''}{R}\right)}{B^2}, \tag{2.2.6}$$

where

$$\begin{aligned}
T^{\Psi}_{00} &= -\dot{\Psi}\left(\frac{2\dot{A}}{A}+\frac{\dot{B}}{B}+\frac{2\dot{R}}{R}\right)+\frac{A^2\Psi'\left(\frac{B'}{B}+\frac{2R'}{R}\right)}{B^2}+\frac{\omega_{BD}\left(\frac{A^2\Psi'^2}{B^2}+\dot{\Psi}^2\right)}{2\Psi}\\
&+ \frac{A^2\Psi''}{B^2}+\frac{1}{2}V(\Psi)A^2,\\
T^{\Psi}_{01} &= -\frac{A'\dot{\Psi}}{A}-\frac{\dot{B}\Psi'}{B}+\frac{\omega_{BD}}{\Psi}\dot{\Psi}\Psi'+\dot{\Psi}',\\
T^{\Psi}_{11} &= -\Psi'\left(\frac{A'}{A}+\frac{2B'}{B}+\frac{2R'}{R}\right)+\frac{B^2\dot{\Psi}\left(\frac{\dot{A}}{A}+\frac{2\dot{R}}{R}\right)}{A^2}+\frac{\omega_{BD}\left(\frac{B^2\dot{\Psi}^2}{A^2}+\Psi'^2\right)}{2\Psi}\\
&+ \frac{B^2\ddot{\Psi}}{A^2}-\frac{1}{2}V(\Psi)B^2,\\
T^{\Psi}_{22} &= -\frac{R^2\Psi'\left(\frac{A'}{A}+\frac{B'}{B}+\frac{R'}{R}\right)}{B^2}+\frac{R^2\dot{\Psi}\left(\frac{\dot{A}}{A}+\frac{\dot{B}}{B}+\frac{\dot{R}}{R}\right)}{A^2}-\frac{\omega_{BD}R^2\left(\frac{\Psi'^2}{B^2}-\frac{\dot{\Psi}^2}{A^2}\right)}{2\Psi}\\
&+ \frac{R^2\ddot{\Psi}}{A^2}-\frac{R^2\Psi''}{B^2}-\frac{1}{2}V(\Psi)R^2.
\end{aligned}$$

Here $\cdot$ denotes derivative with respect to the temporal co-ordinate. The conservation equations corresponding to the anisotropic matter source are expressed as

$$\begin{aligned}
&\dot{T}^{0(\mathrm{eff})}_0+(T^{0(\mathrm{eff})}_0-T^{1(\mathrm{eff})}_1)\frac{\dot{B}}{B}+2(T^{0(\mathrm{eff})}_0-T^{2(\mathrm{eff})}_2)\frac{\dot{R}}{R}+(T^{1(\mathrm{eff})}_0)'\\
&+(T^{1(\mathrm{eff})}_0)(\frac{A'}{A}+\frac{B'}{B}+2\frac{R'}{R})=0, \qquad (2.2.7)\\
&\dot{T}^{1(\mathrm{eff})}_0+(T^{1(\mathrm{eff})}_1)'+T^{1(\mathrm{eff})}_0(\frac{\dot{A}}{A}+\frac{\dot{B}}{B}+2\frac{\dot{R}}{R})-(T^{0(\mathrm{eff})}_0-T^{1(\mathrm{eff})}_1)\frac{A'}{A}\\
&+2(T^{1(\mathrm{eff})}_1-T^{2(\mathrm{eff})}_2)\frac{R'}{R}=0, \qquad (2.2.8)
\end{aligned}$$

whereas the wave equation takes the following form

$$\Box\Psi = \frac{\Psi'\left(\frac{A'}{A}-\frac{B'}{B}+\frac{2R'}{R)}\right)}{B^2}-\frac{\dot{\Psi}\left(\frac{-\dot{A}}{A}+\frac{\dot{B}}{B}+\frac{2\dot{R}}{R}\right)}{A^2}-\frac{\ddot{\Psi}}{A^2}+\frac{\Psi''}{B^2}$$

$$= \frac{1}{3+2\omega_{BD}}\left[-\rho+3P+\left(\Psi\frac{dV(\Psi)}{d\Psi}-2V(\Psi)\right)\right]. \quad (2.2.9)$$

Kinematical quantities (such as four acceleration, expansion scalar and shear tensor) are used to study the motion of cosmic objects. These quantities for the considered setup turn out to be

$$a_1 = \frac{A'}{A}, \quad a^2 = a_\gamma a^\gamma = (\frac{A'}{AB})^2, \quad (2.2.10)$$

$$\vartheta = \frac{1}{A}(\frac{\dot{B}}{B}+2\frac{\dot{R}}{R}), \quad (2.2.11)$$

$$\sigma_{11} = \frac{2}{3}B^2\sigma, \quad \sigma_{22} = -\frac{1}{3}R^2\sigma, \quad (2.2.12)$$

with $a_\gamma = as_\gamma$ and $\sigma = \sqrt{\frac{3}{2}\sigma^{\gamma\delta}\sigma_{\gamma\delta}} = \frac{1}{A}(\frac{\dot{B}}{B}-\frac{\dot{R}}{R})$.

In order to avoid a discontinuity at the junction, the Darmois conditions must be fulfilled. For this purpose, we assume that outgoing radiations are massless as depicted in Vaidya spacetime given by

$$ds^2 = -(1-\frac{2M(\upsilon)}{r})d\upsilon^2 - 2rdrd\upsilon + r^2(d\theta^2+\sin^2\theta d\phi^2),$$

where $M(\upsilon)$ and υ are the total mass and retarded time, respectively. The matching of the two spacetimes is smooth and continuous when $(m(t,r))_\Sigma = (M(\upsilon))_\Sigma$, $(q)_\Sigma = (p_r)_\Sigma$, $(\Psi_-)_\Sigma = (\Psi_+)_\Sigma$, $(\Psi'_-)_\Sigma = (\Psi'_+)_\Sigma$ and $(\dot{\Psi}_-)_\Sigma = (\dot{\Psi}_+)_\Sigma$. We use Misner and Sharp formula for calculating mass of the collapsing model as

$$m = \frac{R}{2}\left[\left(\frac{\dot{R}}{A}\right)^2 - \left(\frac{R'}{B}\right)^2 + 1\right]. \quad (2.2.13)$$

In order to discuss the dynamics of the self-gravitating system, we introduce the proper time and radial derivatives expressed as

$$D_T = \frac{1}{A}\frac{\partial}{\partial t}, \quad D_R = \frac{1}{R'}\frac{\partial}{\partial r}.$$

The velocity of the collapsing fluid in terms of areal radius of the spherical surface within the fluid is defined as $U = D_T R < 0$. The mass and velocity of the sphere are related as

$$E \equiv \frac{R'}{B} = \left(1 + U^2 - \frac{2m}{R}\right)^{\frac{1}{2}}. \tag{2.2.14}$$

Taking proper time and radial derivative of mass leads to

$$D_T m = -\frac{R^2}{2}\left(\frac{T_{11}^{(\text{eff})}}{B^2}U - \frac{T_{01}^{(\text{eff})}}{AB}E\right), \tag{2.2.15}$$

$$D_R m = -\frac{R^2}{2}\left(\frac{T_{00}^{(\text{eff})}}{A^2} + \frac{T_{01}^{(\text{eff})}}{AB}\frac{U}{E}\right), \tag{2.2.16}$$

which imply

$$\frac{3m}{R^3} = -\frac{T_0^{0(\text{eff})}}{2} + \frac{1}{2R^3}\int_0^r R' R^3 (D_R T_0^{0(\text{eff})} - \frac{3T_{01}^{(\text{eff})}}{ABR}\frac{U}{E})dr. \tag{2.2.17}$$

Tidal forces play a significant role in the evolution of a celestial system. The Weyl tensor incorporates the effects of these forces and is expressed as

$$C^{\gamma}_{\alpha\beta\sigma} = \mathcal{R}^{\gamma}_{\alpha\beta\sigma} - \frac{\mathcal{R}^{\gamma}_{\beta}}{2}g_{\alpha\sigma} + \frac{\mathcal{R}_{\alpha\beta}}{2}\delta^{\gamma}_{\sigma} - \frac{\mathcal{R}_{\alpha\sigma}}{2}\delta^{\gamma}_{\beta} + \frac{\mathcal{R}^{\gamma}_{\sigma}}{2}g_{\alpha\beta} + \frac{1}{6}(\delta^{\gamma}_{\beta}g_{\alpha\sigma} + g_{\alpha\beta}\delta^{\gamma}_{\sigma}). \tag{2.2.18}$$

The electric part of the Weyl tensor in the non-static scenario reads

$$E_{\gamma\delta} = C_{\gamma\alpha\delta\beta}v^{\alpha}v^{\beta} = \varepsilon(\mathfrak{s}_{\gamma}\mathfrak{s}_{\delta} + \frac{h_{\gamma\delta}}{3}), \tag{2.2.19}$$

where

$$\varepsilon = \frac{1}{2}\left(\frac{\left(\frac{R'}{R} - \frac{A'}{A}\right)\left(\frac{B'}{B} + \frac{R'}{R}\right) + \frac{A''}{A} - \frac{R''}{R}}{B^2} + \frac{\frac{\ddot{R}}{R} - \frac{\ddot{B}}{B} - \left(\frac{\dot{A}}{A} + \frac{\dot{R}}{R}\right)\left(\frac{\dot{R}}{R} - \frac{\dot{B}}{B}\right)}{A^2} - \frac{1}{R^2}\right). \tag{2.2.20}$$

Moreover, the relation

$$[\varepsilon - \frac{1}{2}(-T_0^{0(\text{eff})} - T_1^{1(\text{eff})} + T_2^{2(\text{eff})})]^{\cdot} = \frac{3\dot{R}}{R}[\frac{1}{2}(-T_0^{0(\text{eff})} + T_2^{2(\text{eff})}) - \varepsilon] - \frac{3R'}{2R}T_0^{1(\text{eff})}), \tag{2.2.21}$$

demonstrates the influence of scalar field on energy density, pressure and Weyl tensor.

2.2.1 Structure Scalars

The Riemann tensor in the current setup is decomposed as

$$\mathcal{R}^{\alpha\delta}_{\beta\gamma}=\mathcal{R}^{\alpha\delta}_{(I)\beta\gamma}+\mathcal{R}^{\alpha\delta}_{(II)\beta\gamma}+\mathcal{R}^{\alpha\delta}_{(III)\beta\gamma}+\mathcal{R}^{\alpha\delta}_{(IV)\beta\gamma}+\mathcal{R}^{\alpha\delta}_{(V)\beta\gamma}, \tag{2.2.22}$$

where $\mathcal{R}^{\alpha\delta}_{(I)\beta\gamma}$, $\mathcal{R}^{\alpha\delta}_{(III)\beta\gamma}$, $\mathcal{R}^{\alpha\delta}_{(IV)\beta\gamma}$ and $\mathcal{R}^{\alpha\delta}_{(V)\beta\gamma}$ are the same as mentioned in Eqs.(2.1.28) and (2.1.30)-(2.1.32) whereas $\mathcal{R}^{\alpha\delta}_{(II)\beta\gamma}$ turns out to be

$$\mathcal{R}^{\alpha\delta}_{(II)\beta\gamma} = \frac{2}{\Psi}\left[\Pi^{[\alpha}_{[\beta}\delta^{\delta]}_{\gamma]}+q\left(v^{[\alpha}\mathfrak{s}_{[\beta}\delta^{\delta]}_{\gamma]}+\mathfrak{s}^{[\alpha}v_{[\beta}\delta^{\delta]}_{\gamma]}\right)\right].$$

Here, we evaluate only $X_{\gamma\delta}$ and $Y_{\gamma\delta}$ as

$$\begin{aligned}
X_{\gamma\delta} &= \frac{1}{\Psi}\left(\frac{\rho h_{\gamma\delta}}{3}+\frac{\Pi_{\gamma\delta}}{2}\right)-E_{\gamma\delta}+\frac{1}{2\Psi}(\Psi_{,\gamma;\mu}h^{\mu}_{\delta}+\frac{\omega_{BD}}{2\Psi}\Psi_{,\gamma}\Psi_{,\mu}h^{\mu}_{\delta}) \\
&+ \frac{h_{\gamma\delta}}{4\Psi}(\Box\Psi+7V(\Psi)), \qquad (2.2.23)\\
Y_{\gamma\delta} &= \frac{1}{\Psi}\left(\frac{(\rho+3P)h_{\gamma\delta}}{6}+\frac{\Pi_{\gamma\delta}}{2}\right)+E_{\gamma\delta}+\frac{1}{2\Psi}(-\Psi_{,\gamma;\delta}-\Psi_{,\gamma;\mu}v_{\delta}v^{\mu} \\
&- \Psi_{,\mu;\delta}v_{\gamma}v^{\mu}+\Psi_{,\alpha;\beta}v_{\alpha}v^{\beta}g_{\gamma\delta})+\frac{\omega_{BD}}{2\Psi^2}(-\Psi_{,\gamma}\Psi_{,\delta}-\Psi_{,\gamma}\Psi_{,\mu}v^{\mu}v_{\delta} \\
&- \Psi_{,\mu}\Psi_{,\delta}v^{\mu}v_{\gamma}-\Psi_{,\alpha}\Psi_{,\beta}v^{\alpha}v^{\beta}g_{\gamma\delta})+\frac{h_{\gamma\delta}}{6\Psi}\left(\frac{\omega_{BD}}{\Psi}\Psi_{,\mu}\Psi^{,\mu}-V(\Psi)\right). \qquad (2.2.24)
\end{aligned}$$

The four structure scalars in the presence of scalar field turn out to be

$$\begin{aligned}
X_T &= X^{(\mathrm{m})}_T+X^{\Psi}_T=\frac{1}{\Psi}(\rho)+\frac{1}{2\Psi}\left(\frac{5}{2}\Box\Psi+\Psi_{,\alpha;\gamma}v^{\alpha}v^{\gamma}+\frac{\omega_{BD}}{2\Psi}(\Psi_{,\alpha}\Psi^{,\alpha}\right. \\
&+ \left.\Psi_{,\gamma}\Psi_{,\alpha}v^{\alpha}v^{\gamma}+\frac{21}{2}V(\Psi)\right), \qquad (2.2.25)\\
X_{TF} &= X^{(\mathrm{m})}_{TF}+X^{\Psi}_{TF}=-\frac{1}{\Psi}(\frac{\Pi}{2}+\varepsilon\Psi)+\frac{1}{2\Psi}\left(\Box\Psi+\Psi_{,\alpha;\gamma}v^{\alpha}v^{\gamma}+\frac{\omega_{BD}}{2\Psi}(\Psi_{,\alpha}\Psi^{,\alpha}\right. \\
&+ \left.\Psi_{,\gamma}\Psi_{,\alpha}v^{\alpha}v^{\gamma})\right), \qquad (2.2.26)\\
Y_T &= Y^{(\mathrm{m})}_T+Y^{\Psi}_T=\frac{1}{2\Psi}(\rho+3p_r-2\Pi)-\frac{1}{2\Psi}\left(\Box\Psi+\Psi_{,\gamma;\alpha}v^{\gamma}v^{\alpha}\right.
\end{aligned}$$

$$+ \quad \frac{\omega_{BD}}{\Psi}(\Psi_{,\gamma}\Psi_{,\alpha}v^{\gamma}v^{\alpha}) + V(\Psi)\Big), \tag{2.2.27}$$

$$Y_{TF} = Y_{TF}^{(\mathrm{m})} + Y_{TF}^{\Psi} = \frac{1}{\Psi}(\varepsilon\Psi - \frac{\Pi}{2}) - \frac{1}{2\Psi}\Big(\Box\Psi + \frac{\omega_{BD}}{\Psi}(\Psi_{,\alpha}\Psi^{,\alpha}$$

$$+ \quad \Psi_{,\gamma}\Psi_{,\beta}v^{\gamma}v^{\beta}) + \Psi_{,\gamma;\mu}v^{\gamma}v^{\mu}\Big). \tag{2.2.28}$$

The above equations indicate that X_T and Y_T govern the total energy density and principal stresses of the system, respectively in the presence of the massive scalar field. Moreover, X_{TF} and Y_{TF} together determine the local anisotropy of the fluid. The impact of anisotropy and inhomogeneity on the evolution of the sphere can be measured through Y_{TF} as

$$Y_{TF} = T_2^{2(\mathrm{eff})} - T_1^{1(\mathrm{eff})} + \frac{1}{2R^3}\int_0^r R'R^3(-D_R T_0^{0(\mathrm{eff})} + \frac{3T_{01}^{(\mathrm{eff})}}{ABR}\frac{U}{E})dr$$

$$+ \quad \left[\frac{\dot{\Psi}}{A^2}(\frac{2\dot{A}}{A} + \frac{3\dot{R}}{R}) - \frac{3\Psi' R'}{B^2 R}\right]. \tag{2.2.29}$$

2.2.2 Complexity and Evolution of the System

In general, the complexity of a cosmic system depends on various physical properties such as anisotropic pressure and inhomogeneous density. The scalar Y_{TF} was chosen as the complexity factor of the static sphere because it incorporated the essential features of the system and determined their effects on Tolman mass (or active gravitational mass). Equation (2.2.29) indicates that Y_{TF} contains the contribution of the significant factors which induce complexity in the current setup. Therefore, we proceed by assuming that the scalar Y_{TF} is the best fit for the complexity factor. Moreover, heat dissipation is an additional factor contributing to the complexity of the dynamical setup. Therefore, it is essential to take into account the pattern of evolution of the system to construct a satisfactory complexity factor. Furthermore, in order to minimize the complexity, we will consider the anisotropic fluid evolving

through the simplest mode of evolution. For this purpose, we identify two patterns of evolution: homologous and homogeneous.

The Homologous Evolution:

The collapse of a celestial body is homologous if the rate at which matter is pulled to the core is the same throughout, i.e., the velocity of the matter falling inward is directly proportional to the radial distance. On the other hand, if density at the center increases rapidly as compared to other regions, then the cosmic object evolves in a non-homologous pattern. In this section, we derive the condition for a homologous collapse. Heat flow can be expressed in terms of shear and expansion scalars through Eqs.(2.2.4) and (2.2.14) as

$$\frac{1}{2E\Psi}\left(q-\frac{T_{01}^{\Psi}}{AB}\right)=\frac{1}{3}D_R(\vartheta-\sigma)-\frac{\sigma}{R}, \tag{2.2.30}$$

which yields

$$D_R\left(\frac{U}{R}\right)=\frac{1}{2E\Psi}\left(q-\frac{T_{01}^{\Psi}}{AB}\right)+\frac{\sigma}{R}. \tag{2.2.31}$$

Integration of the above equation leads to

$$U=R\int_0^r R'\left[\frac{1}{2E\Psi}\left(q-\frac{T_{01}^{\Psi}}{AB}\right)+\frac{\sigma}{R}\right]dr+c(t)R, \tag{2.2.32}$$

where $c(t)=\frac{U_\Sigma}{R_\Sigma}$ is an integration function. If the fluid is non-dissipative and shear-free then the integral in the above equation vanishes providing the necessary condition of homologous evolution $U\sim R$ [109]. Thus, the ratio of areal radii of any two concentric circles must be constant. Assume that R is a separable function of t and r. The homologous condition corresponding to the current setup is

$$\frac{1}{2E\Psi}\left(q-\frac{T_{01}^{\Psi}}{AB}\right)+\frac{\sigma}{R}=0. \tag{2.2.33}$$

The Homogeneous Expansion:

The evolution of a cosmic structure is homogeneous if the rate of expansion or collapse is independent of r. In other words, homogeneous expansion corresponds to $\vartheta' = 0$. Applying this constraint along with Eq.(2.2.30) to (2.2.33) implies

$$D_R\sigma = 0,$$

which leads to $\sigma = 0$ (due to the regularity conditions at the core). Thus, Eq.(2.2.30) yields

$$q = \frac{T_{01}^{\Psi}}{AB}, \tag{2.2.34}$$

i.e., the fluid is dissipative. It must be noted that in GR, a shear-free matter distribution evolving under the condition $\vartheta' = 0$ must also be non-dissipative and consequently, homologous.

2.2.3 Kinematical Variables

In this section, we analyze the behavior of different physical quantities to choose the simplest pattern of evolution. Imposing the homologous condition on Eq.(2.2.30) produces

$$(\vartheta - \sigma)' = \left(\frac{3\dot{R}}{AR}\right)' = 0 \Rightarrow A' = 0.$$

Thus, the homologous fluid is geodesic ($a = 0$) in the current scenario. This implies that homologous pattern can be considered as the simplest mode of evolution. Without loss of generality, we take $A = 1$. Conversely, the geodesic condition produces

$$(\vartheta - \sigma) = \frac{3\dot{R}}{R}.$$

Successive derivatives with respect to r close to the center imply that the fluid is homologous [3].

It must be noted that the counterpart of this structure in GR is shear-free when $q=0$. However, in the presence of scalar field, the non-dissipative as well as homologous fluid is geodesic but not shear-free as

$$\sigma=\frac{RT^{\Psi}_{01}}{2R'}.$$

If the non-dissipative fluid undergoes homogeneous expansion, then Eq.(2.2.34) implies $T^{\Psi}_{01}=0$. Moreover, shear scalar is evaluated from Eq.(2.2.30) as

$$\sigma = \frac{3}{2R^3}\int_0^r \frac{R^3}{A}T^{\Psi}_{01}dr+\frac{g(t)}{R^3}=\frac{g(t)}{R^3},$$

where $g(t)$ is an arbitrary function of integration. Since at the center $R=0$ therefore, $g(t)$ must be zero. It follows that in the non-dissipative case, homogeneous expansion implies homologous evolution (since $T^{\Psi}_{01}=0\Rightarrow\sigma=0\Rightarrow U\sim R$). Conversely, if $\sigma=\frac{RT^{\Psi}_{01}}{2R'}$ then $\vartheta'=(\frac{RT^{\Psi}_{01}}{2R'})'$. Thus, homologous evolution implies homogeneous expansion only if $T^{\Psi}_{01}=0$. In the subsequent sections, we obtain solutions satisfying the conditions for vanishing complexity as well as homologous fluid. For this purpose, we assume an exponential form of the scalar field as $\Psi(t,r)=\Psi(t)=\Psi_0 t^{\beta}$, where β is a constant and Ψ_0 is the present day value of the scalar field.

Case 1: $q=0$

We first consider the non-dissipative case. It is worthwhile to mention here that the homologous fluid for the chosen scalar field satisfies $T^{\Psi}_{01}=0$. Hence, in the non-dissipative case, there is a unique criterion for the simplest evolution (since homologous evolution fulfils the conditions of homogeneous expansion and vice versa).

The homologous condition yields

$$B(t,r)=g_1(r)R(t,r), \tag{2.2.35}$$

where $g_1(r)$ is an arbitrary function of integration. Employing the above relation in the condition of vanishing complexity and wave equation generates the following expressions

$$\begin{aligned}
&V(\Phi)=\frac{\Phi_0 t^{\beta-2}}{g_1(r)^3R^4}\left[2t^2R'\left(g_1(r)R'+g_1'(r)\right)-2t^2g_1(r)RR''+g_1(r)^3R^3\right.\\
&\times\left.\left(t\left(5\beta\dot{R}+4t\ddot{R}\right)+\beta(\beta(\omega_{BD}+2)-2)R\right)+2tg_1(r)^3R^2\dot{R}\left(t\dot{R}+\beta R\right)\right],\\
&\frac{\Phi_0 t^{\beta-1}}{\beta(2\omega_{BD}+3)g_1(r)R}\left[2t^2g_1'(r)\left(-2\beta R'R^2+R\left(R'\left(t\dot{R}+\beta\right)+t\dot{R}'\right)\right.\right.\\
&\left.-\ 4tR'\dot{R}\right)+2t^2g_1(r)\left(R^2\left(\beta R''-t\dot{R}''\right)+t\left(3R''\dot{R}+2R'\dot{R}'\right)R\right.\\
&\left.\left.-\ 4tR'^2\dot{R}\right)+g_1(r)^3R^2\left(-4t^3\dot{R}^3-\beta t^2\left(11\dot{R}^2+2\right)R+tR^2\left(\beta(6\beta\omega_{BD}\right.\right.\right.\\
&\left.\left.\left.+7\beta-7)\dot{R}\ +t\left(5\beta\ddot{R}+4t\dddot{R}\right)\right)+2(\beta-2)\beta(\beta\omega_{BD}+\beta-1)R^3\right)\right]=0.
\end{aligned}$$

A complete solution can be determined for a suitable choice of $g_1(r)$.

Case 2: $q\neq 0$

In the non-dissipative case, the homologous, zero complexity and wave equations, respectively, read

$$\begin{aligned}
&B=g_2(r)\exp\left(\int_1^t\frac{\Psi_0t^\beta R\dot{R}'-R'\dot{R}}{\left(\Psi_0t^\beta-1\right)RR'}\,dt\right),\\
&V(\Psi)=\frac{\Psi_0t^{\beta-2}}{B^3R}\left[2t^2B'R'+2t\dot{B}B^2\left(t\dot{R}+\beta R\right)-2t^2BR''+B^3\left(t\left(5\beta\dot{R}\right.\right.\right.\\
&\left.\left.\left.+\ 4t\ddot{R}\right)+\beta(\beta(\omega_{BD}+2)-2)R\right)\right],\\
&\frac{\Psi_0t^{\beta-1}}{\beta(2\omega_{BD}+3)BR}\left[-6t^3B'\dot{B}RR'+2tB^3\left(-t^2\dot{B}\dot{R}^2+tR\left(\dot{B}\left(t\ddot{R}-\beta\dot{R}\right)\right.\right.\right.
\end{aligned}$$

$$+\ t\ddot{B}\dot{R}\Big)+\beta(\beta\omega_{BD}+\beta-1)\dot{B}R^2\Big)-2t^2B^2\left(R\left(t\dot{B}^2\dot{R}-\beta R''+t\dot{R}''\right)\right.$$
$$+\ \beta\dot{B}^2R^2-\beta R'^2-tR''\dot{R}\Big)+2t^2B\left(R\left(B'\left(t\dot{R}'-\beta R'\right)+t\left(2\dot{B}R''\right.\right.\right.$$
$$+\ \left.\left.\left.\dot{B}'R'\right)\right)-tB'R'\dot{R}\Big)+B^4\left(t^2\left(-\left(7\beta\dot{R}^2+4t\ddot{R}\dot{R}+2\beta\right)\right)+tR\,(\beta\right.$$
$$\times\ (4\beta\omega_{BD}+5\beta-5)\dot{R}+t\left(5\beta\ddot{R}+4t\dddot{R}\right)\Big)+2(\beta-2)\beta(\beta\omega_{BD}+\beta$$
$$\left.-1)R^2)\right]=0,$$

where $g_2(r)$ is an integration function. The above system of equations provide a solution corresponding to an appropriate form of $g_2(r)$ for $\Psi(t,r)=\Psi(t)=\Psi_0t^\beta$.

2.2.4 Stability of $Y_{TF}=0$ Condition

In this section, we examine whether the state of zero complexity can prevail throughout the evolution of homologous matter distribution for $\Psi(t,r)=\Psi(t)=\Psi_0t^\beta$. The evolution of the complexity factor is obtained through Eqs.(2.2.7) and (2.2.21) as

$$\dot{Y}_{TF}+\frac{\dot{\Pi}}{\Psi}+\frac{3\dot{R}}{R}Y_{TF}+(\rho+P_r)\frac{\sigma}{2\Psi}+\frac{1}{2B\Psi}(q'-\frac{qR'}{R})+\frac{2\Pi\dot{R}}{R\Psi}+S_1=0, \quad (2.2.36)$$

where the term S_1, containing the effects of scalar field, is given as

$$\begin{aligned}S_1 &= \frac{(T_1^{1\Psi}-T_2^{2\Psi})^{\cdot}}{2\Psi}-\frac{(T_0^{1\Psi})'}{\Psi}-\frac{(T_0^{1\Psi})'}{2\Psi}(\frac{B'}{B}-\frac{R'}{R})-\frac{(T_0^{0\Psi}-T_1^{1\Psi})\dot{B}}{2B\Psi}\\ &- \frac{5(T_0^{0\Psi}-T_2^{2\Psi})\dot{R}}{2R\Psi}-\dot{Y}_{TF}^{\Psi}-Y_{TF}.\end{aligned}$$

In the non-dissipative scenario, we assume that $q=\Pi=\sigma=Y_{TF}=0$ at $t=0$ which leads to the following forms of Eq.(2.2.36) and its derivative with respect to t

$$S_1 = -(\dot{Y}_{TF}+\dot{\Pi}), \quad (2.2.37)$$
$$\ddot{Y}_{TF}+\frac{\ddot{\Pi}}{\Psi}-\frac{\dot{\Pi}\dot{\Psi}}{\Psi^2} = 3S_1-\dot{S}_1+\frac{\dot{\Pi}\dot{R}}{R\Psi}. \quad (2.2.38)$$

Employing the above relations, the first and second t-derivatives of Eq.(2.2.29) can be written as

$$\begin{aligned} S_1+3\left(\frac{\dot{\Psi}\dot{R}}{R}\right)^{\cdot} &= \frac{\partial}{\partial t}\left(\int_0^r R^3(T_0^{0(\mathrm{eff})})'dr\right), \\ 3S_1-\dot{S}_1+\frac{\dot{\Pi}\dot{R}}{R\Psi}-3\left(\frac{\dot{\Psi}\dot{R}}{R}\right)^{\cdot\cdot} &= \frac{\partial^2}{\partial t^2}\left(\int_0^r -R^3(T_0^{0(\mathrm{eff})})'dr\right). \end{aligned}$$

We can proceed in the same manner and calculate the higher derivatives of Eq.(2.2.29). It is noted that the stability of vanishing complexity depends on state determinants (pressure and energy density) as well as the massive scalar field. Thus, anisotropy and inhomogeneity in pressure and energy density, respectively induce complexity in the system. For the general case, i.e., when $q \neq 0$, it can be clearly deduced from Eq.(2.2.36) that heat dissipation is an additional factor influencing the $Y_{TF}=0$ condition.

Chapter 3

Cosmological Solution through Gravitational Decoupling in SBD Gravity

The focus of this chapter is to derive an anisotropic extension of FLRW metric through decoupling in the framework of SBD theory. The radial deformation decouples the system of field equations into two arrays. We use FLRW universe model to obtain a solution of the system governed by the isotropic matter source. For this purpose, power-law models of the scale factor as well as massive scalar field are assumed while isotropic pressure and density are related via barotropic equation of state. Finally, we investigate the physical behavior, viability and stability of the extended FLRW solution for different values of the EoS parameter.

This chapter is organized as follows. In section **3.1**, we formulate the field equations after inducing anisotropy in the matter. Section **3.2** gives an overview of MGD formalism in a non-static setup. The resulting anisotropic spacetime is inspected for viability as well as stability in section **3.3**. The results of this chapter have been published in the form of a research paper [110].

3.1 SBD Field Equations for Non-static Sphere with Additional Matter Source

The action of SBD theory (with $8\pi G_0 = 1$) in the presence of an additional source is

$$S = \int \sqrt{-g}(\mathcal{R}\Psi - \frac{\omega_{BD}}{\Psi}\nabla^{\gamma}\nabla_{\gamma}\Psi - V(\Psi) + L_m + \varrho L_{\Theta})d^4x, \tag{3.1.1}$$

where L_{Θ} represents the Lagrangian density of the new anisotropic source. The field equations and wave equation corresponding to the above action are, respectively, given as

$$G_{\gamma\delta} = T^{(\text{eff})}_{\gamma\delta} = \frac{1}{\Psi}(T^{(m)}_{\gamma\delta} + \varrho\Theta_{\gamma\delta} + T^{\Psi}_{\gamma\delta}), \tag{3.1.2}$$

$$\Box\Psi = \frac{g^{\gamma\delta}T^{(m)}_{\gamma\delta} + \varrho g^{\gamma\delta}\Theta_{\gamma\delta}}{3+2\omega_{BD}} + \frac{1}{3+2\omega_{BD}}(\Psi\frac{dV(\Psi)}{d\Psi} - 2V(\Psi)). \tag{3.1.3}$$

The energy-momentum tensor $T^{(m)}_{\gamma\delta}$ describes the perfect fluid distribution in terms of density and isotropic pressure as

$$T^{(m)}_{\gamma\delta} = (\rho + p)v_{\gamma}v_{\delta} - pg_{\delta\gamma}. \tag{3.1.4}$$

We assume a non-static spherical system that corresponds to the following line-element

$$ds^2 = e^{\lambda(t,r)}dt^2 - e^{\chi(t,r)}dr^2 - C^2(t,r)(d\theta^2 + \sin^2\theta d\phi^2). \tag{3.1.5}$$

The corresponding SBD field equations incorporating the new source are

$$\begin{aligned}\frac{\rho + \varrho\Theta^0_0 + T^{0\Psi}_0}{\Psi} &= \frac{e^{-\lambda}}{C}\left(\dot{C}\dot{\chi} + \frac{\dot{C}^2}{C}\right) - \frac{e^{-\chi}}{C}\left(2C'' - C'\chi' + \frac{C'^2}{C}\right) \\ &+ \frac{1}{C^2}, \\ \frac{p - \varrho\Theta^1_1 - T^{1\Psi}_1}{\Psi} &= \frac{e^{-\chi}}{C}\left(C'\lambda' + \frac{C'^2}{C}\right) - \frac{e^{-\lambda}}{C}\left(2\ddot{C} - \dot{C}\dot{\lambda} + \frac{\dot{C}^2}{C}\right) - \frac{1}{C^2},\end{aligned} \tag{3.1.6}$$

(3.1.7)

$$\frac{p-\varrho\Theta_2^2-T_2^{2\Psi}}{\Psi} = e^{-\chi}\left(\frac{C'\left(\lambda'-\chi'\right)}{2C}+\frac{C''}{C}-\frac{\chi'\lambda'}{4}+\frac{\lambda'^2}{4}+\frac{\lambda''}{2}\right)$$

$$- e^{-\lambda}\left(-\frac{\dot{C}\left(\dot{\lambda}-\dot{\chi}\right)}{2C}+\frac{\ddot{C}}{C}-\frac{\dot{\chi}\dot{\lambda}}{4}+\frac{\dot{\chi}^2}{4}+\frac{\ddot{\chi}}{2}\right), \tag{3.1.8}$$

$$\frac{1}{\Psi}(\varrho\Theta_1^0+T_1^{0\Psi}) = e^{-\lambda}\left(-\frac{C'\dot{\chi}}{C}-\frac{\dot{C}\lambda'}{C}+\frac{2\dot{C}'}{C}\right), \tag{3.1.9}$$

where

$$\begin{aligned}
T_0^{0\Psi} &= -e^{-\lambda}\dot{\Psi}\left(\frac{2\dot{C}}{C}+\frac{\dot{\chi}}{2}+\frac{\dot{\lambda}}{2}\right)+e^{-\chi}\Psi'\left(\frac{2C'}{C}+\frac{\chi'}{2}\right)+\frac{\omega_{BD}}{2\Psi}\left(e^{-\chi}\Psi'^2\right.\\
&+ \left.e^{-\lambda}\dot{\Psi}^2\right)+e^{-\chi}\Psi''-\frac{V(\Psi)}{2},\\
T_1^{1\Psi} &= e^{-\chi}\Psi'\left(\frac{2C'}{C}+\chi'+\frac{\lambda'}{2}\right)-e^{-\lambda}\dot{\Psi}\left(\frac{2\dot{C}}{C}+\frac{\dot{\lambda}}{2}\right)-\frac{\omega_{BD}}{2\Psi}\left(e^{-\chi}\Psi'^2\right.\\
&+ \left.e^{-\lambda}\dot{\Psi}^2\right)-e^{-\lambda}\ddot{\Psi}-\frac{V(\Psi)}{2},\\
T_2^{2\Psi} &= e^{-\chi}\Psi'\left(\frac{C'}{C}+\frac{\chi'}{2}+\frac{\lambda'}{2}\right)-e^{-\lambda}\dot{\Psi}\left(\frac{\dot{C}}{C}+\frac{\dot{\chi}}{2}+\frac{\dot{\lambda}}{2}\right)-\frac{\omega_{BD}}{2\Psi}\left(e^{-\lambda}\dot{\Psi}^2\right.\\
&- \left.e^{-\chi}\Psi'^2\right)+e^{-\chi}\Psi''-e^{-\lambda}\ddot{\Psi}-\frac{V(\Psi)}{2},\\
T_1^{0\Psi} &= e^{-\lambda}\left(-\frac{\dot{\chi}\Psi'}{2}-\frac{\lambda'\dot{\Psi}}{2}+\frac{\omega_{BD}\Psi'\dot{\Psi}}{\Psi}+\dot{\Psi}'\right).
\end{aligned}$$

The wave equation (3.1.3) for the considered non-static scenario is

$$\begin{aligned}
\Box\Psi &= e^{-\lambda}\left[\left(\frac{2\dot{C}}{C}+\frac{\dot{\chi}}{2}+\frac{\dot{\lambda}}{2}\right)\dot{\Psi}+\ddot{\Psi}\right]-e^{-\chi}\left[\left(\frac{2C'}{C}+\frac{\chi'}{2}+\frac{\lambda'}{2}\right)\Psi'+\Psi''\right]\\
&= \frac{1}{3+2\omega_{BD}}\left[g^{\gamma\delta}T_{\gamma\delta}^{(m)}+g^{\gamma\delta}\Theta_{\gamma\delta}+\left(\Psi\frac{dV(\Psi)}{d\Psi}-2V(\Psi)\right)\right].
\end{aligned} \tag{3.1.10}$$

For $\Theta_2^2-\Theta_1^1\neq 0$, Eqs.(3.1.6)-(3.1.10) correspond to an anisotropic fluid.

3.2 Gravitational Decoupling via MGD Approach

In this section, we apply the MGD approach to reduce the degrees of freedom in the system (3.1.6)-(3.1.10). Currently, these independent equations contain ten unknowns: $\lambda(t,r),\ \chi(t,r),\ \rho,\ p,\ \Theta_0^0,\ \Theta_1^0,\ \Theta_1^1,\ \Theta_2^2,\ \Psi,\ V(\Psi)$. The MGD technique splits the system of field equations into two sets through the following geometric deformation in the radial metric component

$$e^{-\chi(t,r)} \mapsto e^{-\xi(t,r)}(1+\varrho g(t,r)), \tag{3.2.1}$$

whereas the temporal metric potential remains unaffected. It is worthwhile to mention here that the transformation proposed by Ovalle [25] is suitable for static sources only and does not successfully decouple the non-static field equations. For $\varrho=0$, the effects of anisotropy are excluded and a system representing isotropic configuration is obtained as

$$\begin{aligned}
\rho &= \frac{1}{2}\Bigg(\frac{e^{-\lambda}\dot{\Psi}\left(4\dot{C}+C\left(\dot{\lambda}+\dot{\xi}\right)\right)}{C}+\frac{2\Psi}{C^2}\Big(\dot{C}e^{-\lambda}\left(\dot{C}+C\dot{\xi}\right)-e^{-\xi}\left(-CC'\xi'\right.\\
&+ \left.C'^2+2CC''\right)+1\Big)-\frac{e^{-\xi}\Psi'\left(4C'+C\xi'\right)}{C}-\frac{\omega_{BD}\left(e^{-\lambda}\dot{\Psi}^2+e^{-\xi}\Psi'^2\right)}{\Psi}\\
&- 2e^{-\xi}\Psi''+V(\Psi)\Big), \qquad (3.2.2)\\
p &= \frac{1}{2}\Bigg(\frac{e^{-\xi}\Psi'\left(4C'+C\left(\lambda'+2\xi'\right)\right)}{C}+\frac{2\Psi}{C^2}\Big(C'e^{-\xi}\left(C'+C\lambda'\right)-e^{-\lambda}\Big(2C\ddot{C}\\
&+ \dot{C}^2-C\dot{C}\dot{\lambda}\Big)-1\Big)-\frac{e^{-\lambda}\dot{\Psi}\left(4\dot{C}+C\dot{\lambda}\right)}{C}-\frac{\omega_{BD}\left(e^{-\lambda}\dot{\Psi}^2+e^{-\xi}\Psi'^2\right)}{\Psi}\\
&- 2e^{-\lambda}\ddot{\Psi}-V(\Psi)\Big), \qquad (3.2.3)\\
p &= \frac{1}{4}\Bigg(\frac{2e^{-\xi}\Psi'\left(2C'+C\left(\lambda'+\xi'\right)\right)}{C}-\frac{2e^{-\lambda}\dot{\Psi}\left(2\dot{C}+C\left(\dot{\lambda}+\dot{\xi}\right)\right)}{C}\\
&+ \frac{\Psi e^{-\lambda-\xi}}{C}\Big(2C'e^{\lambda}\left(\lambda'-\xi'\right)+2\Big(e^{\xi}\Big(\dot{C}\left(\dot{\lambda}-\dot{\xi}\right)-2\ddot{C}\Big)+2C''e^{\lambda}\Big)
\end{aligned}$$

$$+ \quad C\left(-e^{\lambda}\lambda'\xi' + e^{\xi}\left(\dot{\lambda}\dot{\xi} - \dot{\xi}^2 - 2\ddot{\xi}\right) + e^{\lambda}\lambda'^2 + 2e^{\lambda}\lambda''\right)\Big) + \frac{2\omega_{BD}}{\Psi}\left(e^{-\xi}\Psi'^2\right.$$

$$- \quad \left.e^{-\lambda}\dot{\Psi}^2\right) - 4e^{-\lambda}\ddot{\Psi} + 4e^{-\xi}\Psi'' - 2V(\Psi)\Big), \tag{3.2.4}$$

$$0 \quad = \quad \frac{-2\Psi\left(\dot{C}\lambda' + C'\dot{\xi} - 2\dot{C}'\right)}{C} + \Psi\left(\lambda'\dot{\Psi} + \dot{\xi}\Psi' - 2\dot{\Psi}'\right) - \frac{2\omega_{BD}}{\Psi}\Psi'\dot{\Psi}. \tag{3.2.5}$$

The six unknowns $(\lambda(t,r),\ \xi(t,r),\ \rho,\ p, \Psi,\ V(\Psi))$ involved in the above system can be determined through a known isotropic solution in SBD gravity. On the other hand, the anisotropic effects of the extra source $\Theta_{\gamma\delta}$ appear in the second set as

$$\Theta_0^0 \quad = \quad \frac{1}{2C^2}\left(e^{-\xi}\left(Cg'\left(C\Psi' - 2C'\Psi\right) - g\left(C\left(\Psi'\left(4C' + C\xi'\right) + 2C\Psi''\right) + 2\Psi\right.\right.\right.$$

$$\times \quad \left.\left.\left.\left(C'^2 - CC'\xi' + 2CC''\right) + \frac{\omega_{BD}C^2\Psi'^2}{\Psi}\right)\right) - \frac{\dot{g}e^{-\lambda}\frac{d\left(\Psi C^2\right)}{dt}}{\varrho g + 1}\right), \tag{3.2.6}$$

$$\Theta_1^1 \quad = \quad -\frac{e^{-\xi}}{2C^2}\left(C\Psi'\left(g\left(4C' + C\left(\lambda' + 2\xi'\right)\right) - 2Cg'\right) + 2C'g\Psi\left(C' + C\lambda'\right)\right.$$

$$- \quad \left.\frac{\omega_{BD}}{\Psi}C^2g\Psi'^2\right), \tag{3.2.7}$$

$$\Theta_2^2 \quad = \quad -\frac{1}{4C}\left(e^{-\lambda}\left(\dot{g}\left(\Psi\frac{\left(2\dot{C}(\varrho g+1) - C\left(3\varrho\dot{g} + (\varrho g+1)\left(\dot{\lambda} - 2\dot{\xi}\right)\right)\right)}{(\varrho g+1)^2}\right.\right.\right.$$

$$+ \quad \left.\left.\left.\frac{2C\dot{\Psi}}{(\varrho g+1)}\right) + \frac{2C\ddot{g}\Psi}{(\varrho g+1)}\right) + \frac{e^{-\xi}}{\Psi}\left(2\Psi\left(\Psi'\left(g\left(2C' + C\left(\lambda' + \xi'\right)\right)\right.\right.\right.$$

$$- \quad \left.\left.\left.Cg'\right) + 2Cg\Psi''\right) + \Psi^2\left(2C'\left(g' + g\left(\lambda' - \xi'\right)\right) + 4C''g + C\left(\lambda'\left(g'\right.\right.\right.\right.$$

$$+ \quad \left.\left.\left.\left.g\left(\lambda' - \xi'\right)\right) + 2g\lambda''\right)\right) + 2\omega_{BD}Cg\Psi'^2\right)\Big), \tag{3.2.8}$$

$$\Theta_1^0 \quad = \quad \frac{\dot{g}\left(C\Psi' - 2C'\Psi\right)}{C(\varrho g+1)}. \tag{3.2.9}$$

As the second system has five $(g(t,r),\ \Theta_0^0,\ \Theta_1^0,\ \Theta_1^1,\ \Theta_2^2)$ undetermined variables, it is often solved by imposing either an EoS or a mimic constraint (such as $p = \Theta_1^1$).

3.3 Anisotropic FLRW Solution

In this section, we formulate anisotropic cosmological model by assuming that the isotropic sector represents a homogeneous universe described by the FLRW metric given in Eq.(1.3.1). The functions $\lambda,\ \xi$ and C, in relation to FLRW spacetime, are defined as

$$e^{\lambda(t,r)} = 1, \quad e^{\xi(t,r)} = \frac{a^2(t)}{1-kr^2}, \quad C(t,r) = a(t)r. \tag{3.3.1}$$

Setting $\Psi(t,r) = \Psi(t)$, Eqs.(3.2.2)-(3.2.4) reduce to

$$\rho = \frac{6\Psi^2\left(\dot{a}^2+k\right)+6a\dot{a}\Psi\dot{\Psi}+a^2\left(\Psi V(\Psi)-\omega_{BD}\dot{\Psi}^2\right)}{2a^2\Psi}, \tag{3.3.2}$$

$$p = \frac{2\Psi^2\left(\dot{a}^2+k\right)+4a\Psi\frac{d(\Psi\dot{a})}{dt}+a^2\left(\Psi V(\Psi)+2\Psi\ddot{\Psi}+\omega_{BD}\dot{\Psi}^2\right)}{-2a^2\Psi}, \tag{3.3.3}$$

while Eq.(3.2.5) identically equals to zero. The wave equation for the FLRW metric is

$$\frac{3\dot{a}\Psi'}{a}+\Psi'' = \frac{\rho-3p}{2\omega_{BD}+3}+\frac{2V(\Psi)-\Psi\frac{dV(\Psi)}{d\Psi}}{2\omega_{BD}+3}. \tag{3.3.4}$$

The system (3.3.2)-(3.3.4) obeys the conservation equation

$$\dot{\rho}+3\frac{\dot{a}}{a}(p+\rho)=0.$$

As there are three independent equations and six unknowns ($a(t),\ \Psi(t),\ \rho,\ p,$ $\omega_{BD},\ V(\Psi)$), we apply the EoS (1.5.1).

In order to completely determine the isotropic solution we choose power-law functional forms of the scale factor and massive scalar field as

$$a(t) = a_0 t^{\alpha}, \quad \Psi(t) = \Psi_0 t^{\beta}, \tag{3.3.5}$$

where a_0 is the present value of scale factor. Moreover, $\alpha > 0$ and β are constants. Similar power-law forms have been used in literature to study the phenomenon of expanding universe in the framework of SBD gravity [48, 111]. The potential function and coupling parameter corresponding to the above ansatz are, respectively, evaluated through evolution equation and EoS as

$$\begin{aligned} V(\Psi) &= (4a_0^2)^{-1}[\Psi_0 t^{\beta-2(\alpha+1)}\left(a_0^2 t^{2\alpha}\left(6\alpha(\beta\omega_{BD}+1)-12\alpha^2+(\beta-2)\beta\omega_{BD}\right)\right. \\ &- \left. 6kt^2\right)], \qquad (3.3.6) \\ \omega_{BD} &= [2t^{-2\alpha}\left(a_0^2 t^{2\alpha}\left(6\alpha^2(\varsigma+1)+\alpha(4\beta(3\varsigma+2)+3\varsigma-5)+4(\beta^2-\beta)\right)\right. \\ &+ \left.(9\varsigma+1)kt^2\right)]\left(a_0^2\beta(3\beta\varsigma-6\alpha(\varsigma+1)-5\beta+2\varsigma+2)\right)^{-1}. \qquad (3.3.7) \end{aligned}$$

As the coupling parameter is constant in the context of SBD theory, therefore the analysis of anisotropic FLRW cosmos is valid for $k = 0$ only. The setup corresponding to the additional source is re-written in terms of FLRW metric as

$$\begin{aligned} \Theta_0^0 &= \frac{1}{2(ra)^2}\left(2\Psi\left(r\left(kr^2-1\right)g'+\left(3kr^2-1\right)g\right)-\frac{r^2\dot{g}\frac{d}{dt}(a^2\Psi)}{\varrho g+1}\right), \qquad (3.3.8) \\ \Theta_1^1 &= \frac{\left(kr^2-1\right)\Psi g}{r^2a^2}, \qquad (3.3.9) \\ \Theta_2^2 &= \frac{1}{4ra}\left(\frac{2\Psi\left(\left(kr^2-1\right)g'+2krg\right)}{a}-r\left(\Psi\left(\frac{6\dot{a}\dot{g}}{(\varrho g+1)}+a\left(\frac{2\ddot{g}}{(\varrho g+1)}\right.\right.\right.\right. \\ &- \left.\left.\left.\left.\frac{3\varrho\dot{g}^2}{(\varrho g+1)^2}\right)\right)+\frac{2a\dot{\Psi}\dot{g}(\varrho g+1)}{(\varrho g+1)^2}\right)\right), \qquad (3.3.10) \\ \Theta_1^0 &= \frac{\Psi\dot{g}}{\varrho rg+r}, \qquad (3.3.11) \end{aligned}$$

with the conservation equation

$$\frac{d}{dt}\left(\frac{\Theta_0^0}{\Psi}\right)+\frac{\dot{a}}{a\Psi}(3\Theta_0^0-\Theta_1^1-2\Theta_2^2)=0. \qquad (3.3.12)$$

It is noteworthy to mention here that perfect fluid and extra source cannot exchange matter between them as they are individually conserved.

The field equations representing the extension of FLRW to anisotropic domain are expressed through a combination of isotropic and additional sources as

$$G_0^0 = \rho + \varrho\Theta_0^0, \tag{3.3.13}$$

$$G_1^1 = p_r = p + \varrho\Theta_1^1, \tag{3.3.14}$$

$$G_2^2 = p_\perp = p + \varrho\Theta_2^2, \tag{3.3.15}$$

$$G_1^0 = 0 = \Theta_1^0. \tag{3.3.16}$$

Equations (3.3.11) and (3.3.16) imply $\dot{g} = 0$ leading to the following relation between components of Θ_δ^γ

$$\Theta_0^0 = \Theta_1^1 + 2\Theta_2^2.$$

Employing the above equation in the conservation equation (3.3.12) yields the following decoupling function

$$g(r) = \frac{c_1}{r\left(1 - kr^2\right)} - \frac{c_2^2 r^2}{3\left(1 - kr^2\right)}, \tag{3.3.17}$$

where c_1 and c_2 are constants of dimensions L and $\frac{1}{L^2}$, respectively (L is the dimension of length).

In the subsequent subsections, we investigate the salient characteristics of the anisotropic flat FLRW cosmos corresponding to different values of ϱ. For this purpose, we set $c_1 = 1$ and $c_2 = 0.0001$. Figure **3.1** shows that $g(r)$ is negative throughout its domain for the chosen values of the constants. The current values of the scale factor and scalar field are normalized to 1. Recent observations show that the range of the deceleration parameter ($\mathfrak{q} = \frac{-\ddot{a}a}{\dot{a}^2}$) is [-1,0] [112] which implies that $\alpha > 1$. Furthermore, β measures the change in the scalar field with time and must be greater than zero for the expanding cosmos. Thus, we choose $\alpha = 1.1$ and $\beta = 0.2$ to analyze graphically different phases of the universe for $\varrho = 0.1,\ 0.5$.

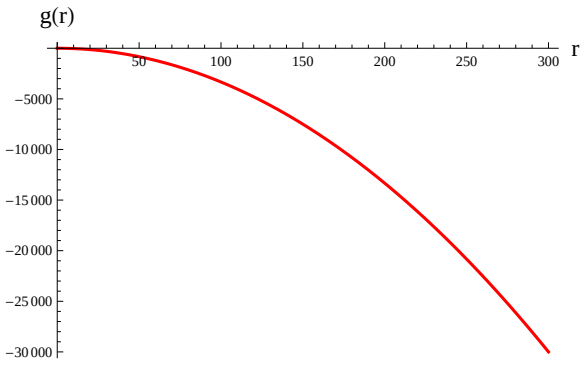

Figure 3.1: Behavior of $g(r)$ for $k = 0,\ c_1 = 1$ and $c_2 = 0.0001$.

3.3.1 Massless Scalar Field Dominated Era

When $\varsigma = 1$, the energy within the cosmos is purely kinetic. A scalar field is responsible for the inflation of spacetime at 10^{-32} seconds after the big bang. Figure **3.2** shows that the density of this anisotropic model decreases with respect to cosmic time corresponding to the expansion of the universe. The pressure components are positive and decrease as ϱ increases from 0.1 to 0.5. Moreover, the anisotropy is negative indicating $p_r > p_\perp$.

The viability of the developed model is checked through four energy conditions defined in Eqs.(1.9.4)-(1.9.7). If the cosmological model is consistent with SEC and DEC then the first two conditions are automatically satisfied. Thus, we will check viability of the anisotropic model via last two conditions only. The plots in Figure **3.3** indicate that the scalar field is consistent with the energy bounds. In order to examine the stability of the universe represented by the anisotropic FLRW spacetime, the criteria of causality condition is employed. Figure **3.4** confirms that the extension of FLRW is stable corresponding to $\varsigma = 1$.

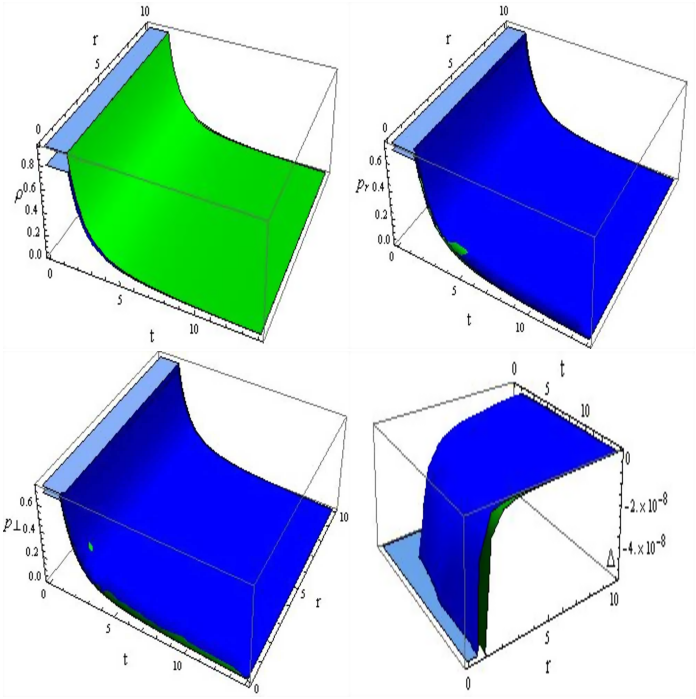

Figure 3.2: Plots of ρ, p_r and $p_\perp$ of anisotropic FLRW solution with $\varsigma = 1$ for $\varrho = 0.1$ (blue) and 0.5 (green).

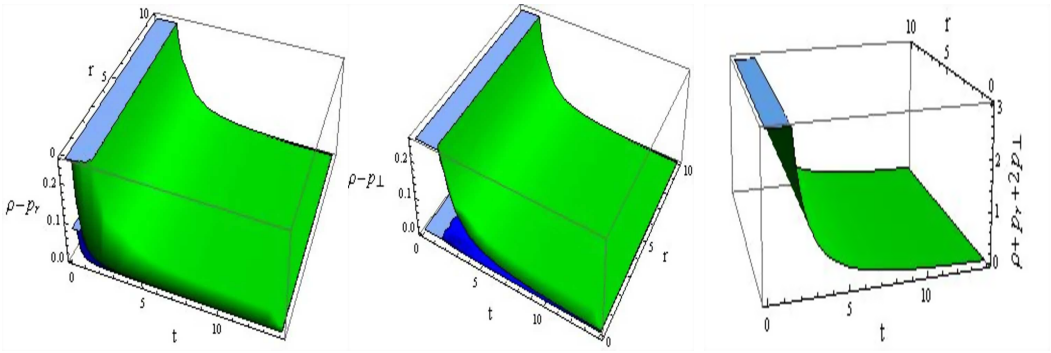

Figure 3.3: Energy conditions with $\varsigma = 1$ for $\varrho = 0.1$ (blue) and 0.5 (green).

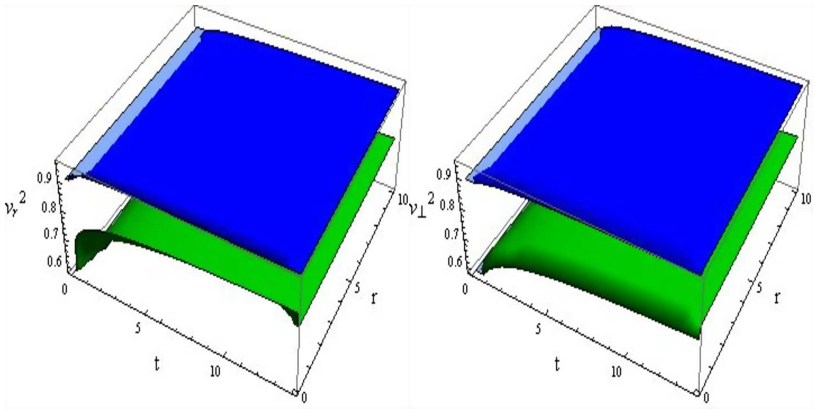

Figure 3.4: Plots of v_r^2 and $v_\perp^2$ with $\varsigma = 1$ for $\varrho = 0.1$ (blue) and 0.5 (green).

3.3.2 Radiation-Dominated Era

During this phase, the pressure is approximately equal to one-third of the total density and the cosmos is dominated by matter composed of relativistic particles (photons and neutrinos). In this era, momentum is larger as compared to mass within the universe. The behavior of density and pressure components corresponding to this cosmic model is presented in Figure **3.5**. The rapid decrease in density with time suggests that the universe is in expansion mode. A higher value of the decoupling parameter correlates with a more dense cosmos but pressure decreases as the decoupling parameter attains higher values. Negative anisotropy indicates that more pressure is exerted in the radial direction as compared to the transverse direction. The cosmic model is consistent with all the energy conditions (Figure **3.6**) and the stability criterion (Figure **3.7**). Thus, the extended solution represents a viable and stable spacetime for $\varsigma = 1/3$.

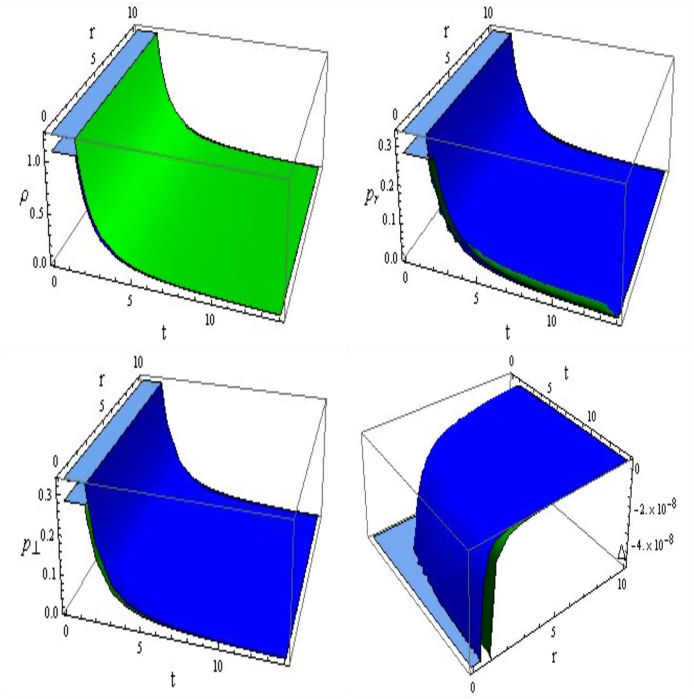

Figure 3.5: Plots of ρ, p_r and $p_\perp$ of anisotropic FLRW solution with $\varsigma = 1/3$ for $\varrho = 0.1$ (blue) and 0.5 (green).

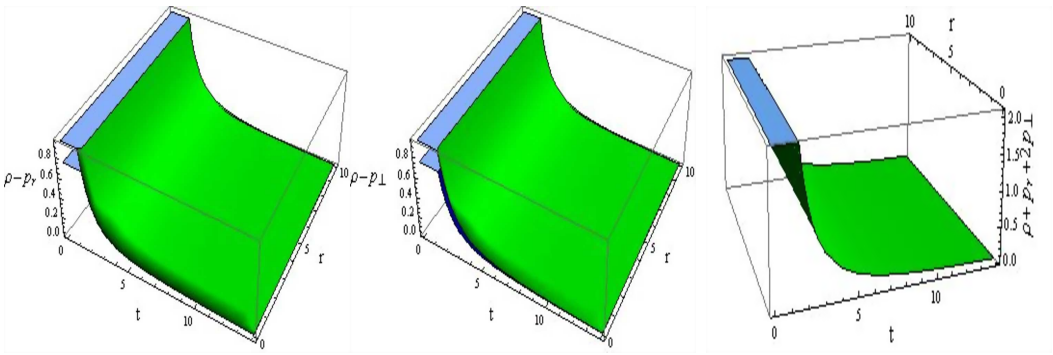

Figure 3.6: Energy conditions with $\varsigma = 1/3$ for $\varrho = 0.1$ (blue) and 0.5 (green).

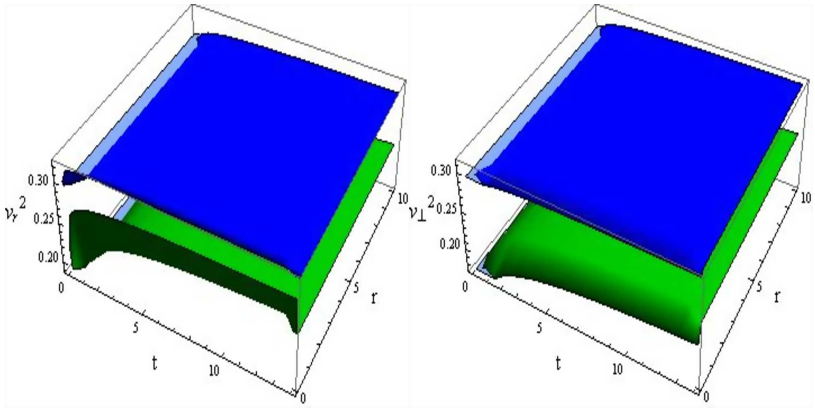

Figure 3.7: Plots of v_r^2 and $v_\perp^2$ with $\varsigma = 1/3$ for $\varrho = 0.1$ (blue) and 0.5 (green).

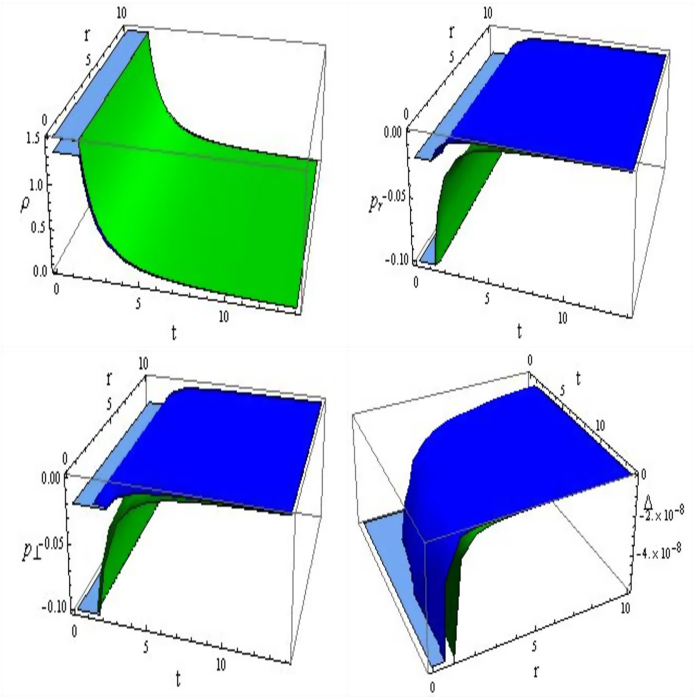

Figure 3.8: Plots of ρ, p_r and $p_\perp$ of anisotropic FLRW solution with $\varsigma = 0$ for $\varrho = 0.1$ (blue) and 0.5 (green).

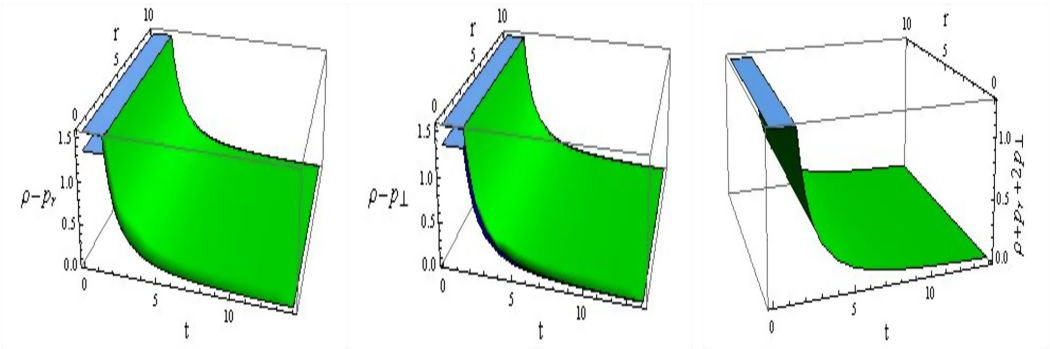

Figure 3.9: Energy conditions with $\varsigma = 0$ for $\varrho = 0.1$ (blue) and 0.5 (green).

3.3.3 Matter-Dominated Era

The constituent particles of the universe in the matter-dominated era are non-relativistic (baryons), i.e., their kinetic energy is smaller as compared to the mass energy. The matter encompassing all the non-relativistic elementary particles is also dubbed as dust. Plots of corresponding matter variables are presented in Figure **3.8**. Energy density is directly proportional to the decoupling parameter and follows a decreasing trend in relation to time. From the barotropic EoS, it is noted that pressure is negligible in the isotropic case ($\varrho = 0$). However, plots in Figure **3.8** indicate the presence of negative pressure (in radial/transverse directions) which approaches to zero as time progresses. The anisotropic solution is compatible with the energy constraints as shown in Figure **3.9**. However, the causality condition, presented in Figure **3.10** is violated for $\varsigma = 0$.

3.3.4 Vacuum Energy Dominated Era

This era is the last of the four phases of the known universe. Matter density decreases in comparison to vacuum energy (also referred to as dark energy) and the universe

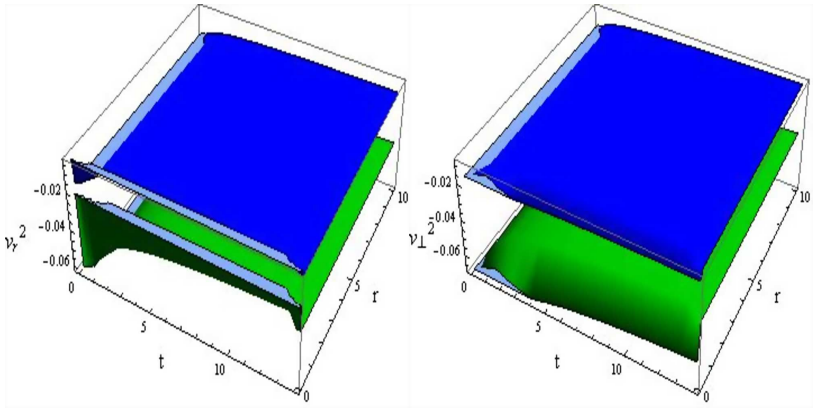

Figure 3.10: Plots of v_r^2 and $v_\perp^2$ with $\varsigma = 0$ for $\varrho = 0.1$ (blue) and 0.5 (green).

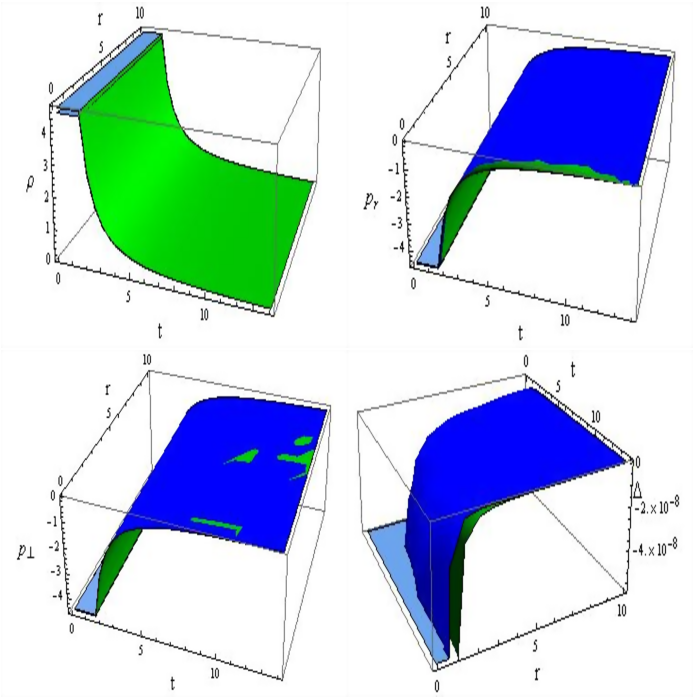

Figure 3.11: Plots of ρ, p_r and $p_\perp$ of anisotropic FLRW solution with $\varsigma = -1$ for $\varrho = 0.1$ (blue) and 0.5 (green).

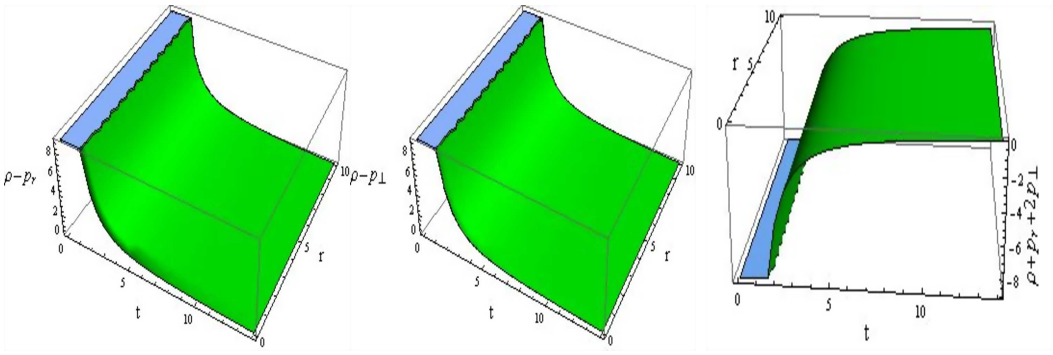

Figure 3.12: Energy conditions with $\varsigma = -1$ for $\varrho = 0.1$ (blue) and 0.5 (green).

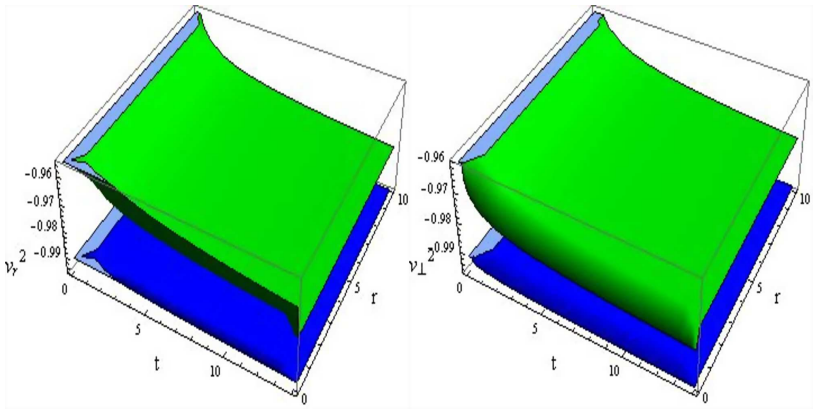

Figure 3.13: Plots of v_r^2 and $v_\perp^2$ with $\varsigma = -1$ for $\varrho = 0.1$ (blue) and 0.5 (green).

enters a phase of accelerated expansion. The graphical analysis of energy density and pressure components is displayed in Figure **3.11**. Negative pressure indicates the presence of a repulsive force which is responsible for the increased rate of expansion. The expansion rate drops when the decoupling parameter increases. Moreover, negative anisotropy indicates that the cosmos is expanding at a faster rate in the radial direction. The extended solution satisfies all energy bounds except SEC as shown in Figure **3.12**. Furthermore, the anisotropic model violates the causality condition (Figure **3.13**).

Chapter 4

Extended Gravitational Decoupled Solutions in SBD Theory

In this chapter, we construct anisotropic spherical solutions from known isotropic solutions through EGD method in the background of SBD theory. The field equations are decoupled into two sets by applying geometric deformations on radial as well as temporal metric components. The first array, corresponding to seed source is determined through metric functions of isotropic (Tolman IV/KB) as well as vacuum (Schwarzschild) solutions whereas two constraints on the anisotropic source are required to close the second system. The impact of the massive scalar field as well as the decoupling parameter on the physical characteristics of the anisotropic solutions is analyzed graphically for $V(\Psi) = \frac{1}{2}m_{\Psi}^{2}\Psi^{2}$.

This chapter is organized as follows. In the next section, viable anisotropic versions of Tolman IV and KB solutions are formulated while section **4.2** discusses the efficiency of EGD technique in extending vacuum spacetime. The findings of this chapter have been published in [113, 114].

4.1 EGD Approach and SBD Field Equations for Static Sphere

The field equations incorporating the anisotropic source are formulated via Eqs.(2.1.1) and (3.1.1)-(3.1.4) as

$$\frac{1}{r^2}-e^{-\chi}\left(\frac{1}{r^2}-\frac{\chi'}{r}\right) = \frac{1}{\Psi}(\rho+\varrho\Theta_0^0+T_0^{0\Psi}), \tag{4.1.1}$$

$$-\frac{1}{r^2}+e^{-\chi}\left(\frac{1}{r^2}+\frac{\lambda'}{r}\right) = \frac{1}{\Psi}(p-\varrho\Theta_1^1-T_1^{1\Psi}), \tag{4.1.2}$$

$$\frac{e^{-\chi}}{4}\left(2\lambda''+\lambda'^2-\chi'\lambda'+2\frac{\lambda'-\chi'}{r}\right) = \frac{1}{\Psi}(p-\varrho\Theta_2^2-T_2^{2\Psi}), \tag{4.1.3}$$

with $T_0^{0\Psi},\ T_1^{1\Psi}$ and $T_2^{2\Psi}$ given in Eqs.(2.1.6)-(2.1.8), respectively. Moreover, the evolution equation (2.1.9) for the metric (2.1.1) involves the traces of energy-momentum tensors representing seed as well as additional source.

Equations (4.1.1)-(4.1.3) form a system of non-linear differential equations with eight unknowns: two metric potentials ($\lambda,\ \chi$), five matter variables ($\rho,\ p,\ \Theta_0^0$, $\Theta_1^1,\ \Theta_2^2$) and a massive scalar field. In order to evaluate the unknown functions, we implement the novel technique of EGD [31] on SBD field equations. This technique determines the effect of Θ_δ^γ on the matter distribution by inducing the following deformations in the metric potentials

$$\lambda(r) \mapsto \mu(r)+\varrho g(r), \tag{4.1.4}$$

$$e^{-\chi(r)} \mapsto e^{-\xi(r)}+\varrho f(r), \tag{4.1.5}$$

where $f(r)$ and $g(r)$ encode the translations in radial and temporal metric components, respectively. It is noteworthy that spherical symmetry of the compact object is preserved under these geometric deformations. Substituting the deformed metric potentials in Eqs.(4.1.1)-(4.1.3) splits the system into two sets. The first set corresponds

to $\varrho=0$ and exclusively describes the isotropic configuration as

$$\begin{aligned}
\rho &= \frac{1}{2r^2\Psi(r)}\left\{e^{-\xi(r)}\left(r^2e^{\xi(r)}V(\Psi)\Psi(r)+r^2(-\omega_{BD})\Psi'^2(r)+((r\xi'(r)\right.\right.\\
&- \left.\left.4)\,\Psi'(r)-2r\Psi''(r))\,r\Psi(r)+2\Psi^2(r)\left(r\xi'(r)+e^{\xi(r)}-1\right)\right)\right\}, \qquad (4.1.6)\\
p &= \frac{1}{2}\left\{\frac{1}{r^2\Psi(r)}\left(e^{-\xi(r)}\left(-r^2\omega_{BD}\Psi'^2(r)+\Psi^2(r)\left(2r\mu'(r)-2e^{\xi(r)}+2\right)\right.\right.\right.\\
&+ \left.\left.\left.r\Psi(r)\,(r\mu'(r)+4)\,\Psi'(r)\right)\right)-V(\Psi)\right\}, \qquad (4.1.7)\\
p &= \frac{1}{4r\Psi(r)}\left\{e^{-\xi(r)}\left(2\Psi(r)\,(\Psi'(r)\,(r\mu'(r)-r\xi'(r)+2)+2r\Psi''(r))+\Psi^2(r)\right.\right.\\
&\times \left.\left(2r\mu''(r)+\mu'(r)\,(2-r\xi'(r))+r\mu'^2(r)-2\xi'(r)\right)-2re^{\xi(r)}\Psi(r)V(\Psi)\right.\\
&+ \left.\left.2r\omega_{BD}\Psi'^2(r)\right)\right\}. \qquad (4.1.8)
\end{aligned}$$

The conservation of isotropic matter distribution in (μ,ξ) coordinates is represented by the conservation equation

$$T_1^{1'(\text{eff})}-\frac{\mu'(r)}{2}(T_0^{0(\text{eff})}-T_1^{1(\text{eff})})=0. \qquad (4.1.9)$$

The second set containing evolution equations for the anisotropic source is given as

$$\begin{aligned}
\Theta_0^0 &= \frac{-1}{2r^2\Psi(r)}\left\{\left(r\Psi(r)f'(r)\,(r\Psi'(r)+2\Psi(r))+f(r)\left(r^2\omega_{BD}\Psi'^2(r)\right.\right.\right.\\
&+ \left.\left.\left.2r\Psi(r)\,(r\Psi''(r)+2\Psi'(r))+2\Psi^2(r)\right)\right)\right\}, \qquad (4.1.10)\\
\Theta_1^1 &= \frac{-f(r)}{2r^2\Psi(r)}\left(-r^2\omega_{BD}\Psi'^2(r)+r\Psi(r)\,(r\lambda'(r)+4)\,\Psi'(r)+2\Psi^2(r)\,(r\lambda'(r)\right.\\
&+ \left.1)\right)-\frac{e^{-\xi(r)}g'(r)\,(r\Psi'(r)+2\Psi(r))}{2r}, \qquad (4.1.11)\\
\Theta_2^2 &= \frac{-f(r)}{4r\Psi(r)}\left(2\Psi(r)\,((r\lambda'(r)+2)\,\Psi'(r)+2r\Psi''(r))+\Psi^2(r)\,(2r\lambda''(r)\right.\\
&+ \left.r\lambda'^2(r)+2\lambda'(r)\right)+2r\omega_{BD}\Psi'^2(r)\Big)-\frac{f'(r)}{4r}\,(\Psi(r)\,(r\lambda'(r)+2)\\
&+ 2r\Psi'(r))-\frac{e^{-\xi(r)}}{4r}\left(2rg'(r)\Psi'(r)+\Psi(r)\left(2rg''(r)+\varrho rg'^2(r)+g'(r)\right.\right.
\end{aligned}$$

$$\times \quad (2r\mu'(r) - r\xi'(r) + 2))) \,. \tag{4.1.12}$$

The divergence of the source Θ^{γ}_{δ} leads to

$$\Theta_1^{1'(\text{eff})} - \frac{\lambda'(r)}{2}(\Theta_0^{0(\text{eff})} - \Theta_1^{1(\text{eff})}) - \frac{2}{r}(\Theta_2^{2(\text{eff})} - \Theta_1^{1(\text{eff})}) = \frac{g'(r)}{2}(T_0^{0(\text{eff})} - T_1^{1(\text{eff})}), \tag{4.1.13}$$

where

$$\begin{aligned}
\Theta_0^{0(\text{eff})} &= \frac{1}{\Psi}\left(\Theta_0^0 + \frac{1}{2}f'(r)\Psi'(r) + f(r)\Psi'' + \frac{\omega_{BD}f(r)\Psi'^2}{2\Psi} + \frac{2f(r)\Psi'(r)}{r}\right), \\
\Theta_1^{1(\text{eff})} &= \frac{1}{\Psi}\left(\Theta_1^1 + \frac{1}{2r\Psi}e^{-\xi(r)}\Psi'(r)\left(f(r)e^{\xi(r)}\left(\Psi(r)\left(r\lambda'(r)+4\right) - r\omega_{BD}\right.\right.\right. \\
&\times \quad \left.\left.\left.\Psi'(r)\right) + r\Psi(r)g'(r)\right)\right), \\
\Theta_2^{2(\text{eff})} &= \frac{1}{\Psi}\left(\Theta_2^2 + \frac{1}{2r\Psi}e^{-\xi(r)}\left(r\Psi(r)\Psi'(r)\left(e^{\xi(r)}f'(r) + g'(r)\right) + f(r)\right.\right. \\
&\times \quad \left.\left.e^{\xi(r)}\left(\Psi(r)\left(\left(r\lambda'(r)+2\right)\Psi'(r) + 2r\Psi''(r)\right) + r\omega_{BD}\Psi'^2(r)\right)\right)\right).
\end{aligned}$$

The conservation equation of the energy-momentum tensor $T^{\gamma(\text{eff})}_{\delta}$ in (λ, χ)-coordinate system yields

$$\nabla_\gamma T^{\gamma(\text{eff})}_{\beta} = \nabla^{(\mu,\xi)}_{\gamma} T^{\gamma(\text{eff})}_{\beta} - \frac{g'(r)}{2}(T_0^{0(\text{eff})} - T_1^{1(\text{eff})})\delta^1_\beta, \tag{4.1.14}$$

where $\nabla^{(\mu,\xi)}_{\gamma}$ represents the divergence of a tensor in (μ, ξ)-frame. As a direct consequence of Eqs.(4.1.9) and (4.1.13), we have

$$\nabla^{(\mu,\xi)}_{\gamma} T^{\gamma(\text{eff})}_{\beta} = 0, \quad \nabla_\gamma \Theta^{\gamma(\text{eff})}_{\beta} = \frac{g'(r)}{2}(T_0^{0(\text{eff})} - T_1^{1(\text{eff})})\delta^1_\beta. \tag{4.1.15}$$

Equations (4.1.14) and (4.1.15) imply that exchange of energy takes place between the sources $T^{(m)}_{\gamma\delta}$ and $\Theta_{\gamma\delta}$ but the overall energy and momentum of the system remain unchanged. Thus, these sources can be decoupled provided that energy can be transferred from one setup to the other. However, if $T^{(m)}_{\gamma\delta}$ represents either a vacuum solution or a barotropic fluid, matter sources interacting only gravitationally can also be decoupled via EGD approach.

4.1.1 Anisotropic Solutions

When we apply the EGD technique, the system (4.1.1)-(4.1.3) is decomposed into two sets: Eqs.(4.1.6)-(4.1.8) represent the seed source in terms of $T^{(m)}_{\gamma\delta}$, μ and ξ whereas the influence of the additional source is determined by the second set (4.1.10)-(4.1.12) with five unknowns $(g(r),\ f(r),\ \Theta^0_0,\ \Theta^1_1,\ \Theta^2_2)$. The undetermined variables of the second set can be evaluated if a viable solution for the isotropic sector is known. Thus, EGD approach has simplified the process of extracting solutions of the field equations by reducing the degrees of freedom from 4 to 2. In this section, we obtain anisotropic analogues of two solutions: Tolman IV and KB.

In 1939, Tolman [115] constructed eight static spherically symmetric solutions for perfect fluid and explored the conditions for smooth matching of interior and exterior geometries. Tolman IV is one of the physically acceptable solutions [116] which corresponds to a non-vanishing surface density. It has previously been employed to investigate different features of self-gravitating systems [33, 117]. The line element of Tolman IV solution is written as

$$ds^2 = B^2(1+\frac{r^2}{A^2})dt^2 - \frac{1+\frac{2r^2}{A^2}}{(1+\frac{r^2}{A^2})(1-\frac{r^2}{F^2})}dr^2 - r^2(d\theta^2+\sin^2\theta d\phi^2), \quad (4.1.16)$$

where the constants $A,\ B$ and F are determined through the matching of internal and external (Schwarzschild) spacetimes at the boundary of the celestial object. The junction conditions evaluate the constants $A,\ B$ and F (for $\varrho = 0$) as

$$A^2 = -\frac{R^2\left(R^2\zeta + M\left(28R - 2R\zeta\right) + 2M^2(\omega_{BD}-12) - 8R^2\right)}{R\zeta(R-2M) + 2M^2\omega_{BD}}, \quad (4.1.17)$$

$$B^2 = \frac{(R-2M)\left(3R^2\zeta - 6M\left(R\zeta + 10R\right) + 6M^2(\omega_{BD}+12) + 8R^2\right)}{2R\left(R^2\zeta - 2M\left(R\zeta + 11R\right) + 2M^2(\omega_{BD}+12) + 4R^2\right)}, \quad (4.1.18)$$

$$F^2 = (4R^3(3M-2R)(\zeta+4))(m_\Psi^4R^6 + 4R^2\zeta + M^2\left(4m_\Psi^4R^4 + 2\zeta(\omega_{BD} + 12) + 8(\omega_{BD}+12)\right) - 4M\left(m_\Psi^4R^5 + 6R\zeta + 16R\right))^{-1}. \quad (4.1.19)$$

where $\zeta = m_{\Psi}^2 R^2 \sqrt{1-\frac{2M}{R}}$.

Krori and Barua [118] formulated a physically acceptable solution for a static charged sphere. The highlight of this solution is that no restrictions are imposed on the metric functions to avoid singularities, i.e., it is regular throughout the spacetime. This solution has proved helpful in checking the impact of electromagnetic field on matter source. However, researchers have also employed this ansatz to inspect physical characteristics of uncharged systems [119]. The KB solution is defined by the following line element

$$ds^2 = e^{\hat{a}r^2+\hat{b}}dt^2 - e^{\hat{c}r^2}dr^2 - r^2(d\theta^2+\sin^2\theta d\phi^2), \tag{4.1.20}$$

where the constants $\hat{a}$, $\hat{b}$ and $\hat{c}$ are evaluated (for $\varrho = 0$) through the matching conditions as

$$\hat{a} = \frac{R\zeta(R-2M)+2M^2\omega_{BD}}{4R^2(R-2M)(2R-3M)}, \tag{4.1.21}$$

$$\hat{b} = \frac{R\zeta(R-2M)+2M^2\omega_{BD}}{-4\left(6M^2-7MR+2R^2\right)} + \ln\left(1-\frac{2M}{R}\right), \tag{4.1.22}$$

$$\hat{c} = -\frac{\ln\left(1-\frac{2M}{R}\right)}{R^2}. \tag{4.1.23}$$

The anisotropic model is completely specified by the following matter variables

$$\begin{aligned}
\rho &= \frac{e^{-\xi(r)}}{2r^2\Psi(r)}\left(-r\Psi(r)\left(\Psi'(r)\left(\varrho re^{\xi(r)}f'(r)+4\varrho f(r)e^{\xi(r)}-r\xi'(r)+4\right)\right.\right.\\
&+ \left.2r\Psi''(r)\left(\varrho f(r)e^{\xi(r)}+1\right)\right)-2\Psi^2(r)\left(\varrho re^{\xi(r)}f'(r)+\varrho f(r)e^{\xi(r)}\right.\\
&- \left.r\xi'(r)-e^{\xi(r)}+1\right)+r^2(-\omega_{BD})\Psi'^2(r)\left(\varrho f(r)e^{\xi(r)}+1\right)\\
&+ \left.r^2e^{\xi(r)}\Psi(r)V(\Psi)\right), \qquad (4.1.24)\\
p_r &= \frac{\Psi(r)}{r^2}\left(\left(\varrho f(r)+e^{-\xi(r)}\right)\left(\varrho rg'(r)+r\mu'(r)+1\right)-1\right)-\frac{1}{2r\Psi(r)}\\
&\times \left(\Psi'(r)\left(\varrho f(r)+e^{-\xi(r)}\right)\left(r\omega_{BD}\Psi'(r)-\Psi(r)\left(\varrho rg'(r)+r\mu'(r)+4\right)\right)\right)
\end{aligned}$$

$$- \quad \frac{V(\Psi)}{2}, \tag{4.1.25}$$

$$\begin{aligned} p_\perp &= \left(\varrho f(r)+e^{-\xi(r)}\right)\left(\frac{1}{2}\Psi'(r)\left(\frac{\varrho e^{\xi(r)}f'(r)-\xi'(r)}{\varrho f(r)e^{\xi(r)}+1}+\varrho g'(r)+\mu'(r)\right.\right. \\ &+ \left.\left.\frac{2}{r}\right)+\Psi''(r)+\frac{\omega_{BD}\Psi'^2(r)}{2\Psi(r)}\right)+\frac{1}{2}\Psi(r)\left(\varrho f(r)+e^{-\xi(r)}\right)\left(\left(\left(\varrho e^{\xi(r)}f'(r)\right.\right.\right. \\ &- \left.\left.\xi'(r)\right)\left(\varrho g'(r)+\mu'(r)\right)\right)(2\varrho f(r)e^{\xi(r)}+2)^{-1}+\frac{1}{r}\left(\frac{\varrho e^{\xi(r)}f'(r)-\xi'(r)}{\varrho f(r)e^{\xi(r)}+1}\right. \\ &+ \left.\left.\varrho g'(r)+\mu'(r)\right)+\varrho g''+\frac{1}{2}\left(\varrho g'(r)+\mu'^2(r)\right)+\mu''(r)\right)-\frac{V(\Psi)}{2}. \end{aligned} \tag{4.1.26}$$

In order to extend the seed solutions to the anisotropic domain, we require two constraints on Θ_δ^γ to close the anisotropic system. For this purpose, we choose a mimic constraint

$$\Theta_1^1(r)=p(r), \tag{4.1.27}$$

which fulfills the requirement of vanishing pressure at the hypersurface. Under this constraint, the values of the constants F and $\hat{a}$ remain unchanged. The remaining constants A and $\hat{c}$ appear as free parameters in corresponding extended versions whose values are chosen as presented in Eqs.(4.1.17) and (4.1.21), respectively. For the second constraint, a linear EoS as well as a regularity condition on anisotropy is implemented as cases I and II, respectively.

The limits enforced by the weak-field on values of the coupling parameter can be avoided through a lower bound for mass of the scalar field ($m_\Psi > 10^{-4}$ in dimensionless units). In accordance with this limit, we take $m_\Psi = 0.01$ and solve the wave equation numerically to determine the massive scalar field. Different features of anisotropic models are investigated graphically for three values of ϱ (0.2, 0.55, 0.9) by employing the observed mass ($1.97M_\odot$) and radius (11.29km) of the star PSR J1614-2230.

Case I: Linear Equation of State

We consider a linear EoS for the source Θ_{δ}^{γ} as

$$\Theta_0^0 = a_1\Theta_1^1 + a_2\Theta_2^2. \tag{4.1.28}$$

Setting $a_1 = 1$ and $a_2 = 0$ in the above equation leads to

$$\begin{aligned}
&\frac{e^{-\xi(r)}}{r\Psi(r)}\left(-r\Psi(r)\left(\Psi'(r)\left(re^{\xi(r)}f'(r)+4f(r)e^{\xi(r)}+r\mu'(r)+4\right)+2rf(r)\right.\right.\\
&\times\left.\left. e^{\xi(r)}\Psi''(r)\right)-2\Psi^2(r)\left(re^{\xi(r)}f'(r)+f(r)e^{\xi(r)}+r\mu'(r)-e^{\xi(r)}+1\right)\right.\\
&\left.+r^2(-\omega_{BD})\left(f(r)e^{\xi(r)}-1\right)\Psi'^2(r)+r^2e^{\xi(r)}\Psi(r)V(\Psi)\right)=0,
\end{aligned} \tag{4.1.29}$$

which is solved numerically for $f(r)$ along with the wave equation with the central conditions $\Psi(0) = 0.2,\ \Psi'(0) = 0$ and $f(0) = 0$. On the other hand, the mimic constraint (4.1.27) yields the following temporal geometric function

$$\begin{aligned}
g(r) &= \int\left((r^2\omega_{BD}\left(f(r)e^{\xi(r)}+1\right)\Psi'(r)^2-r\Psi(r)\left(f(r)e^{\xi(r)}+1\right)(r\mu'(r)\right.\\
&+ \left.4)\Psi'(r)-2\Psi^2(r)\left(f(r)e^{\xi(r)}(r\mu'(r)+1)+r\mu'(r)-e^{\xi(r)}+1\right)\right.\\
&+ \left.r^2e^{\xi(r)}\Psi(r)V(\Psi))(r\Psi(r)(r\Psi'(r)+2\Psi(r))\left(\varrho f(r)e^{\xi(r)}+1\right))^{-1}\right)dr.
\end{aligned} \tag{4.1.30}$$

Substituting the metric functions and constants corresponding to Tolman IV solution in Eqs.(4.1.24)-(4.1.26), (4.1.29) and (4.1.30) provides the extended version of this solution.

The graphical analysis of state determinants is provided in Figure **4.1** with $\omega_{BD} = 9.87$. It is observed from Figure **4.1** that energy density as well as pressure components are positive throughout and maximum at the center for $\varrho = 0.2$ and 0.55. However, for $\varrho = 0.9$, the transverse pressure increases monotonically instead of

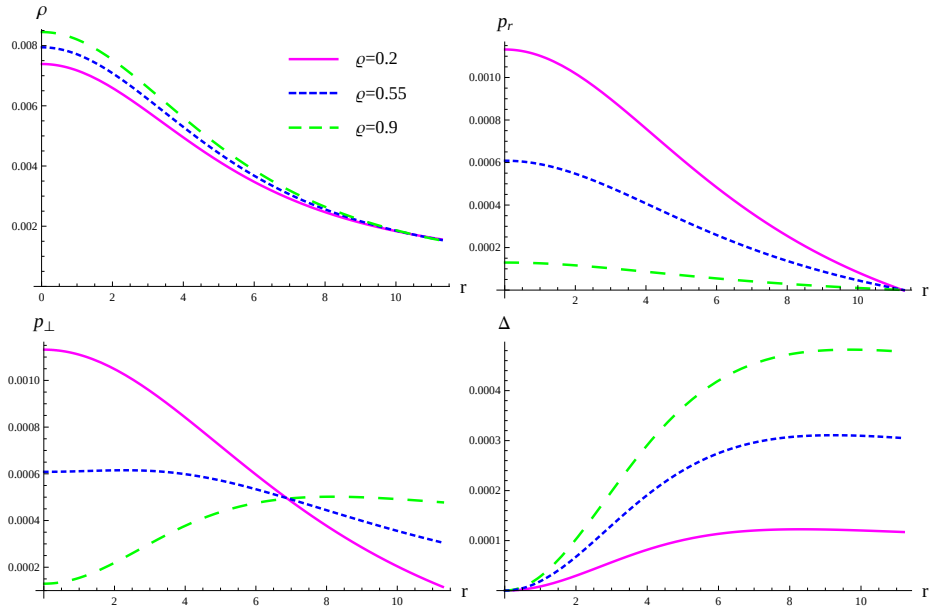

Figure 4.1: Plots of matter variables and anisotropy of extended Tolman IV solution for case I.

decreasing. The anisotropy is zero at the center and increases towards the surface indicating the presence of an outward repulsive force. It is noted that higher values of ϱ increase the density and repulsive force in the interior of the structure whereas the pressure components decrease. We employ energy conditions to ensure the presence of normal matter. The first three conditions (NEC, WEC, SEC) are readily satisfied for extended Tolman IV solution as energy density and pressure (radial/transverse) are positive within the compact object. Figure **4.2** demonstrates that the parameters governing the matter source agree with DEC ensuring viability of the model.

Another important physical feature of a self-gravitating system is its compactness ($u(r)$) in a state of equilibrium. The compactness factor is defined as the relation of mass to the radius of the object. Buchdahl [120] calculated the upper limit of this parameter for a fluid with non-increasing energy density by matching the interior of

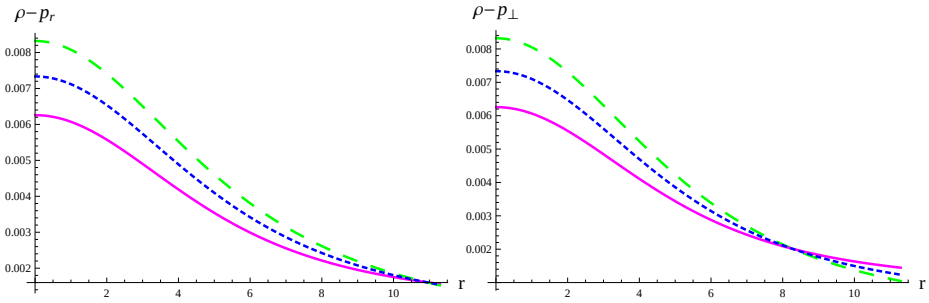

Figure 4.2: DEC for anisotropic Tolman IV with case I.

a static sphere to Schwarzschild exterior solution. This limit is given as

$$u(r) = \frac{m}{R} < \frac{4}{9}, \tag{4.1.31}$$

where $m(r) = \frac{R}{2}(1 - e^{-\chi})$. The compactness factor obtained for anisotropic Tolman IV solution (shown in Figure **4.3**) conforms to Buchdahl limit. The surface redshift ($Z(r)$) of a celestial object gauges the increase in wavelength of electromagnetic radiation due to gravitational force exerted by the star. It is defined as

$$Z(r) = \frac{1}{\sqrt{1-2u}} - 1. \tag{4.1.32}$$

For a perfect fluid distribution, Buchdahl limit restricts the value of redshift at the stellar surface as $Z(r) < 2$. However, for an anisotropic configuration, the upper limit of surface redshift changes to 5.211 [121]. It is observed from Figure **4.3** that the range of redshift parameter complies with the above limit.

The internal structure of compact objects is determined by the gravitational (M_g) as well as baryonic (M_b) mass. The gravitational mass of a spherical gravitationally bound system is measured using Kepler's law (when a satellite orbits the star) and is defined as

$$M_g = \frac{1}{2}\int_0^R \rho r^2 dr. \tag{4.1.33}$$

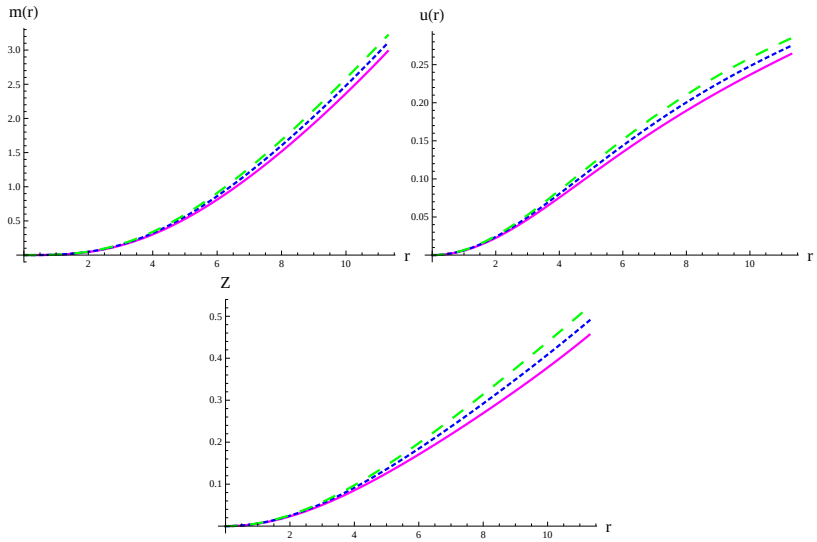

Figure 4.3: Plots of mass, compactness and redshift parameters corresponding to anisotropic Tolman IV for case I.

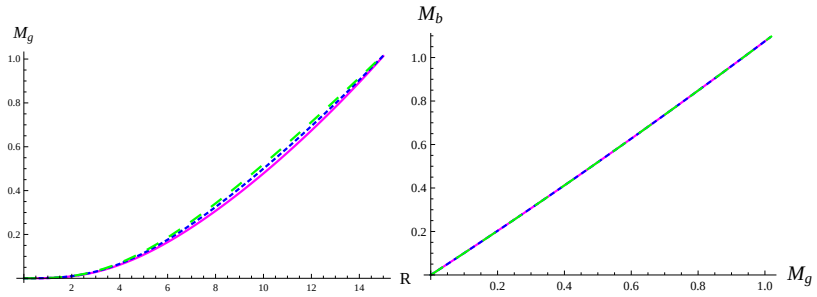

Figure 4.4: Plots of gravitational mass versus radius (left) and baryonic mass versus gravitational mass (right) corresponding to anisotropic Tolman IV with case I.

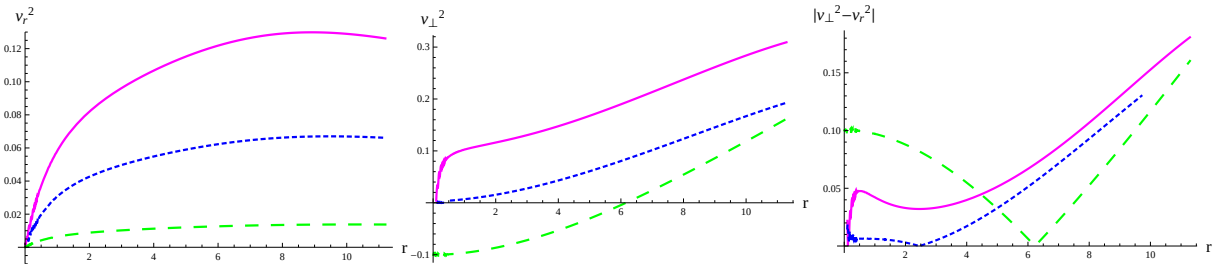

Figure 4.5: Plots of radial/tangential velocities and $|v_\perp^2 - v_r^2|$ corresponding to anisotropic Tolman IV for case I.

The gravitational mass associated with the anisotropic star is obtained by numerically solving the above equation along with the wave equation and (4.1.29) under the condition $M_g(0) = 0$. The mass is presented in Figure **4.4** as a function of radius for chosen values of ϱ. It is noted that the gravitational mass of the spherical system increases with an increase in the decoupling parameter. On the other hand, baryonic mass is directly related to the massive iron core at the center of the stellar remnant and is defined as the volume integral of baryon number density times mass of a baryon. Burrows and Lattimer [122] provided the relation between gravitational and baryonic mass as

$$M_b = M_g + \varpi M_g^2, \tag{4.1.34}$$

where $\varpi = 0.075$ for a large number of nuclear EoS [123]. The relation between gravitational and baryonic masses, presented in Figure **4.4**, shows that maximum baryonic mass is attained for $\varrho = 0.9$.

The stability of the constructed model is investigated through causality condition and Herrera's cracking approach. The plots in Figure **4.5** clearly show that the anisotropic model is stable for $\varrho = 0.2,\ 0.55$ whereas tangential velocity becomes positive after a certain distance corresponding to $\varrho = 0.9$. Moreover, the extended

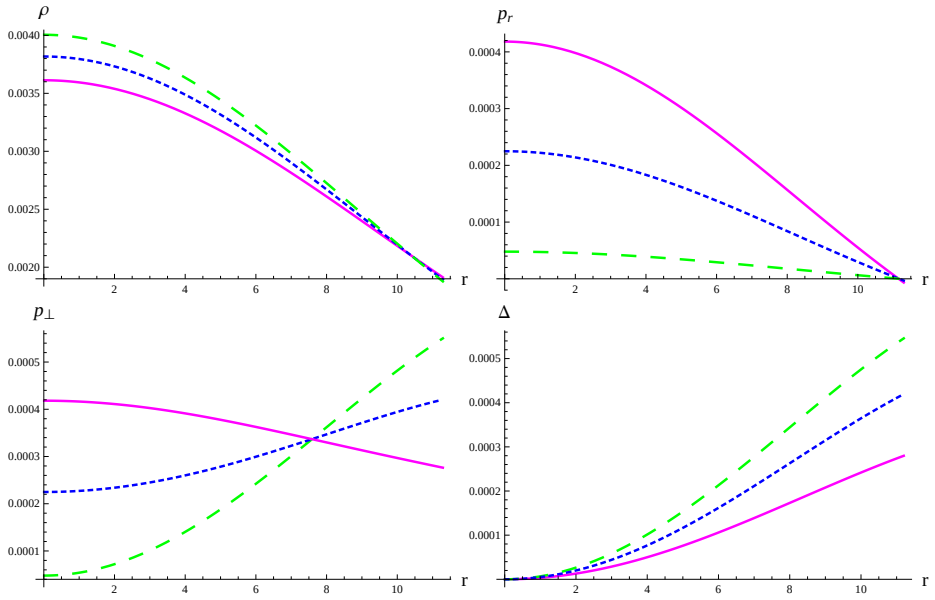

Figure 4.6: Matter variables and anisotropy of extended KB solution for case I.

Tolman IV solution complies with this condition for $\varrho = 0.2,\ 0.55$ as shown in Figure **4.5**.

The anisotropic version of the KB solution is formulated in SBD gravity through Eqs.(4.1.20), (4.1.24)-(4.1.26), (4.1.29) and (4.1.30). Plots of state variables are presented in Figure **4.6** for $\omega_{BD} = 9.87$. The profiles of energy density and pressure components attain maximum value at the center and decrease towards the surface for $\varrho = 0.2$. However, for higher values of the decoupling parameter (0.55, 0.9), tangential pressure exhibits monotonically increasing behavior. Furthermore, the anisotropy vanishes at the center as required. This anisotropic solution is consistent with all energy bounds for chosen values of ϱ (Figure **4.7**) leading to a viable configuration. The compactness factor and surface redshift obey the desired restraints as shown in Figure **4.8**. Figure **4.9** shows an increment in the gravitational mass as ϱ increases

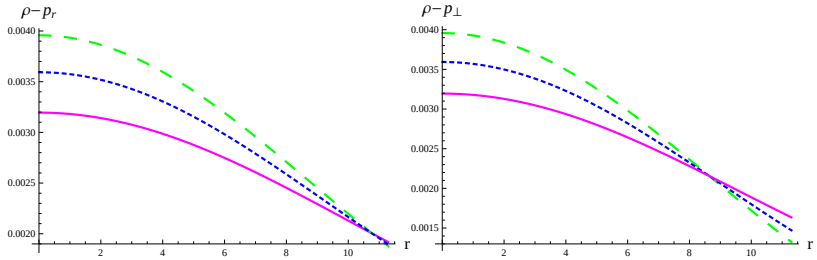

Figure 4.7: DEC for extended KB solution with case I.

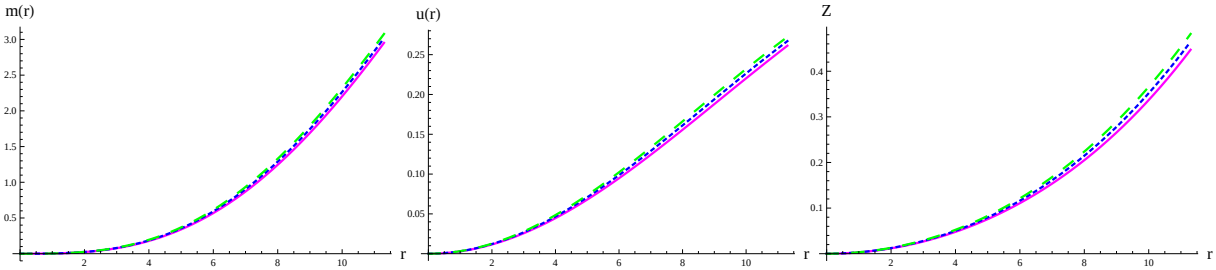

Figure 4.8: Plots of mass, compactness and redshift parameters corresponding to extended KB solution for case I.

from 0.2 to 0.55. However, a drop in the mass is observed for a higher value of ϱ. Moreover, the baryonic mass is maximum for $\varrho = 0.55$. The anisotropic model violates the causality condition as tangential velocity is negative throughout the system for selected values of ϱ (refer to Figure **4.10**). However, the compact object is stable with respect to Herrera's cracking approach.

Case II: Regularity Condition on Anisotropy

Bowers and Liang [124] proposed that singularities in the Tolman-Oppenheimer-Volkoff equation can be avoided if the following condition is imposed on the anisotropy

$$p_\perp - p_r = Ch(p_r, r)(\rho + p_r)r^{\mathfrak{m}},$$

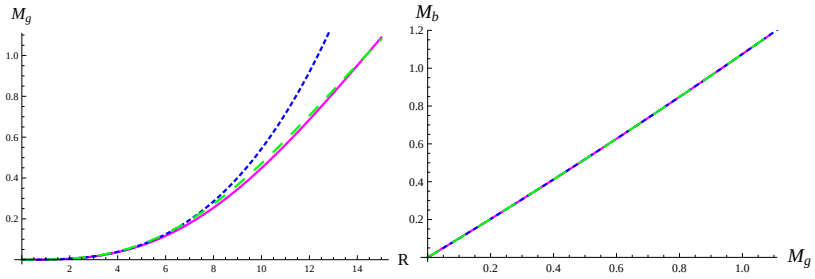

Figure 4.9: Plots of gravitational mass versus radius (left) and baryonic mass versus gravitational mass (right) for extended KB solution with case I.

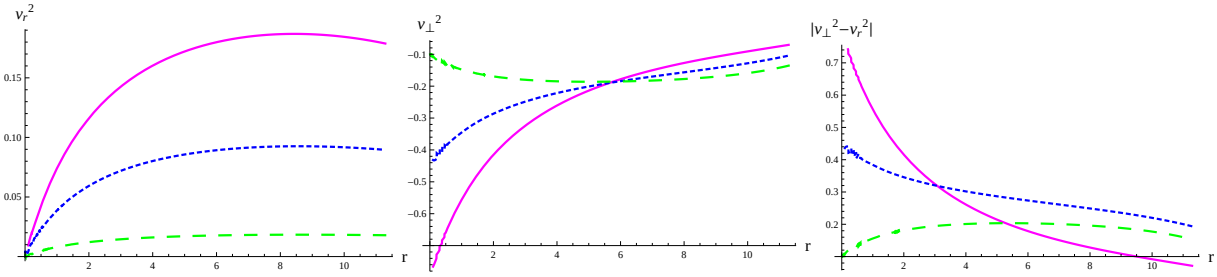

Figure 4.10: Plots of radial/tangential velocities and $|v_\perp^2 - v_r^2|$ for extended KB solution with case I.

where the parameter C measures the strength of the anisotropy and $\mathfrak{m} > 1$. For the present work, we have taken $C = -0.5$. Moreover, h is an arbitrary function of radial pressure and contains information about the anisotropy of the system. In 1981, Cosenza et al. [125] evaluated anisotropic solutions from known isotropic solutions by assuming the energy density of a perfect fluid and taking $h(p_r, r) = \frac{\lambda'(r)}{2} r^{1-\mathfrak{m}}$. These conditions have already been employed in MGD approach to obtain new anisotropic solutions [126, 127]. In this section, we obtain anisotropic analogues of seed solutions by imposing Bowers-Liang constraint on Θ-sector as

$$\Theta_2^2 - \Theta_1^1 = Ch(\Theta_1^1, r)(-\Theta_0^0 + \Theta_1^1) r^{\mathfrak{m}}, \tag{4.1.35}$$

with $h(\Theta_1^1, r) = \frac{\lambda'(r)}{2} r^{1-\mathfrak{m}}$. Substituting Eqs.(4.1.10)-(4.1.12) in the above equation leads to

$$\begin{aligned}
&\frac{e^{-\xi(r)}}{r\Psi(r)} \left(f(r) e^{\xi(r)} \left(r\Psi(r) \left(\Psi'(r) \left(C\varrho r^2 g'(r)\lambda'(r) + Cr^2\mu'(r)\lambda'(r) + 4 \right) \right. \right. \right. \\
&- \left. 2r\Psi''(r) \left(Cr\lambda'(r) + 2 \right) \right) + \Psi^2(r) \left(- \left(2 \left(\varrho r^2 g''(r) + r^2 \mu''(r) - 2 \right) \right. \right. \\
&+ \left. \varrho^2 r^2 g'^2(r) + 2\varrho r g'(r) \left(r\mu'(r) - Cr\lambda'(r) - 1 \right) + r^2 \mu'^2(r) - 2r\mu'(r) \right. \\
&\times \left. \left. \left. \left(Cr\lambda'(r) + 1 \right) \right) \right) - 2r^2 \omega_{BD} \Psi'^2(r) \left(Cr\lambda'(r) + 2 \right) \right) - r\Psi(r) \left(r\Psi'(r) \right. \\
&\times \left. \left(e^{\xi(r)} f'(r) \left(Cr\lambda'(r) + 2 \right) - Crg'(r)\lambda'(r) \right) + \Psi(r) \left(e^{\xi(r)} f'(r) \left(\varrho r g'(r) \right. \right. \right. \\
&+ \left. r\mu'(r) + 2Cr\lambda'(r) + 2 \right) + 2rg''(r) + \varrho r g'^2(r) + g'(r) \left(2r\mu'(r) - r\xi'(r) \right. \\
&- \left. \left. \left. 2Cr\lambda'(r) - 2 \right) \right) \right) \right) = 0.
\end{aligned} \tag{4.1.36}$$

We obtain the deformation function $g(r)$ by simultaneously solving Eq.(4.1.36) and wave equation numerically with the initial conditions $\Psi(0) = 0.1,\ \Psi'(0) = 0,\ g(0) = 0$ and $g'(0) = 0.5$. The function $f(r)$ is evaluated from the constraint (4.1.27) as

$$\begin{aligned}
f(r) \ = \ & e^{-\xi(r)} \left(2\Psi^2(r) \left(-rg'(r) - r\mu'(r) + e^{\xi(r)} - 1 \right) - r\Psi(r)\Psi'(r) \left(rg'(r) \right. \right.
\end{aligned}$$

$$+ \quad r\mu'(r)+4)+r^2e^{\xi(r)}\Psi(r)V(\Psi)+r^2\omega_{BD}\Psi'^2(r)\big)\,(r\Psi(r)\Psi'\,(\varrho rg'(r)$$

$$+ \quad r\mu'(r)+4)+2\Psi^2(r)\,(\varrho rg'(r)+r\mu'(r)+1)-r^2\omega_{BD}\Psi'^2(r))^{-1}. \quad (4.1.37)$$

Tolman IV solution is extended via constraint (4.1.35) by employing the associated constants in Eqs.(4.1.24)-(4.1.26), (4.1.36) and (4.1.37). The physical characteristics of this solution are investigated graphically for $\omega_{BD} = 17.95$. Figure **4.11** displays the energy density and pressures as decreasing functions of r for the considered values of ϱ. A decrease in the physical parameters $(\rho,\ p_r,\ p_\perp)$ is observed for higher values of the decoupling parameter whereas anisotropy increases as ϱ increases. Moreover, the anisotropy within the star increases for some distance and then decreases indicating the presence of a weaker repulsive force near the stellar surface. Figure **4.12** shows that the system corresponding to extended Tolman IV solution is viable as it adheres to the restrictions imposed by energy bounds. Moreover, the compactness and redshift parameters (Figure **4.13**) adhere to the respective bounds. The gravitational and baryonic masses calculated from Eqs.(4.1.33) and (4.1.34), respectively are plotted in Figure **4.14**. The compact structure becomes more massive as ϱ increases form 0.2 to 0.55 but decreases for $\varrho = 0.9$. Furthermore, the model has maximum baryonic mass for $\varrho = 0.55$. Finally, the extended Tolman IV solution is stable for the considered values of the decoupling parameter as it complies with the causality condition and cracking approach as shown in Figure **4.15**.

The extended version of KB solution under Bowers-Liang constraint is constructed by plugging the associated metric potentials and constants in Eqs.(4.1.24)-(4.1.26), (4.1.36) and (4.1.37). It is noted from Figure **4.16** that energy density and tangential pressure are positive for the selected values of ϱ but decrease monotonically only for $\varrho = 0.2$. However, the radial pressure has a maximum value at the center and vanishes

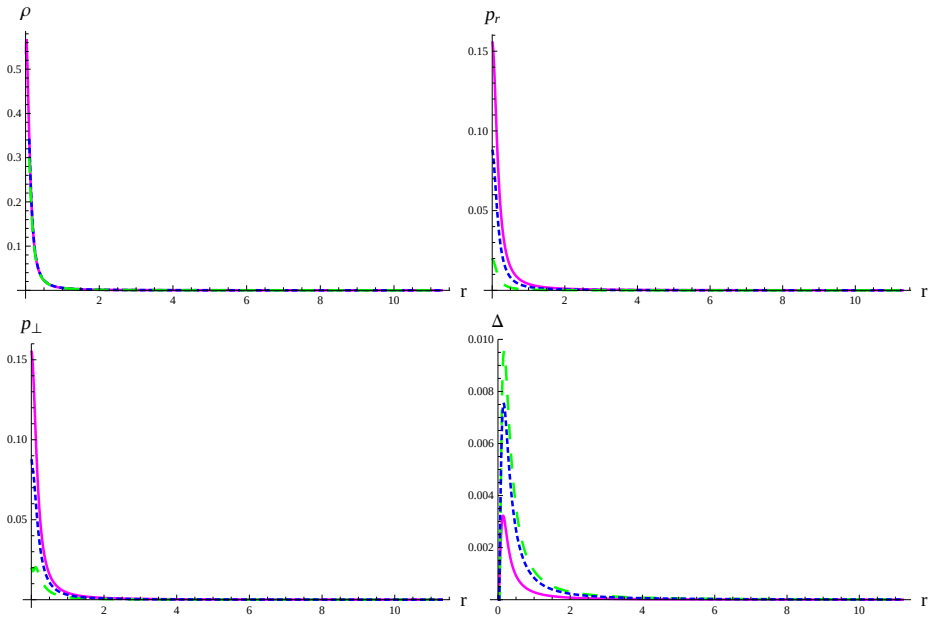

Figure 4.11: Plots of matter variables and anisotropy of extended Tolman IV for case II.

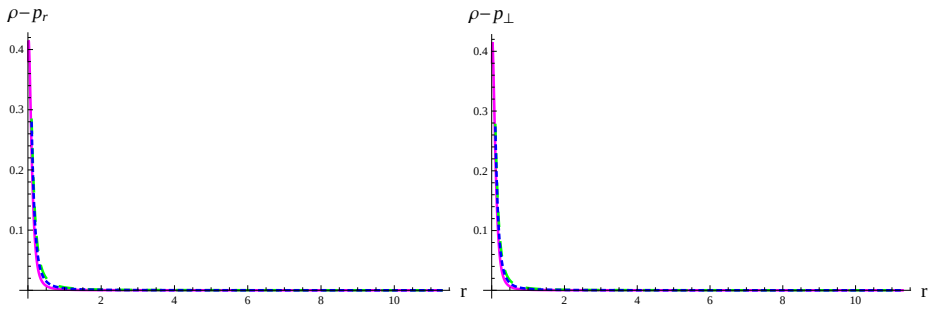

Figure 4.12: DEC for anisotropic Tolman IV with case II.

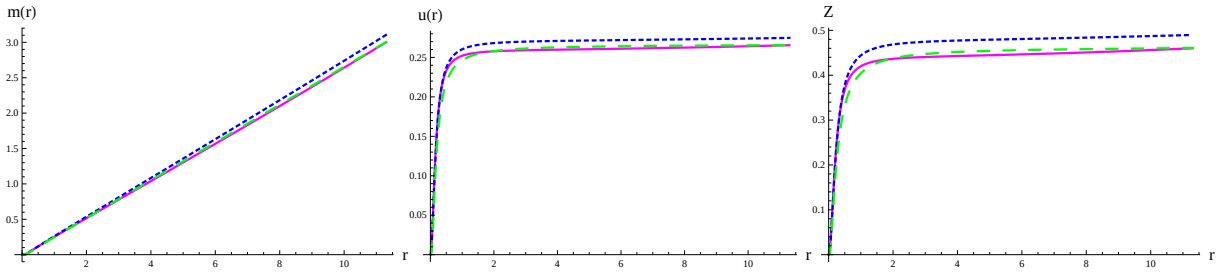

Figure 4.13: Plots of mass, compactness and redshift parameters corresponding to anisotropic Tolman IV for case II.

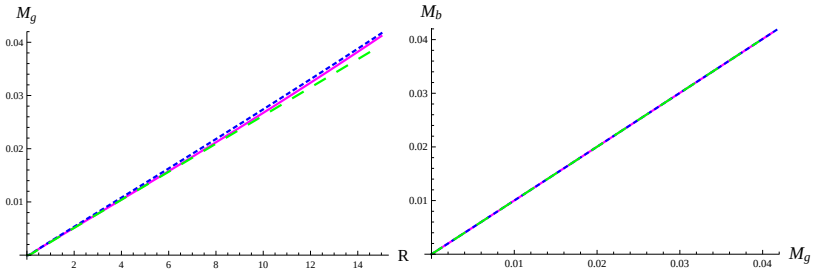

Figure 4.14: Plots of gravitational mass versus radius (left) and baryonic mass versus gravitational mass (right) corresponding to anisotropic Tolman IV for case II.

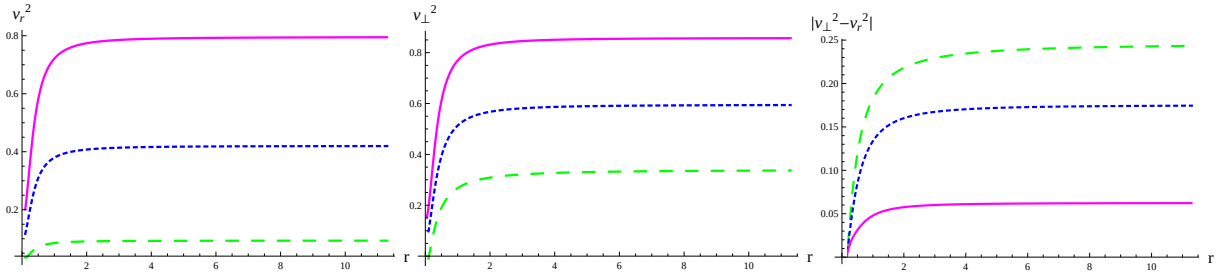

Figure 4.15: Plots of radial/tangential velocities and $|v_\perp^2 - v_r^2|$ corresponding to anisotropic Tolman IV for case II.

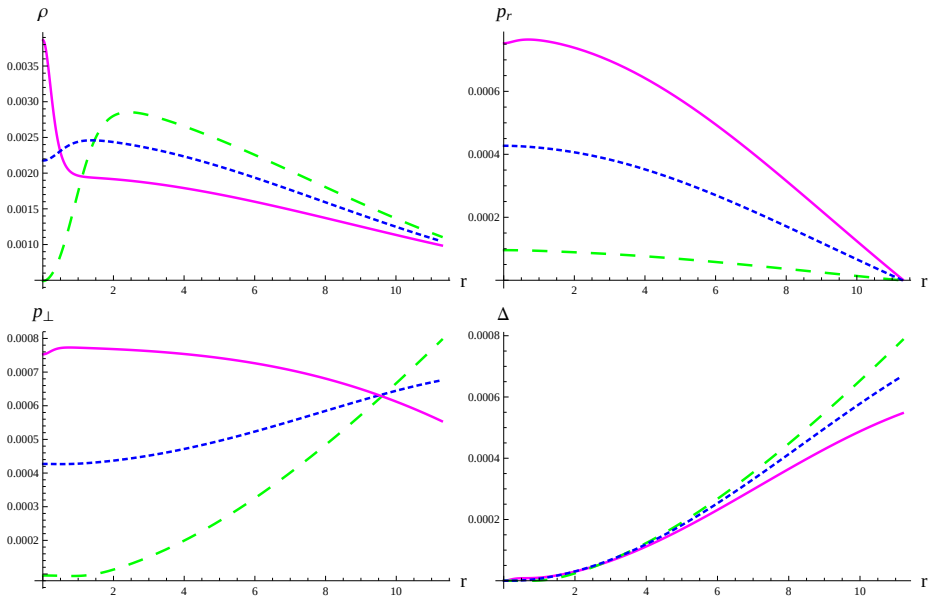

Figure 4.16: Plots of matter variables and anisotropy of extended KB solution for case II.

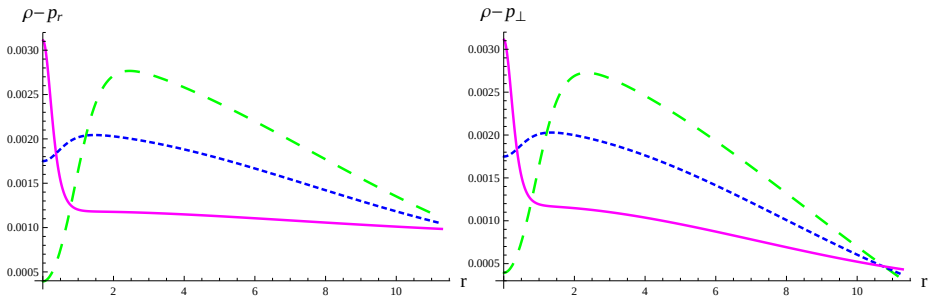

Figure 4.17: DEC for extended KB solution with case II.

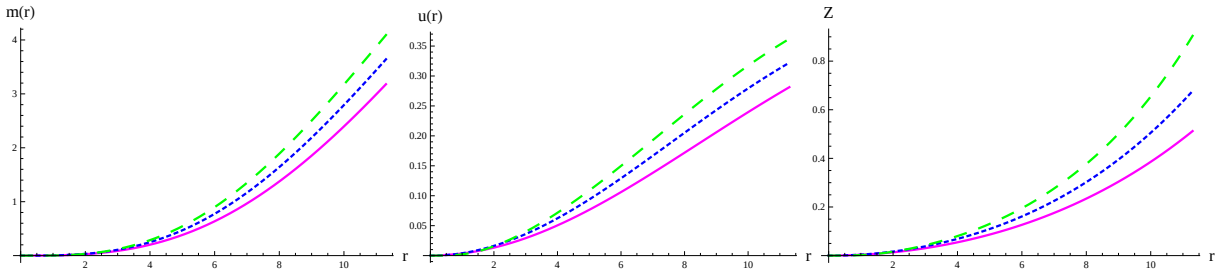

Figure 4.18: Plots of mass, compactness and redshift parameters corresponding to extended KB solution for case II.

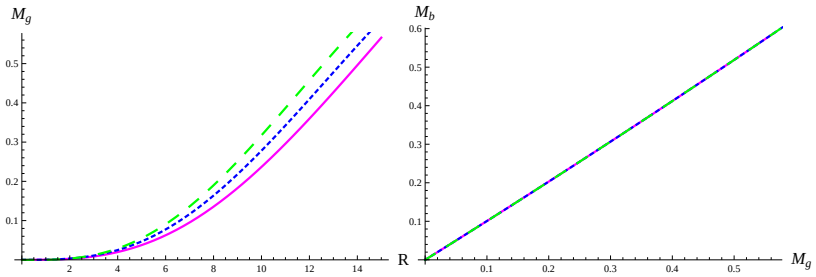

Figure 4.19: Plots of gravitational mass versus radius (left) and baryonic mass versus gravitational mass (right) corresponding to extended KB solution for case II.

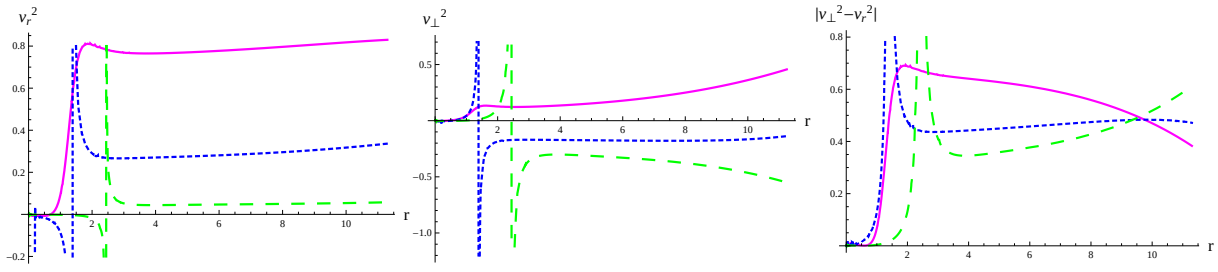

Figure 4.20: Plots of radial/tangential velocities and $|v_\perp^2 - v_r^2|$ corresponding to extended KB solution for case II.

at $r = R$ for all values of the decoupling parameter. Moreover, the state parameters are inversely proportional to ϱ while the anisotropy is directly proportional to the decoupling parameter. The plots of DEC in Figure **4.17** show that the anisotropic solution is physically valid for the chosen values of ϱ. The values of compactness parameter and surface redshift also lie in the desired range as displayed in Figure **4.18**. The gravitational mass increases with increase in the decoupling parameter as shown in Figure **4.19**. Moreover, the baryonic mass is maximum for $\varrho = 0.9$. The constructed model is stable only for $\varrho = 0.2$ as it violates causality and cracking conditions for higher values of the decoupling parameter (Figure **4.20**).

4.2 Extended Schwarzschild Solutions

In this section, we consider the Schwarzschild metric in Eq.(1.4.1) to determine the set (4.1.6)-(4.1.8). Consequently, $e^{\mu} = e^{-\xi} = 1 - \frac{2M}{r}$. The Schwarzschild spacetime has a singularity at $r = 0$ hidden behind an event horizon at $r = 2M$. According to the no-hair theorem, information about the BH is lost behind the event horizon as physical state of matter is unknown beyond this boundary. However, efforts have been made to study BHs in different perspectives in order to avoid this theorem [22]. The addition of scalar field [128] or another generic source of matter [35] in the vacuum leads to different BH solutions known as hairy BHs (with mass M and a discrete set of charges as primary hair). The major benefit of the EGD scheme is the transformation in temporal as well as radial metric components which increases the probability of hairy BH solutions with different horizons.

As there are five unknowns in the system (4.1.10)-(4.1.12), we apply two constraints to obtain the extended solution. In order to have a well-defined causal structure of the resultant spacetime, it is necessary that the causal horizon ($e^{-\chi}=0$) either covers the Killing horizon ($e^{\lambda}=0$) or coincides with it. Therefore, the first constraint is applied to the metric potentials as

$$\lambda=-\chi, \tag{4.2.1}$$

which leads to coinciding Killing and causal horizons. Setting $e^{-\chi}=0$ implies that both Killing and causal horizons occur at $r=2M$. The second constraint is applied to Θ-components through a linear EoS expressed in Eq.(4.1.28). Applying the condition (4.2.1) to Eqs.(4.1.4) and (4.1.5) yields the following relation between the deformation functions

$$f(r)=-\frac{(2M-r)\left(e^{\varrho g(r)}-1\right)}{\varrho r}. \tag{4.2.2}$$

The presence of an essential singularity is confirmed through Kretschmann scalar which is evaluated as

$$\begin{aligned}
\mathcal{K} &= \frac{1}{r^6}\left[\varrho^2r^4(r-2M)^2e^{2\varrho g(r)}g''^2+8\varrho Mr^2(2M-r)e^{2\varrho g(r)}g''(r)+\varrho^4r^4(r\right.\\
&- 2M)^2e^{2\varrho g(r)}g'^4-8\varrho^3Mr^3(2M-r)e^{2\varrho g(r)}g'^3+2\varrho^2r^2e^{2\varrho g(r)}g'^2\left(\varrho r^2\right.\\
&\times (r-2M)^2g''(r)+2\left(12M^2-6Mr+r^2\right)\Big)-8\varrho Mre^{2\varrho g(r)}g'(r)\left(\varrho r^2\right.\\
&\times (2M-r)g''(r)+8M-2r)+4\left(\left(12M^2-4Mr+r^2\right)e^{2\varrho g(r)}\right.\\
&+ \left.\left.2r(2M-r)e^{\varrho g(r)}+r^2\right)\right].
\end{aligned}$$

In the subsequent subsections, $\mathcal{K}$ is plotted to indicate the presence of a singularity at $r=0$. We compute decoupled solutions by choosing different values of the constants a_1 and a_2 corresponding to different scenarios in Eq.(4.1.28). Moreover, we determine

the massive scalar field by solving the wave equation numerically for $m_\Psi = 0.1$ and $\omega_{BD} = 60$. The behavior of the obtained BH solutions is checked for $\varrho = -0.4,\ -0.5,\ -0.7$. It is noteworthy to mention here that under the applied constraints, the positive behavior of density is achieved for negative values of the decoupling parameter only.

4.2.1 Traceless Θ^{γ}_{δ}

The additional source has a traceless energy-momentum tensor when

$$\Theta^0_0 + \Theta^1_1 = -2\Theta^2_2,$$

(since $\Theta^2_2 = \Theta^3_3$), i.e., Θ^{γ}_{δ} is traceless when $a_1 = -1$ and $a_2 = -2$ in Eq.(4.1.28) which yields

$$\begin{aligned}
&\frac{1}{r\Psi(r)}\left(e^{-\xi(r)}\left(\varrho\Psi(r)r\left(3\Psi'(r)r\left(e^{\xi(r)}f'(r)+g'(r)\right)+\Psi(r)\left(e^{\xi(r)}f'(r)\right.\right.\right.\right.\\
&\times(\varrho rg'(r)+r\mu'(r)+4)+2rg''(r)+g'(r)(\varrho rg'(r)+2r\mu'(r)-r\\
&\times\xi'(r))+4))+\varrho f(r)e^{\xi(r)}(3r\Psi(r)(\Psi'(r)(\varrho rg'(r)+r\mu'(r)+4)\\
&+2r\Psi''(r))+\Psi^2(r)\left(r\left(r\left(2\left(\varrho g''(r)+\mu''(r)\right)+\mu'^2(r)\right)+\varrho^2rg'^2(r)\right.\right.\\
&\left.\left.\left.\left.+2\varrho g'(r)(r\mu'(r)+2)+4\mu'(r))+4)+2r^2\omega_{BD}\Psi'^2(r)\right)\right)\right)=0. \qquad (4.2.3)
\end{aligned}$$

The deformation function $g(r)$ is evaluated by solving the above equation numerically along with the wave equation subject to the initial conditions $\Psi(2M) = 0.8,\ \Psi'(2M) = 0.1,\ g(2M) = 1$ and $g'(2M) = 0.1$. The Kretschmann scalar shown in Figure **4.21** approaches to infinity when $r \to 0$. Thus, a singularity exists at $r = 0$. The graphical analysis of state variables is done in the region accessible to an outer-observer with $M = 1$ (Figure **4.22**). The energy density and tangential pressure increase as the

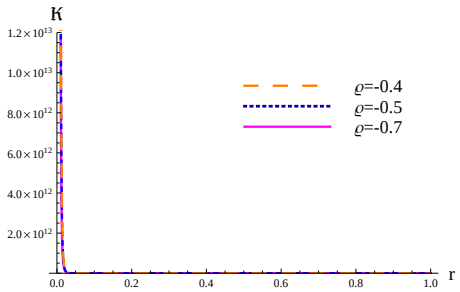

Figure 4.21: Plot of $\mathcal{K}$ for case I.

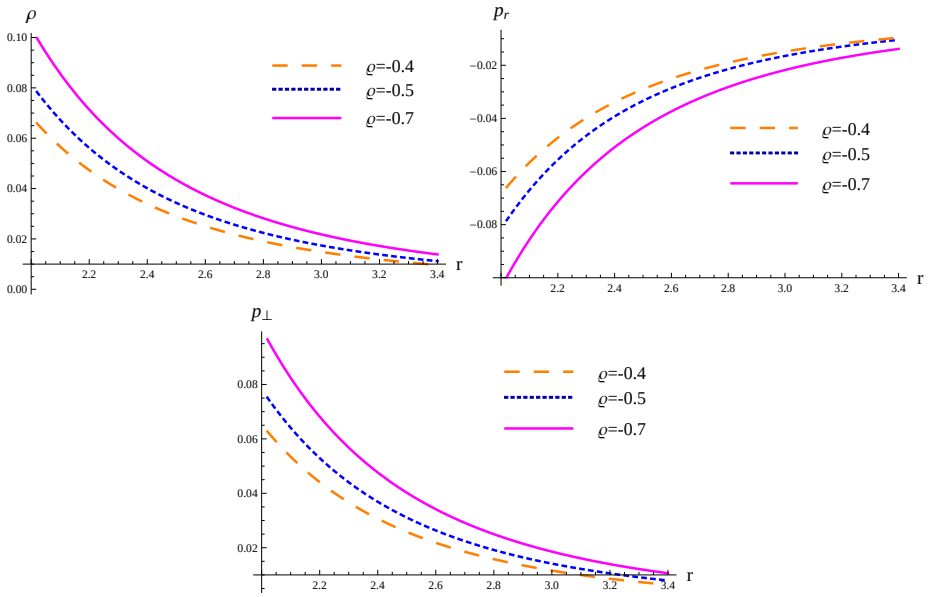

Figure 4.22: Plots of matter variables for case I.

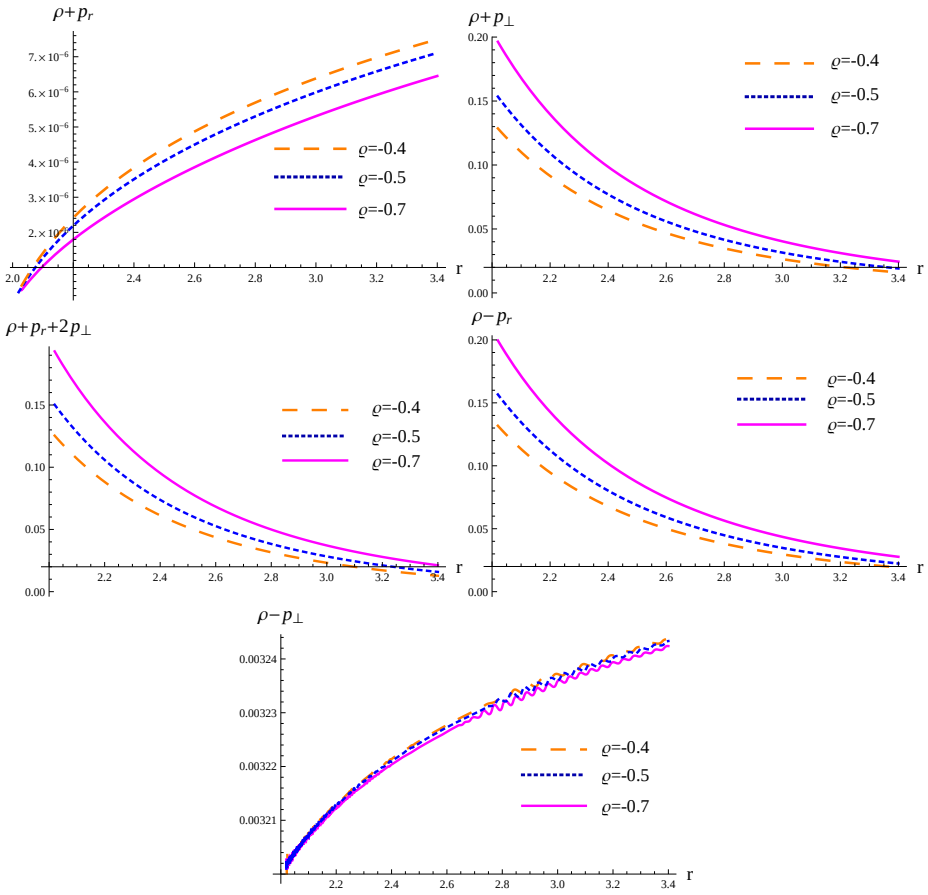

Figure 4.23: Energy conditions for case I.

decoupling parameter decreases. However, radial pressure is directly proportional to ϱ. It is noted that positive energy density is obtained when radial pressure is negative. Figure **4.23** shows that all bounds on energy density and pressure components are satisfied in the considered setup. The plot of metric potentials in Figure **4.24** indicates that the new solution preserves asymptotic flatness for large values of the radial coordinate.

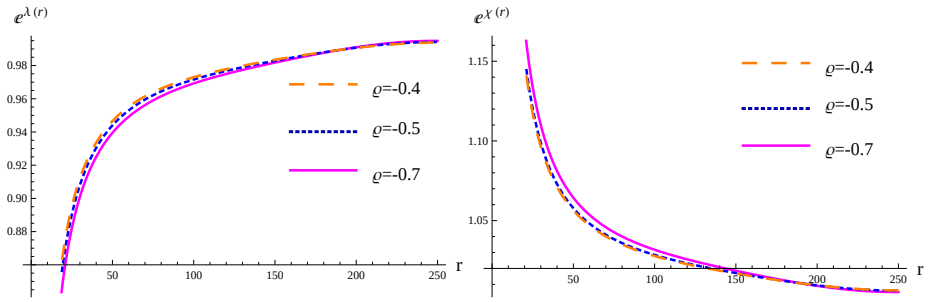

Figure 4.24: Metric potentials for case I.

4.2.2 Barotropic Equation of State

The new source is polytropic if it satisfies the EoS

$$\Theta_1^1 = K(\Theta_0^0)^{1+\frac{1}{n}}.$$

Different values of the polytropic index correspond to different types of fluids. We proceed by taking the simplest case of barotropic fluid (isothermal sphere of gas). The resulting EoS is equivalent to Eq.(4.1.28) for $a_1 = -\frac{1}{K}$ and $a_2 = 0$ which is expressed as

$$\begin{aligned}&\frac{1}{Kr\Psi(r)}\left(\varrho e^{-\xi(r)}\left(r\Psi(r)\left(r\Psi'(r)+2\Psi(r)\right)\left(Ke^{\xi(r)}f'(r)+g'(r)\right)\right.\right.\\&+f(r)e^{\xi(r)}\left(r\Psi(r)\left(\Psi'(r)\left(\varrho r g'(r)+4K+r\mu'(r)+4\right)+2Kr\Psi''(r)\right)\right.\\&\left.\left.+2\Psi^2(r)\left(\varrho\, r g'(r)+K+r\mu'(r)+1\right)+(K-1)r^2\omega_{BD}\Psi'^2(r)\right)\right)\right)=0.\end{aligned} \tag{4.2.4}$$

Employing Eq.(4.2.2) and the initial conditions used in case I, wave equation and Eq.(4.2.4) are solved simultaneously for $\Psi(r)$ and $g(r)$, respectively with $M = 1$.

Figure **4.25** demonstrates the presence of a singularity at $r = 0$ in the current setup. The plots of energy density and pressure components are displayed in Figure

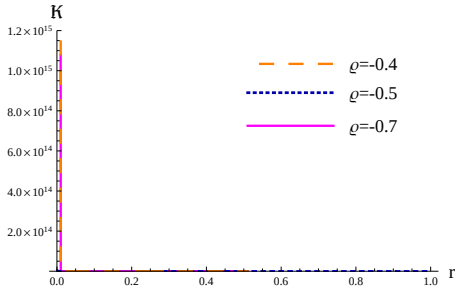

Figure 4.25: Plot of $\mathcal{K}$ for case II.

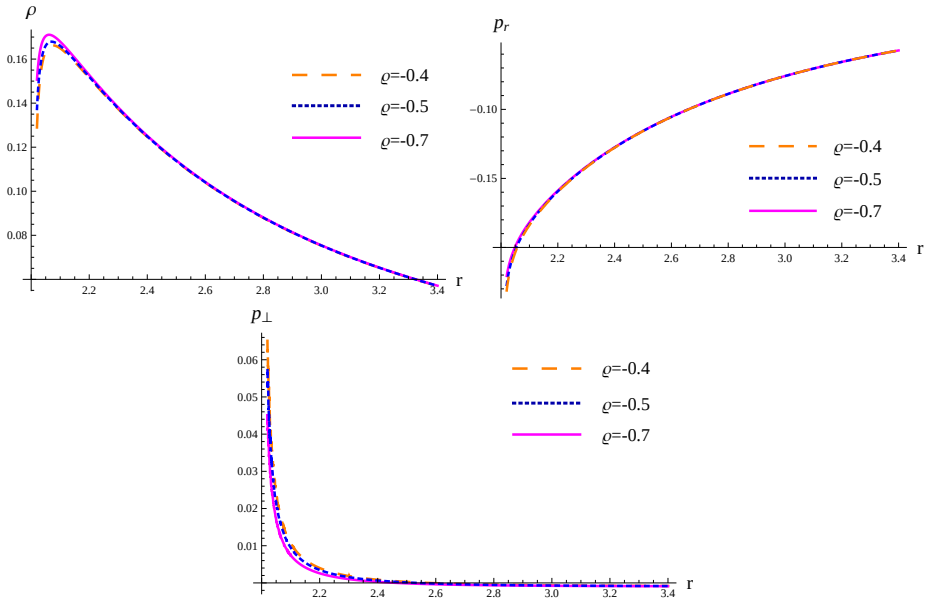

Figure 4.26: Matter variables for case II.

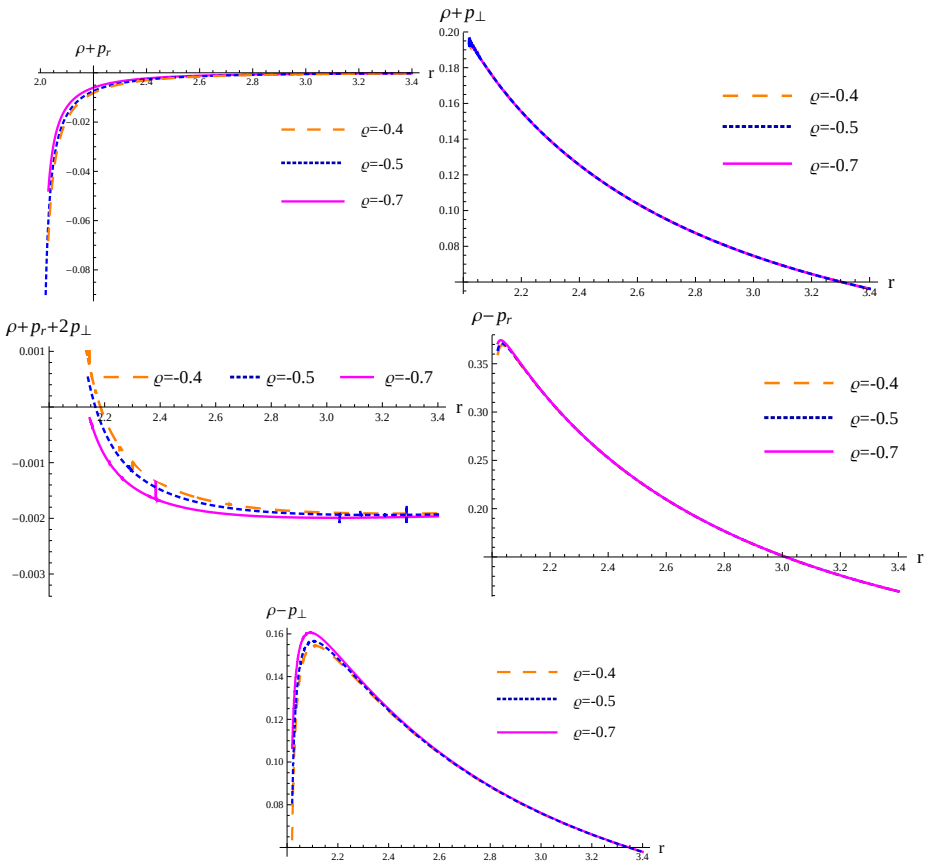

Figure 4.27: Energy conditions for case II.

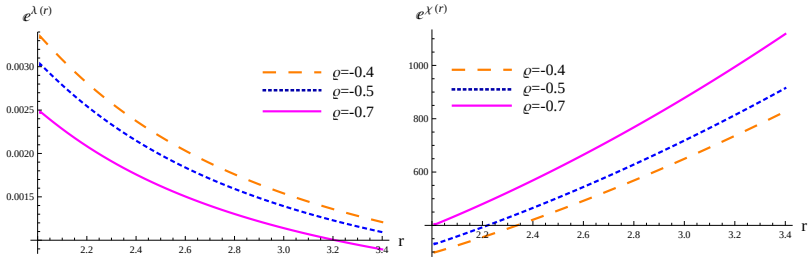

Figure 4.28: Metric potentials for case II.

4.26 for $K = 0.01$. The celestial object becomes less dense for higher values of ϱ. The density increases to a maximum and then decreases monotonically for $r > 2M$. Moreover, the radial pressure decreases while tangential pressure increases as the decoupling parameter takes on higher values. The plots in Figure **4.27** indicate that the extended solution fails to satisfy the energy conditions as $\rho + p_r < 0$ and $\rho + p_r + 2p_\perp < 0$ for the chosen values of ϱ. Thus, the unknown source Θ_δ^γ can be treated as exotic matter in this case. Finally, the metric potentials representing the spacetime of this setup are shown in Figure **4.28**. It can be clearly observed that trends of e^λ and e^χ do not approach 1 and thus, disobey the criterion of asymptotic flatness.

4.2.3 A Particular Solution

Here, we evaluate a specific solution by inserting $a_1 = 1.4$ and $a_2 = 3$ in Eq.(4.1.28) leading to

$$\frac{1}{r\Psi(r)}\left(\varrho e^{-\xi(r)}\left(r\Psi(r)\left(r\Psi'(r)\left(e^{\xi(r)}f'(r)+2.2g'(r)\right)+\Psi(r)\left(e^{\xi(r)}f'(r)\right.\right.\right.\right.$$
$$\times(0.75\varrho rg'(r)+0.75r\mu'(r)+0.5)+1.5rg''(r)+g'(r)(0.75\varrho rg'(r)$$
$$+1.5r\mu'(r)-0.75r\xi'(r)+2.9)))+f(r)e^{\xi(r)}(r\Psi(r)(\Psi'(r)(2.2\varrho rg'(r)$$
$$+2.2r\mu'(r)+3.8)+2r\Psi''(r))+\Psi^2(r)\left(r\left(1.5\varrho rg''(r)+0.75\varrho^2rg'^2(r)\right.\right.$$
$$\left.\left.+\varrho g'(r)(1.5r\mu'(r)+2.9)+1.5r\mu''(r)+0.75r\mu'^2(r)+2.9\mu'(r)\right)+0.4\right)$$
$$\left.\left.\left.+0.3r^2\omega_{BD}\Psi'^2(r)\right)\right)\right)=0. \tag{4.2.5}$$

The extended solution is formulated by plugging the values of $\xi(r)$, $\mu(r)$ and $f(r)$ in wave equation and Eq.(4.2.5) and solving them for initial conditions of case I with $M = 1$. A singularity exists at $r = 0$ since the plot of $\mathcal{K}$ in Figure **4.29** tends to

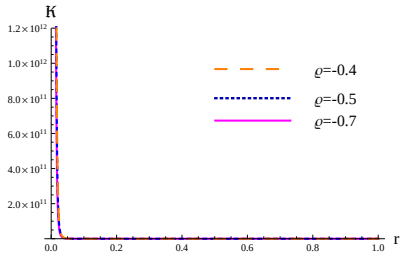

Figure 4.29: Plot of $\mathcal{K}$ for case III.

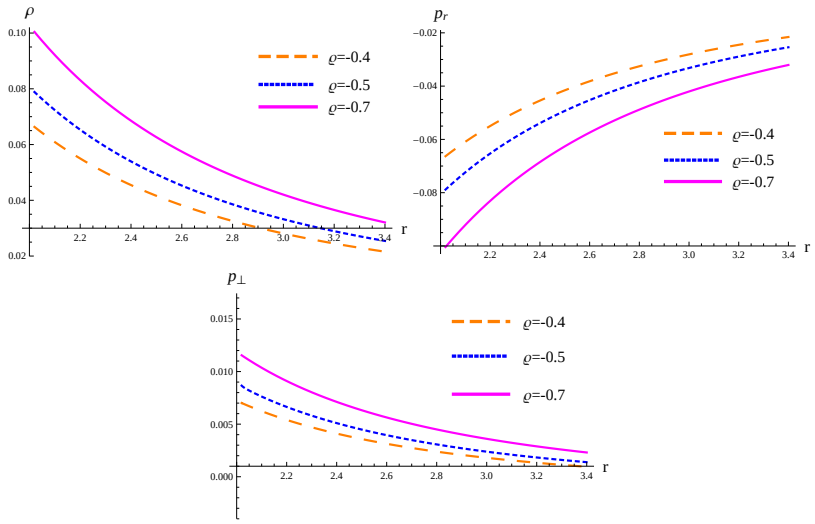

Figure 4.30: Matter variables for case III.

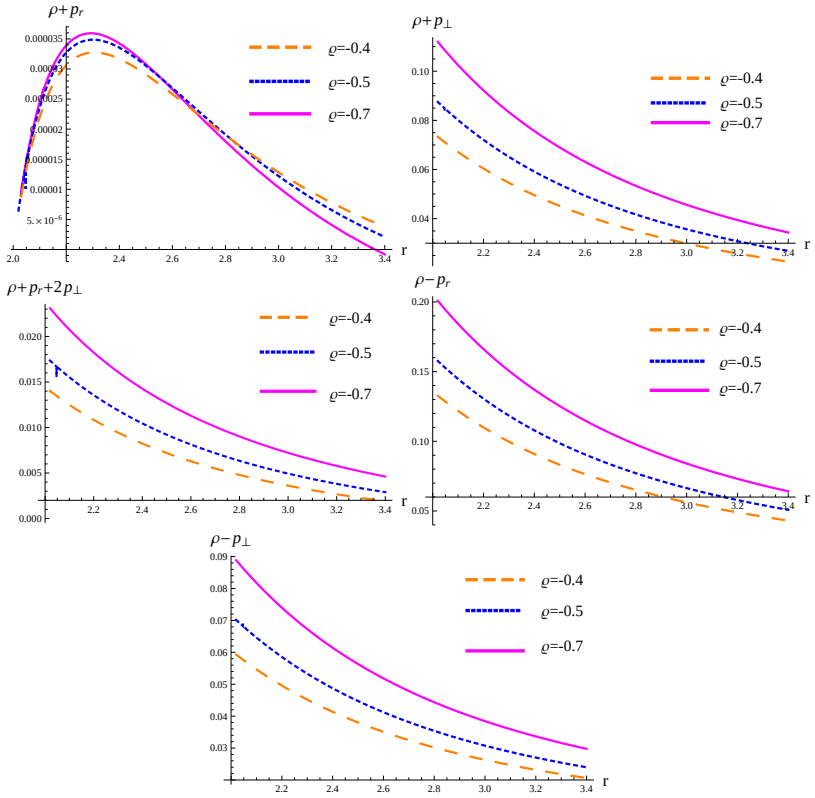

Figure 4.31: Energy conditions for case III.

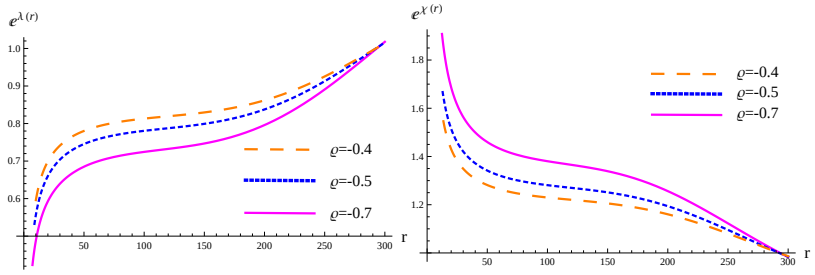

Figure 4.32: Metric potentials for case III.

infinity for $r \to 0$. The state variables of the solution are plotted in Figure **4.30** for chosen values of the decoupling parameter. The energy density and tangential pressure are maximum at the horizon and decrease monotonically as r increases. The decrease in the values of decoupling parameter causes an increase in density and transverse pressure whereas the radial pressure increases with increase in ϱ. The energy constraints are satisfied by Θ_{δ}^{γ} (Figure **4.31**) ensuring the presence of normal matter. The metric functions represent a spacetime that is asymptotically flat as shown in Figure **4.32**.

Chapter 5

Anisotropic Strange Stars through Embedding Technique in MBD Gravity

This chapter investigates the existence and properties of anisotropic strange quark stars in the context of MBD theory. The field equations are constructed by assuming a suitable potential function with MIT bag model. We employ the embedding class-one approach as well as junction conditions to determine the unknown metric functions. Radius of the strange star candidate, LMC X-4, is predicted through its observed mass for different values of the bag constant. We analyze the effects of coupling parameter as well as mass of scalar field on state determinants and execute multiple checks on the stability and viability of the spherical system.

This chapter is organized as follows. In section **5.1**, we construct a system of field equations and physical variables using MIT bag model. Section **5.2** gives an overview of junction conditions for a smooth matching between intrinsic and extrinsic geometries. The physical properties, validity and stability are examined in section **5.3**. The results of this chapter are published in [129].

5.1 Embedding Class-one Solution via MIT Bag Model

The field equations required to construct the anisotropic model are represented by Eqs.(4.1.1)-(4.1.3). The embedding class-one condition (1.8.1) leads to the following differential equation for the metric (2.1.1)

$$(\chi' - \lambda')\lambda' e^{\chi} + 2(1 - e^{\chi})\lambda'' + \lambda'^2 = 0. \tag{5.1.1}$$

The solution of the above equation turns out to be

$$\chi(r) = \ln(1 + \hat{B}\lambda'^2 e^{\lambda}), \tag{5.1.2}$$

where $\hat{B}$ is a constant of integration. Maurya et al. [130] constructed a new class of solutions using the following form of metric potential

$$\lambda(r) = 2r^2\hat{A} + \ln\hat{C}, \tag{5.1.3}$$

where $\hat{A}$ and $\hat{C}$ are positive constants. Using this value in Eq.(4.1.6), we have

$$\chi(r) = \ln(1 + \hat{A}\hat{D}r^2 e^{2\hat{A}r^2}), \tag{5.1.4}$$

where $\hat{D} = 16\hat{A}\hat{B}\hat{C}$ is a constant.

Neutron stars with $M > 3M_{\odot}$ may transform into quark stars which contain up (u), down (d) and strange (s) quark flavors. The matter variables describing the interior configuration of these relativistic stars obey MIT bag EoS. According to the MIT bag model, the quark pressure is stated in Eq.(1.5.3). The simplified form of this EoS has been used in GR and modified theories to examine the features of quark star candidates. In our study, the numerical results of the model have been obtained

by taking $\mathcal{B}$ equal to $64MeV/fm^3$ and $83MeV/fm^3$ which are within the allowed limit [131]. The total mass of a sphere of radius r is evaluated through Misner-Sharp formula (1.2.1).

5.1.1 Matching Conditions

The set of parameters $(\hat{A},\ \hat{B},\ \hat{C},\ \hat{D})$ defining the geometry as well as physical properties (such as mass and radius) of anisotropic compact objects can be determined through the smooth matching of interior and exterior spacetimes on the boundary of the star. The exterior region is taken to be the Schwarzschild spacetime. Moreover, the scalar field corresponding to the vacuum Schwarzschild solution is derived using the technique in [53] which comes out to be $\Psi = e^{(1-\frac{2M}{r})}$. We denote the interior and exterior regions by $\mathcal{V}^-$ and $\mathcal{V}^+$, respectively.

The hypersurface ($\hat{h} = r - R = 0, R$ is constant radius) is defined by the metric

$$ds^2 = d\tau^2 - R^2(d\theta^2 + \sin^2\theta d\phi^2), \tag{5.1.5}$$

where τ is the proper time on the boundary. The extrinsic curvature of Σ is given by

$$K^{\pm}_{ij} = -\mathfrak{n}^{\pm}_{\gamma}\frac{\partial^2 x^{\gamma}_{\pm}}{\partial\nu^i\nu^j} - \mathfrak{n}^{\pm}_{\gamma}\Gamma^{\gamma}_{\delta\mu}\frac{\partial x^{\delta}_{\pm}}{\partial\nu^i}\frac{\partial x^{\mu}_{\pm}}{\partial\nu^j}, \quad i,j = 1,2,3,$$

where ν^i are the coordinates defined on Σ. Moreover, the components of the four-vector normal $(\mathfrak{n}^{\pm}_{\gamma})$ to the hypersurface are defined in the coordinates $(x^{\gamma}_{\pm})$ of $\mathcal{V}^{\pm}$ as

$$\mathfrak{n}^{\pm}_{\gamma} = \frac{d\hat{h}}{dx^{\gamma}}|g^{\delta\mu}\frac{d\hat{h}}{dx^{\delta}}\frac{d\hat{h}}{dx^{\mu}}|^{\frac{-1}{2}},$$

with $\mathfrak{n}_{\gamma}\mathfrak{n}^{\gamma} = 1$. The unit normal vectors have the following form

$$\mathfrak{n}^{-}_{\gamma} = (0, e^{\frac{\chi}{2}}, 0, 0), \quad \mathfrak{n}^{+}_{\gamma} = (0, (1-\frac{2M}{r})^{\frac{-1}{2}}, 0, 0). \tag{5.1.6}$$

Comparing the metrics (1.4.1) and (2.1.1) with (5.1.5), it follows that

$$[\frac{dt}{d\tau}]_\Sigma = [e^{\frac{-\lambda}{2}}]_\Sigma = [(1-\frac{2M}{r})^{\frac{-1}{2}}]_\Sigma, \quad [r]_\Sigma = R. \tag{5.1.7}$$

Using Eq.(5.1.6), the non-zero components of curvature are calculated as

$$\begin{aligned} K^-_{00} &= [-\frac{e^{-\frac{\chi}{2}}\lambda'}{2}]_\Sigma, \quad K^-_{22} = \frac{1}{\sin^2(\theta)}K^-_{33} = [re^{-\frac{\chi}{2}}]_\Sigma, \\ K^+_{00} &= [-\frac{M}{r^2}(1-\frac{2M}{r})^{\frac{-1}{2}}]_\Sigma, \quad K^+_{22} = \frac{1}{\sin^2(\theta)}K^+_{33} = [r(1-\frac{2M}{r})^{\frac{1}{2}}]_\Sigma. \end{aligned}$$

The junction conditions $[K^-_{22}]_\Sigma = [K^+_{22}]_\Sigma$ and $[r]_\Sigma = R$ yield

$$e^{-\frac{\chi(R)}{2}} = (1-\frac{2M}{R})^{\frac{1}{2}}. \tag{5.1.8}$$

Substituting the above equation in the matching condition $[K^-_{00}]_\Sigma = [K^+_{00}]_\Sigma$ gives

$$\lambda'(R) = \frac{2M}{R(R-2M)}. \tag{5.1.9}$$

Thus, the matching conditions in Eqs.(5.1.7)-(5.1.9) provide the following relations at the hypersurface

$$\begin{aligned} e^{\lambda(R)} &= \hat{C}e^{2\hat{A}r^2} = 1-\frac{2M}{R}, \\ e^{-\chi(R)} &= \frac{1}{1+\hat{A}\hat{D}R^2e^{2\hat{A}R^2}} = 1-\frac{2M}{R}, \\ \lambda'(R) &= \frac{2M}{R(R-2M)}. \end{aligned}$$

Inserting $D = 16ABC$ in the above equations, the deterministic parameters of the system are expressed as

$$\hat{A} = \frac{M}{2R^2(R-2M)}, \tag{5.1.10}$$

$$\hat{B} = \frac{R^3}{2M}, \tag{5.1.11}$$

$$\hat{C} = e^{\frac{M}{2M-R}}\frac{R-2M}{R}, \tag{5.1.12}$$

$$\hat{D} = 4e^{\frac{M}{2M-R}}. \tag{5.1.13}$$

For the metric functions in Eqs.(5.1.3) and (5.1.4) along with Eqs.(5.1.10)-(5.1.13), the state variables are expressed in Eqs.(A1)-(A3).

5.2 Physical Features of Compact Stars

The effect of coupling parameter as well as mass of scalar field on stellar structure can now be analyzed through the energy density and radial/transverse pressure components. Numerical results have been obtained for $V(\Psi) = \frac{1}{2}m_{\Psi}^2\Psi^2$, $\omega_{BD} = 20,\ 25,\ 30$ and $m_{\Psi} = 0.001,\ 0.3$ which are in accordance with the constraints imposed by the solar system observations [43]. The expression of scalar field is derived by solving the wave equation numerically with the initial conditions $\Psi(0) = \Psi_c$ =constant and $\Psi'(0) = 0$. The values of Ψ_c for different values of m_{Ψ}, ω_{BD} and $\mathcal{B}$ are given in Tables **5.1** and **5,2**. All deductions have been presented graphically for LMC X-4 ($M = 1.29M_{\odot}$ [132]).

Using the condition $p_r(R) = 0$, radius as well as physical parameters of the strange star candidate are displayed in Tables **5.1** and **5.2** for $m_{\Psi} = 0.001$ and $m_{\Psi} = 0.3$, respectively. Here, the subscripts c and s denote that the quantity has been calculated at the center and surface of the star, respectively. For a physically valid solution, the metric potentials must be positive, regular and monotonically increasing functions of the radial coordinate [133]. The metric potential functions are shown in Figure **5.1** which reveal their regular behavior leading to singularity free system.

The influence of physical variables such as energy density and pressure cannot be

Table 5.1: Physical parameters of LMC X-4 with $m_\Psi = 0.001$ for different values of ω_{BD} and $\mathcal{B}$.

$\mathcal{B} = 64MeV/fm^3$					
ω_{BD}	Ψ_c	Predicted Radius (km)	$\rho_c\ (gm/cm^3)$	$\rho_s\ (gm/cm^3)$	$p_c\ (dyne/cm^2)$
20	0.0204	$8.3141^{+0.3293}_{-0.3285}$	6.6437×10^{14}	4.6155×10^{14}	7.1544×10^{34}
25	003055	$9.6173^{+0.3863}_{-0.3847}$	6.2865×10^{14}	4.5450×10^{14}	5.6021×10^{34}
30	0.04445	$10.9515^{+0.449}_{-0.446}$	6.1019×10^{14}	4.6035×10^{14}	4.8650×10^{34}
GR limit		5.54	9.498×10^{16}	6.823×10^{16}	3.540×10^{36}
$\mathcal{B} = 83MeV/fm^3$					
ω_{BD}	Ψ_c	Predicted Radius (km)	$\rho_c\ (gm/cm^3)$	$\rho_s\ (gm/cm^3)$	$p_c\ (dyne/cm^2)$
20	00264	$8.3397^{+0.3582}_{-0.3315}$	8.5180×10^{14}	5.9133×10^{14}	9.0542×10^{34}
25	0.0399	$9.6669^{+0.3931}_{-0.3908}$	8.1568×10^{14}	5.9266×10^{14}	7.1989×10^{34}
30	0.0578	$11.0422^{+0.4622}_{-0.4577}$	7.9254×10^{14}	5.8838×10^{14}	6.3199×10^{34}
GR limit		5.55	9.498×10^{16}	6.823×10^{16}	3.564×10^{36}

Table 5.2: Physical parameters of LMC X-4 with $m_\Psi = 0.3$ for different values of ω_{BD} and $\mathcal{B}$.

$\mathcal{B} = 64MeV/fm^3$					
ω_{BD}	Ψ_c	Predicted Radius (km)	$\rho_c\ (gm/cm^3)$	$\rho_s\ (gm/cm^3)$	$p_c\ (dyne/cm^2)$
20	0.0204	$8.3141^{+0.3293}_{-0.3285}$	6.7762×10^{14}	4.7467×10^{14}	7.1905×10^{34}
25	0.03055	$9.6173^{+0.3863}_{-0.3847}$	6.6665×10^{14}	4.9018×10^{14}	5.8065×10^{34}
30	0.04555	$10.9515^{+0.449}_{-0.446}$	6.7427×10^{14}	5.1681×10^{14}	4.9215×10^{34}
$\mathcal{B} = 83MeV/fm^3$					
ω_{BD}	Ψ_c	Predicted Radius (km)	$\rho_c\ (gm/cm^3)$	$\rho_s\ (gm/cm^3)$	$p_c\ (dyne/cm^2)$
20	0.0264	$8.3397^{+0.3582}_{-0.3315}$	8.7829×10^{14}	6.1661×10^{14}	9.1757×10^{34}
25	0.0399	$9.6669^{+0.3931}_{-0.3908}$	8.5916×10^{14}	6.3427×10^{14}	7.2289×10^{34}
30	0.0578	$11.0422^{+0.4622}_{-0.4577}$	8.8271×10^{14}	6.9153×10^{14}	6.0806×10^{34}

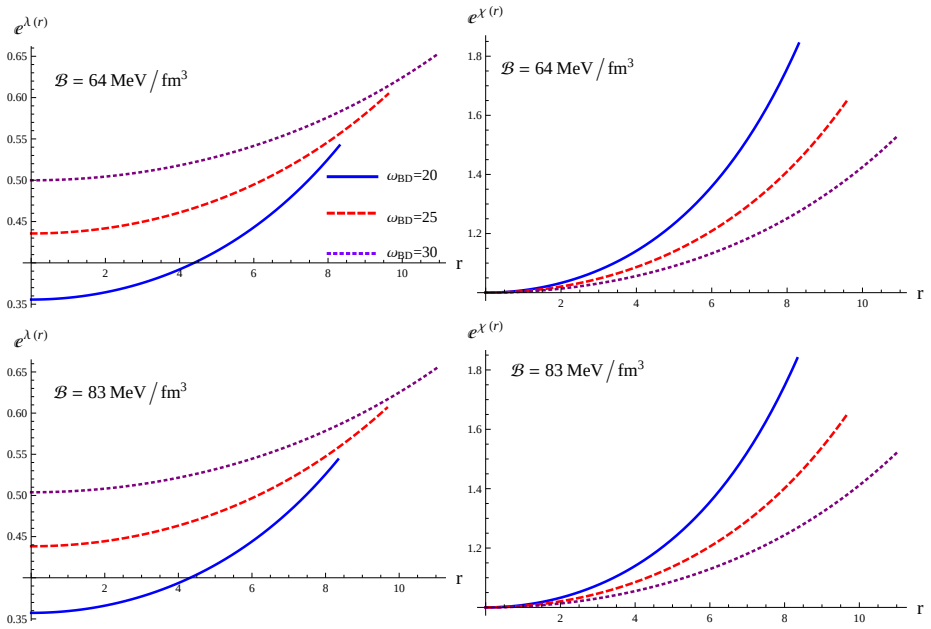

Figure 5.1: Plots of metric potentials for massive scalar field versus radial coordinate.

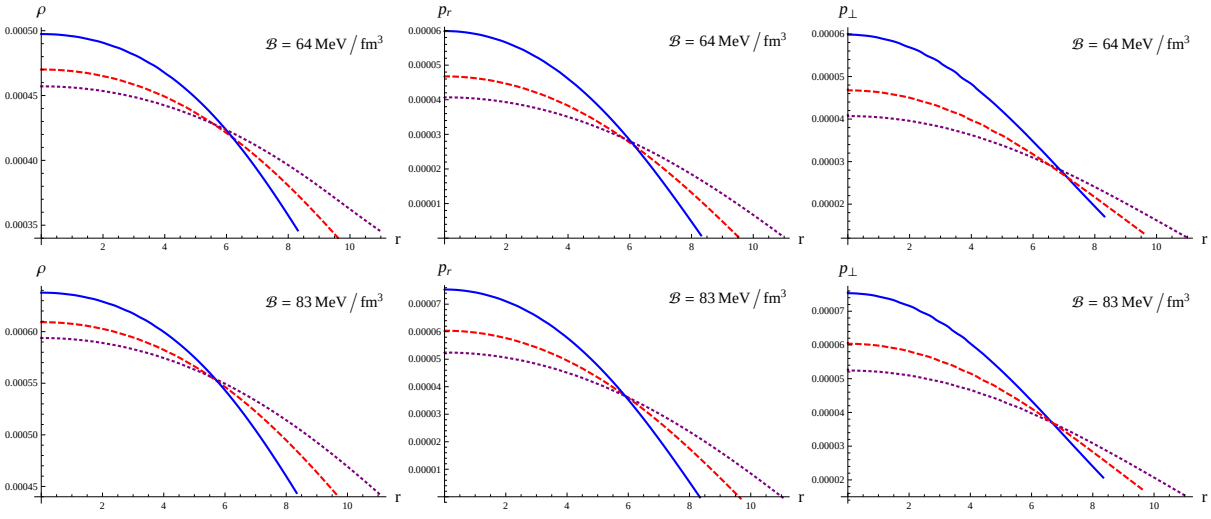

Figure 5.2: Effective energy density, effective radial/transverse pressure as functions of r with $m_\Psi = 0.001$.

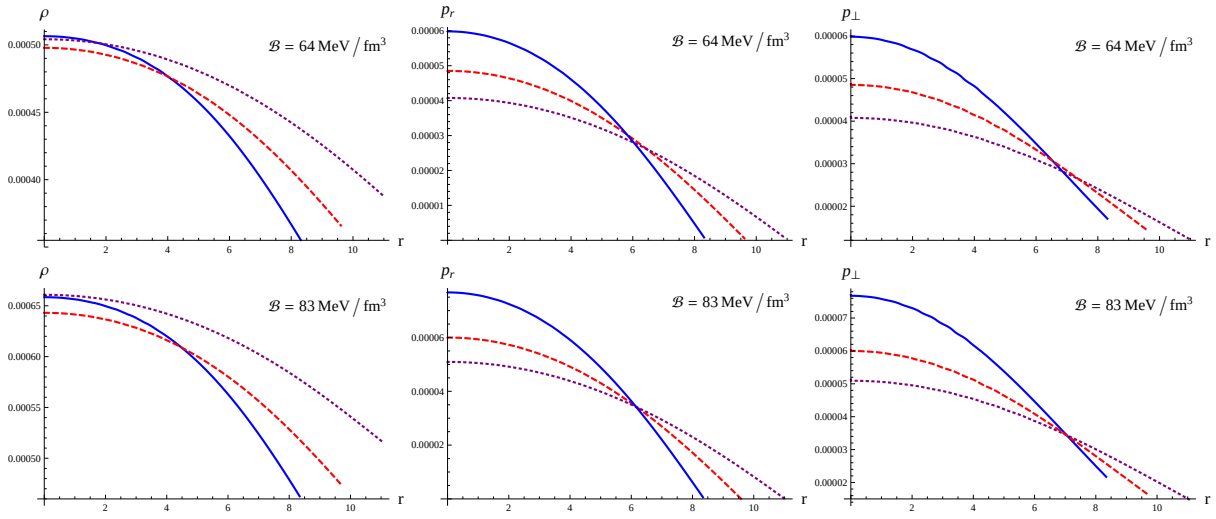

Figure 5.3: Effective energy density, effective radial/transverse pressure as functions of r with $m_\Psi = 0.3$.

neglected in extremely dense strange stars. The behavior of these physical quantities with respect to the radial coordinate is positive throughout and maximum at the center of compact configuration as presented in Figures **5.2** and **5.3** which shows that the core is highly concentrated for the chosen values of the parameters (m_Ψ, ω_{BD}, $\mathcal{B}$). The plots also depict the monotonic decreasing trend of energy density and pressure components away from the center of stars leading to a compact profile. Hence, for the considered values of $\mathcal{B}$, the existence of quark stars is ensured for $V(\Psi) = \frac{1}{2}m_\Psi^2\Psi^2$.

The radial and tangential components of pressure give rise to anisotropy within the structure. The anisotropy of pressure is positive when $p_\perp > p_r$ and negative otherwise. The positive and increasing behavior of anisotropy suggests that an outward directed repelling force is in play in the interior of stellar models stabilizing the system against gravity. Utilizing Eqs.(A2) and (A3), the anisotropy comes out to be

$$\Delta = \frac{\xi\Psi}{r}\left[M^2r^3\Psi^2(r)\left(1-2e^{\frac{M(r-R)(r+R)}{R^2(R-2M)}}\right)^2 - rR^2\omega_{BD}(2M-R)\right.$$

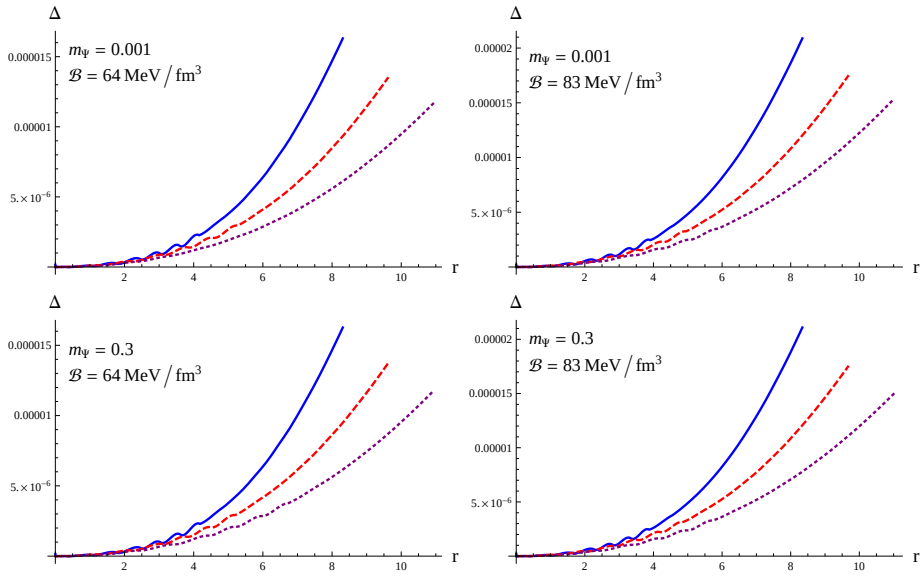

Figure 5.4: Variation of effective anisotropy as a function of r.

$$\times \quad \left(2Mr^2 e^{\frac{M(r-R)(r+R)}{R^2(R-2M)}} + R^2(R-2M)\right)\Psi'^2(r) + \Psi(r)\left(R^4\left(-(R-2M)^2\right)\right.$$
$$\times \quad (\Psi'(r) - r\Psi''(r)) - 2Mr^2 e^{\frac{M(r-R)(r+R)}{R^2(R-2M)}}\left(\left(Mr^2 - 4MR^2 + 2R^3\right)\Psi'(r)\right.$$
$$+ \quad rR^2(2M-R)\Psi''(r))\Big)\Big] .$$

Figure **5.4** indicates that the behavior of anisotropy is acceptable for the selected model.

5.2.1 Energy Conditions

A configuration is said to be realistic if it satisfies all four energy conditions, i.e., NEC, WEC, SEC and DEC. These conditions are expressed in Eqs.(1.9.4)-(1.9.7). As Figures **5.2** and **5.3** depict positive behavior of ρ, p_r and $p_\perp$ throughout the stellar structure, therefore the first three conditions are readily satisfied. The plot of DEC in Figure **5.5** is positive at each point within the stellar structure. Hence,

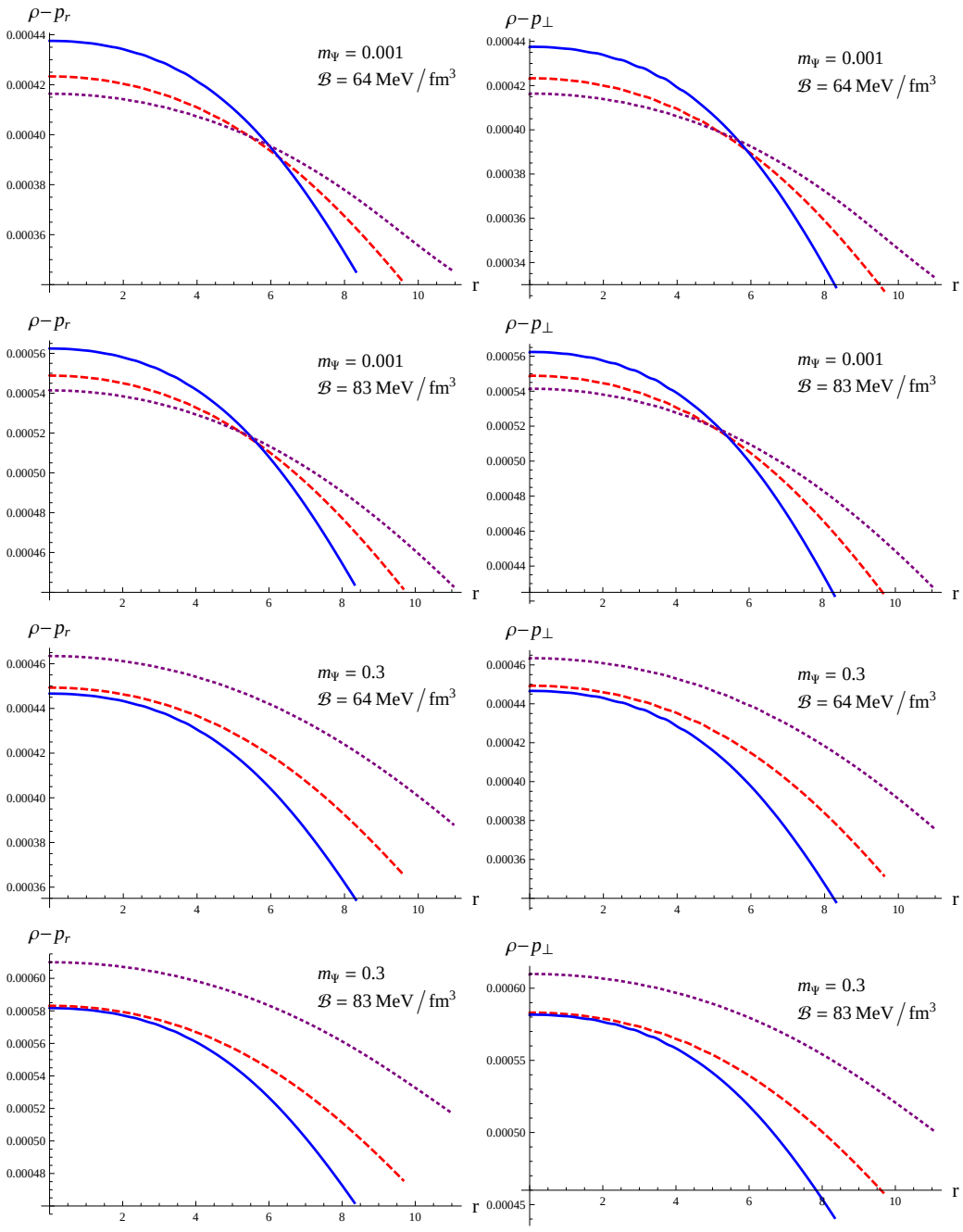

Figure 5.5: DEC plotted against the radial coordinate.

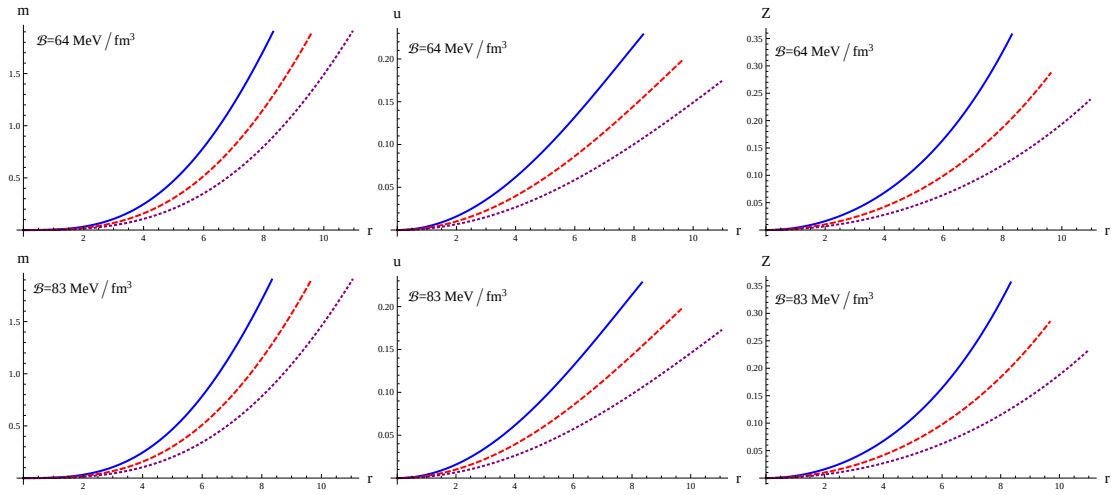

Figure 5.6: Plots of relation between mass, compactness factor and redshift against radial coordinate.

all energy conditions are satisfied which validate the model for the chosen values of m_Ψ, $\mathcal{B}$ and ω_{BD}.

5.2.2 Effective Mass, Compactness and Redshift

The size and mass are two inter-related observable features of a compact object. The effective mass for the current structure is calculated via Eq.(1.2.1) as

$$m(r) = \frac{r}{2}\left[\frac{2Mr^2 e^{\frac{M(R^2-r^2)}{R^2(2M-R)}}}{R^2(R-2M)+2Mr^2 e^{\frac{M(R^2-r^2)}{R^2(2M-R)}}}\right],$$

which is dependent on the radius of celestial body. Figure **5.6** shows a decrease in mass for a larger value of $\mathcal{B}$. The compactness function is the ratio of mass to radius given as

$$u(r) = \frac{m(r)}{r} = \frac{1}{2}\left[\frac{2Mr^2 e^{\frac{M(R^2-r^2)}{R^2(2M-R)}}}{R^2(R-2M)+2Mr^2 e^{\frac{M(R^2-r^2)}{R^2(2M-R)}}}\right].$$

Figure **5.6** displays the compactness factor as a monotonic increasing function with respect to the radial coordinate. The values attained by the function adhere to the upper limit $\frac{m}{R} < \frac{4}{9}$, proposed by Buchdal [120] for both values of bag constant. Further, the gravitational redshift is a measure of the force exerted on light as a consequence of strong gravity. The relativistic effect can be measured from the X-ray spectrum of the cosmic object using the compactness factor which is defined as

$$Z = \frac{1}{\sqrt{1-2u(r)}} - 1,$$

leading to the following expression

$$Z = -1 + \sqrt{1 + \frac{2Mr^2 e^{\frac{M(R^2-r^2)}{R^2(2M-R)}}}{R^2(R-2M)}}.$$

Figure **5.6** exhibits the redshift as an increasing function of radial coordinate. We would like to mention here that the surface redshift for the stellar candidate is consistent with the limit for relativistic stars ($Z < 5.211$) [121].

5.2.3 Stability of Stellar System

In this section, we examine stability of the anisotropic setup through causality condition, cracking approach and adiabatic index. Figures **5.7** and **5.8** shows that anisotropic distribution agrees with the causality condition as well as cracking approach in the framework of MBD theory.

The expression for adiabatic index for our system is given by

$$\Gamma = \frac{p_r + \rho}{p_r}\frac{dp_r}{d\rho} = \frac{p_r + \rho}{p_r}v_r^2.$$

The graphical analysis of adiabatic index in the presence of a scalar field can be seen in Figure **5.9**. The value of this index is more than $\frac{4}{3}$ for all stars which is in

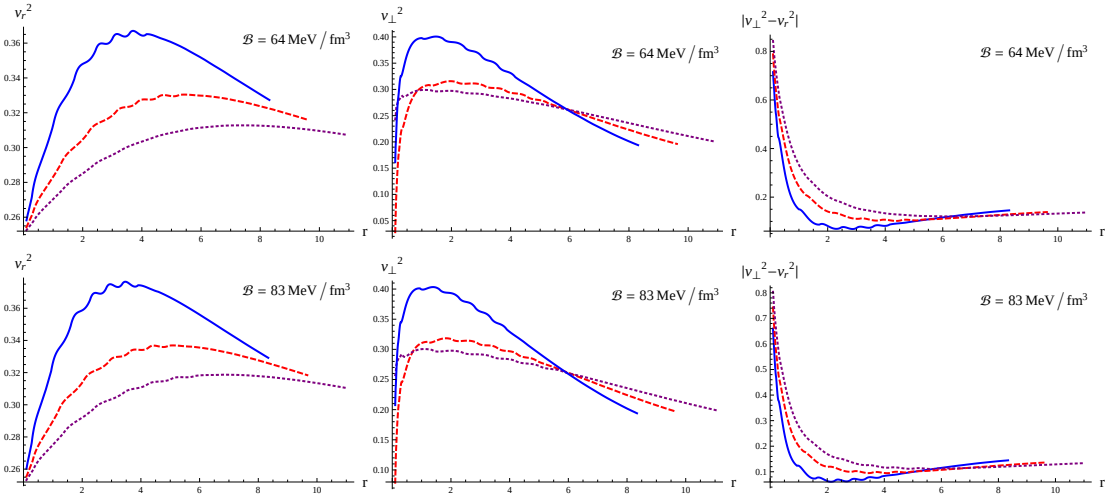

Figure 5.7: Variation of radial velocity, tangential velocity and $|v_\perp^2 - v_r^2|$ with respect to radial coordinate with $m_\Psi = 0.001$.

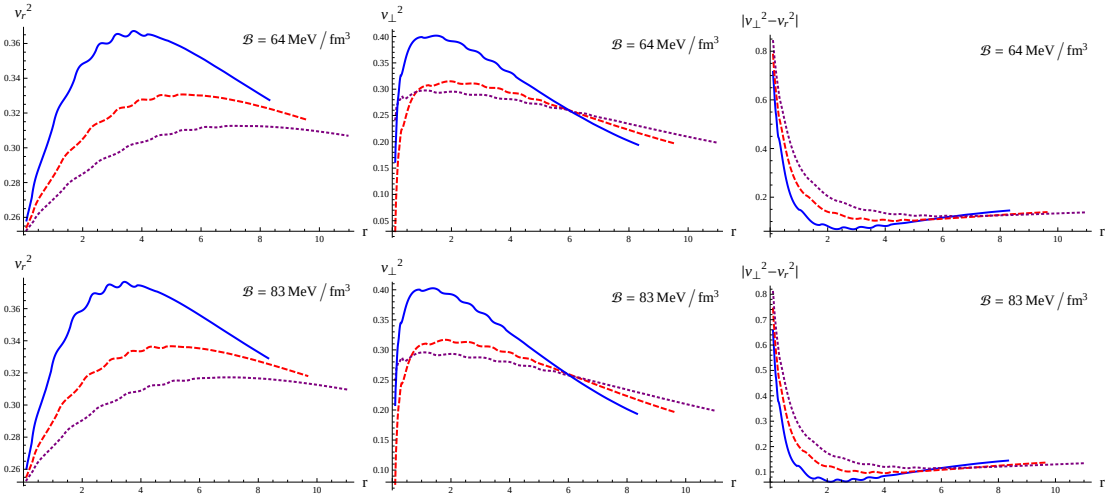

Figure 5.8: Variation of radial velocity, tangential velocity and $|v_\perp^2 - v_r^2|$ with respect to radial coordinate with $m_\Psi = 0.3$.

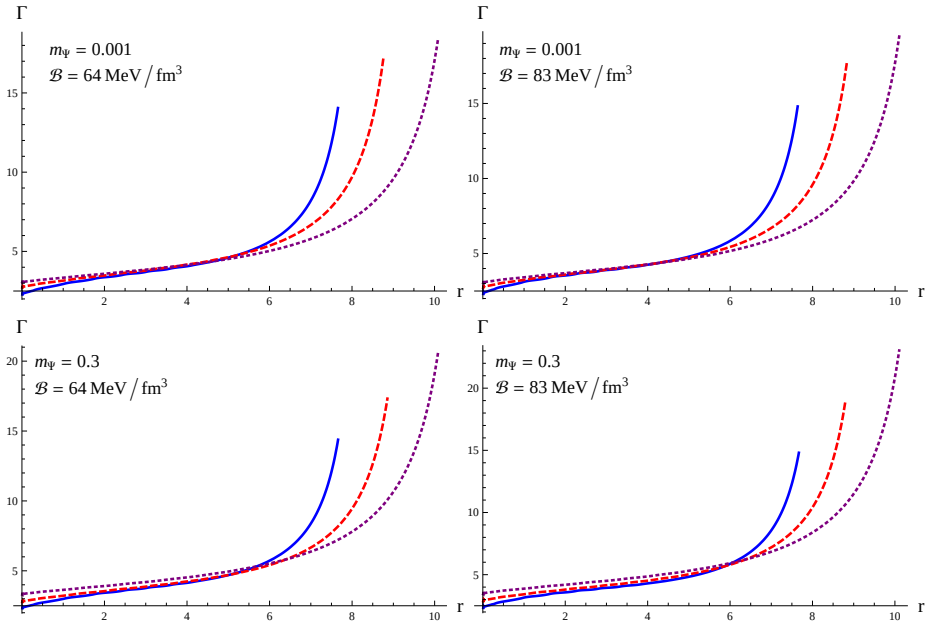

Figure 5.9: Plots of adiabatic index versus r.

agreement with the constraint [103]. Hence, the stellar structure is stable for the considered values of MBD parameters.

Chapter 6

Concluding Remarks

In this thesis, firstly we have formulated definitions of complexity for static as well as non-static spherical systems in the framework of SBD theory. The condition of vanishing complexity has been employed to formulate possible solutions. We have also adopted the technique of MGD to develop anisotropic extension of a non-static spherical system. In particular, we have deformed the radial metric of FLRW spacetime to extend it to anisotropic domain. Furthermore, we incorporated an additional source in the simple seed source (isotropic or vacuum) and used the EGD scheme to devise extended versions of Tolman IV, KB and Schwarzschild spacetimes. We have inspected physical properties of the models constructed via decoupling method graphically. Finally, we have investigated the possible existence of anisotropic strange quark stars in SBD gravity by utilizing embedding class-one condition with MIT bag model.

Chapter 2 comprises of two sections. In the first section, we have investigated the complexity of static sphere. We have used Misner-Sharp and Tolman definitions for calculating the mass of the sphere. We measure the complexity of the self-gravitating objects through the structure scalar Y_{TF} as it establishes a relation between these

factors as well as measures their effect on Tolman mass. In the case of homogeneous energy density and isotropic pressure, the complexity factor of the system vanishes in the context of GR [2]. However, our results do not reduce to a complexity free structure under these assumptions which highlight the effect of including scalar field and potential function to the complexity factor. The simplest configuration in SBD corresponds to two cases of fluids (either the fluid is homogeneous and isotropic or the inhomogeneity and anisotropy terms cancel each other) which must also satisfy an additional condition ($\frac{e^{-\chi}\Psi'}{2r\Psi} = 0$). Hence, the presence of scalar field and self-interacting potential has increased the complexity of the system. The use of vanishing complexity condition in two models representing self-gravitating objects have provided open systems which can be closed by assigning suitable values to $V(\Psi)$.

In the second section of **Chapter 2**, we have considered an anisotropic radiating non-static sphere with inhomogeneous energy density. The structure scalar Y_{TF} has been selected as an appropriate choice for complexity factor based on the following reasons.

- It has already served as an adequate measure of complexity in the static case, thereby ensuring that the current definition of complexity is recovered in the static regime.

- It includes the effects of anisotropy, inhomogeneous energy density and dissipation.

Since the homologous condition has implied that the fluid is geodesic (for both $q = 0$ and $q \neq 0$) therefore, a homologous pattern of evolution has been chosen to minimize the complexity in the evolution of the system. Further, in the non-dissipative case, the complexity factor and shear-tensor do not vanish in contrast to the GR analog

[3]. Furthermore, we have deduced that in SBD gravity the stability of vanishing complexity condition depends on the scalar field in addition to the matter variables (pressure, heat flux, energy density).

In **Chapter 3**, the system of SBD field equations corresponding to FLRW metric are decoupled into two sets through a transformation of the radial metric function. The anisotropic version of flat FLRW model has been graphically analyzed for $\varsigma = 1,\ 1/3,\ 0,\ -1$ which correspond to various phases of the universe. The important results are summarized below.

- In the massless scalar field dominated era, energy density and pressure decrease with respect to cosmic time. The model depicts a stable expanding cosmos which adheres to the energy bounds.

- The universe model dominated by radiation has positive energy density and pressure components which agree with the energy bounds and stability criterion. Moreover, the radiation dominated universe is more dense than the cosmos with a massless scalar field.

- The cosmic model corresponding to $\varsigma = 0$ expands due to the presence of a repulsive force (which is absent in the isotropic case) characterized by the negative pressure. This viable model attains a higher energy density as compared to the previous two phases. However, the solution violates the causality condition.

- The vacuum energy dominated cosmos experiences a stronger repulsive force due to large negative pressure which increases its rate of expansion. This is the most dense cosmic model which violates the SEC as well as causality condition.

We would like to mention here that energy density of the universe in all eras is

directly proportional to the decoupling parameter whereas pressure decreases when σ increases. The negative anisotropy indicates that the cosmos expands more rapidly in the radial direction.

Chapter 4 has been divided into two sections. In the first section, we have examined the efficiency of EGD method by considering metric coefficients of two isotropic solutions: Tolman IV and KB. The anisotropic models corresponding to case I are viable as well as obey Buchdahl limit for compactness and redshift. Moreover, higher values of the decoupling parameter correspond to denser and more compact stellar structures in both models. The extended Tolman IV solution is stable for $\varrho = 0.2,\ 0.55$ whereas anisotropic KB solution is stable according to Herrera's cracking approach but violates the causality condition $0 \leq v_{\perp}^2 \leq 1$ for the considered values of ϱ.

For case II, both solutions satisfy energy conditions as well as the limits on compactness and surface redshift. Moreover, increase in the decoupling parameter leads to a decrease in the density and compactness of both anisotropic models. Finally, the strength of the repulsive force due to positive anisotropy increases with the increase in ϱ in all four solutions. The model corresponding to extended Tolman IV solution is consistent with both stability criteria whereas anisotropic KB solution is stable for $\varrho = 0.2$ only. It is inferred that viability of the extended Tolman IV solutions in GR [33, 126] is preserved in SBD gravity as well. Moreover, the anisotropic analogues of KB solution obtained here are viable for higher values of the decoupling parameter in contrast to the extended KB solutions obtained through MGD technique in [134]. Thus, EGD method yields anisotropic solutions with suitable physical properties.

In the second section of **Chapter 4**, we have considered the seed source as a

vacuum and employed the metric potentials of Schwarzschild spacetime. The number of unknown constants has been reduced by imposing the EoS $\Theta_0^0 = a_1\Theta_1^1 + a_2\Theta_2^2$. Three solutions have been generated corresponding to

- $a_1 = -1$ and $a_2 = -2$ (represents a traceless additional source).
- $a_1 = -\frac{1}{K}$ and $a_2 = 0$ (provides a barotropic fluid distribution).
- $a_1 = 1.4$ and $a_2 = 3$ (yields a particular solution).

The energy density in all cases is positive for negative values of the decoupling parameter only which results in negative radial pressure. This behavior of matter variables is consistent with the work in [26]. Moreover, higher energy density is observed for lower values of ϱ. The analysis of state parameters has revealed that the extended models corresponding to cases I and III are consistent with energy conditions. This implies that Θ_δ^γ is sourced by normal matter. However, the extended model obtained for a barotropic EoS violates the energy conditions indicating the presence of exotic matter. Moreover, the metrics formulated for I and III are asymptotically flat whereas the metric obtained for II does not approach to a flat spacetime when $r \to \infty$. All the BH solutions mentioned above have a singularity covered by the horizon at $r = 2M$. Moreover, the extended Schwarzschild solutions obtained through the technique of MGD in GR violate the DEC. However, in the context of SBD gravity two solutions have been generated that adhere to all the energy constraints.

In **Chapter 5**, we have constructed a static stellar model representing strange star by assuming a well-behaved metric potential and embedding class-one condition with MIT bag model. Tables **5.1** and **5.2** indicate that predicted radius increases while Figure **5.6** implies that the quark star becomes less dense with increase in the

bag constant. Moreover, higher values of scalar field mass lead to more dense stellar systems. The regular behavior of state variables indicates that the system has no singularity. We have established that the interior of star consists of normal matter as all energy conditions are satisfied for the considered values of the parameters as well as the bag constant.

The positive trend of anisotropy confirms the presence of a repelling force required to save the star from further collapse. The graphical analysis of redshift parameter depicts that as the radius of the star increases, the amount of redshift decreases. We have also calculated the compactness factor and the mass-radius ratio which are in agreement with the Buchdahl criterion. Figure **5.6** indicates that a more dense star exerts additional force on light leading to greater redshift. Finally, we have checked the stability conditions for the prototype stellar model using three approaches. All these imply stability of the system coupled to a massive scalar field. However, plots of v_r and $v_\perp$ represent smooth behavior for increasing values of ω_{BD} as shown in Figures **5.7** and **5.8**. Hence, the celestial object is more stable for larger values of coupling parameter. We conclude that the cosmic structure governed by MIT bag model in the framework of SBD is consistent with all the critical requirements and can be treated as a viable and stable model.

It would be interesting to address the following issues in future in the framework of SBD gravity.

- To explore the complexity of anisotropic self-gravitating spheres following either a quasi-homologous or homogeneous regime.

- To extend the definition of complexity to cosmological models.

- To investigate the influence of electromagnetic field on the complexity of static as well as dynamical systems in different symmetries.
- To apply the decoupling approach in the background of other symmetries in the presence as well as absence of charge.
- To devise a configuration representing ultracompact stars with a polynomial form of complexity factor by employing the decoupling approach.
- To develop decoupled compact models using the MIT bag model along with embedding class-one condition.
- To determine the effect of different forms of self-interacting potential functions on charged as well as uncharged quark stellar models for various well-behaved metric functions.

Appendix A

Energy density and pressure components take the following form

$$\begin{aligned}
\rho &= \frac{1}{2r^2}\left\{\xi^2\Psi^2\left[2R^2(2M-R)\left(M\left(r^2-2R^2\right)+R^3\right)\left(r\Psi'(r)+2\Psi(r)\right)\right]\right. \\
&- \xi\left[r^2R^2\omega_{BD}(R-2M)\Psi'^2(r)+2r\Psi(r)\left(\left(R^3-M\left(r^2+2R^2\right)\right)\Psi'(r)\right.\right. \\
&+ \left.\left.rR^2(R-2M)\Psi''(r)\right)-2\Psi^2(r)\left(2M(r-R)(r+R)+R^3\right)\right] \\
&+ \left.r^2V(\Psi)+2\Psi(r)\right\}, \qquad \text{(A1)} \\
p_r &= \frac{\xi}{4r^2}r^2R^2\omega_{BD}(2M-R)\Psi'^2(r)+2\Psi^2(r)\left(2M(r-R)(r+R)+R^3\right) \\
&+ r\Psi(r)\left(\left(2M(r-R)(r+R)+R^3\right)\Psi'(r)+rR^2(2M-R)\Psi''(r)\right) \\
&+ \frac{\xi^2\Psi^2}{4r}(R^2(2M-R)\left(M\left(r^2-2R^2\right)+R^3\right)\left(r\Psi'(r)+2\Psi(r)\right))-\mathcal{B}, \qquad \text{(A2)} \\
p_\perp &= \frac{\Psi\xi}{4r^2}\left[\left(M\left(r^2-2R^2\right)+R^3\right)\left(2\Psi(r)\left(2M(r-R)(r+R)+R^3\right)\right.\right. \\
&+ \left.\left.3rR^2(R-2M)\Psi'(r)\right)\right]+\xi\left[3r^2R^2\omega_{BD}(R-2M)\Psi'^2(r)+r\Psi(r)\right. \\
&\times \left(\left(-2Mr^2+14MR^2-7R^3\right)\Psi'(r)+3rR^2(R-2M)\Psi''(r)\right)-2\Psi^2(r) \\
&\times \left.\left(2M\left(r^2-3R^2\right)+3R^3\right)\right]-\mathcal{B}+\frac{\Psi(r)}{r^2}, \qquad \text{(A3)}
\end{aligned}$$

where $\xi = \frac{\Psi^{-1}(r)}{2Mr^2e^{\frac{M(r-R)(r+R)}{R^2(R-2M)}}+R^2(R-2M)}$.

Appendix B

List of Publications

The contents of this thesis are based on the following research papers published or accepted in journals of International repute. These papers are also attached herewith.

1. Sharif, M. and **Majid, A.**: *Complexity Factor for Static Sphere in Self-interacting Brans-Dicke Gravity,*
   Chin. J. Phys. **61**(2019)38.

2. Sharif, M. and **Majid, A.**: *Complexity of Dynamical Sphere in Self-interacting Brans-Dicke Gravity,*
   Eur. Phys. J. C **80**(2020)1185.

3. Sharif, M. and **Majid, A.**: *Cosmological Solutions through Gravitational Decoupling in Self-interacting Brans-Dicke Gravity,*
   Phys. Scr. **96**(2021)045003.

4. Sharif, M. and **Majid, A.**: *Extended Gravitational Decoupled Solutions in Self-interacting Brans-Dicke Gravity,*
   Phys. Dark Universe **30**(2020)100610.

5. Sharif, M. and **Majid, A.**: *Extended Black Hole Solutions in Self-interacting Brans-Dicke Gravity,*
   Phys. Scr. **96**(2021)035002.

6. Sharif, M. and **Majid, A.**: *Anisotropic Strange Stars through Embedding Technique in Massive Brans-Dicke Gravity,*
   Eur. Phys. J. Plus **135**(2020)558.

Also, the following papers related to this thesis have been published or submitted for publication.

1. Sharif, M. and **Majid, A.**: *Complexity Factors for Static Axial System in Self-interacting Brans-Dicke Gravity,*
   Int. J. Geom. Methods Mod. Phys. **16**(2019)1950174.

2. Sharif, M., **Majid, A.** and Nasir, M.M.M.: *Complexity Factor for Self-gravitating System in Modified Gauss-Bonnet Gravity,*
   Int. J. Mod. Phys. A **34**(2019)1950210.

3. Sharif, M. and **Majid, A.**: *Anisotropic Compact Stars in Self-interacting Brans-Dicke Gravity,*
   Astrophys. Space Sci. **365**(2020)42.

4. Sharif, M. and **Majid, A.**: *Decoupled Anisotropic Spheres in Self-interacting Brans-Dicke Gravity,*
   Chin. J. Phys. **68**(2020)406.

5. **Majid, A.** and Sharif, M.: *Quark Stars in Massive Brans-Dicke Gravity with Tolman-Kuchowicz Spacetime,*
   Universe **6**(2020)124.

6. Sharif, M. and **Majid, A.**: *Compact Stars with MIT Bag Model in Massive Brans-Dicke Gravity,*
   Astrophys. Space Sci. **366**(2021)54.

7. Sharif, M. and **Majid, A.**: *Effects of Charge on Decoupled Solutions in Self-interacting Brans-Dicke Theory,*
   Phys. Dark Universe **32**(2021)100803.

8. Sharif, M. and **Majid, A.**: *Analysis of Strange Quark Stars in Massive Brans-Dicke Gravity,*
   Int. J. Mod. Phys. D **36**(2021)2150054.

9. Sharif, M. and **Majid, A.**: *Complexity Analysis of Dynamical Cylinder in Massive Brans-Dicke Gravity,*
   Eur. Phys. J. Plus **136**(2021)530.

10. Sharif, M. and **Majid, A.**: *Decoupled Embedding Class-one Strange Stars in Self-interacting Brans-Dicke Gravity,*
Universe **7**(2021)161.

11. Sharif, M. and **Majid, A.**: *Complexity Factor for Cylindrical System in Brans-Dicke Gravity,*
Indian J. Phys. **95**(2021)769.

12. Sharif, M. and **Majid, A.**: *Relativistic Models for Strange Stars in Massive Brans-Dicke Gravity,*
Astron. Rep. **65**(2021)1048.

13. Sharif, M. and **Majid, A.**: *Isotropization and Complexity of Decoupled Solutions in Self-interacting Brans-Dicke Gravity,*
Eur. Phys. J. Plus **137**(2022)114.

14. Sharif, M., **Majid, A.** and M. Shafaqat: *Study of Anisotropic Polytropes in $f(\mathcal{R},T)$ Theory,*
Physica Scripta (to appear, 2022).

15. Sharif, M. and **Majid, A.**: *Decoupled Quark Stars in Self-interacting Brans-Dicke Gravity,*
Submitted for publication.

16. Sharif, M. and **Majid, A.**: *Isotropic and Complexity-free Deformed Solutions in Self-interacting Brans-Dicke Gravity,*
Submitted for publication.

Bibliography

[1] Kolmogorov, A.N.: *Three Approaches to the Definition of the Concept Quantity of Information*, Prob. Inform. Theory J. **1**(1965)3; Grassberger, J.: *Toward a Quantitative Theory of Self-generated Complexity*, Int. J. Theor. Phys. **125**(1986)907; Anderson, P.W.: *Is Complexity Physics? Is it Science? What is it?*, Phys. Today **7**(1991)9; Parisi, G.: *Statistical Physics and Biology*, Phys. World **6**(1993)42.

[2] Herrera, L.: *New Definition of Complexity for Self-gravitating Fluid Distributions: The Spherically Symmetric, Static Case*, Phys. Rev. D **97**(2018)044010.

[3] Herrera, L., Di Prisco, A. and Ospino, J.: *Definition of Complexity for Dynamical Spherically Symmetric Dissipative Self-gravitating Fluid Distributions*, Phys. Rev. D **98**(2018)104059.

[4] Sharif, M. and Butt, I.I.: *Complexity Factor for Static Cylindrical System*, Eur. Phys. J. C **78**(2018)850.

[5] Sharif, M. and Butt, I.I.: *Complexity Factor for Charged Spherical System*, Eur. Phys. J. C **78**(2018)688.

[6] Sharif, M. and Butt, I.I.: *Electromagnetic Effects on Complexity Factor for Static Cylindrical System*, Chinese J. Phys. **61**(2019)238.

[7] Herrera, L., Di Prisco, A. and Ospino, J.: *Complexity Factors for Axially Symmetric Static Sources*, Phys. Rev. D **99**(2019)044049.

[8] Herrera, L., Di Prisco, A. and Carot, J.: *Complexity of the Bondi Metric*, Phys. Rev. D **99**(2019)124028.

[9] Sharif, M. and Tariq, S.: *Complexity Factor for Charged Dissipative Dynamical System*, Mod. Phys. Lett. A **35**(2020)28.

[10] Herrera, L., Di Prisco, A. and Ospino, J.: *Quasi-homologous Evolution of Self-gravitating Systems with Vanishing Complexity Factor*, Eur. Phys. J. C **80**(2020)631.

[11] Wu, K.K.S., Lahav, O. and Rees, M.J.: *The Large-scale Smoothness of the Universe*, Nature **397**(1999)225.

[12] Schwarz, D.J. and Weinhorst, B.: *(An)isotropy of the Hubble Diagram: Comparing Hemispheres*, Astron. Astrophys. **474**(2007)717; Antoniou, I. and Perivolaropoulos, L.: *Searching for a Cosmological Preferred Axis: Union 2 Data Analysis and Comparison with Other Probes*, J. Cosmol. Astropart. Phys. **12**(2010)012; Colin, J. *et al.*: *Probing the Anisotropic Local Universe and Beyond with SNe Ia data*, Mon. Not. R. Soc. **414**(2011)264; Javanmardi, B. *et al.*: *Probing the Isotropy of Cosmic Acceleration Traced by Type Ia Supernovae*, Astrophys. J.**810**(2015)47.

[13] Yoon, M. *et al.: Dipolar Modulation in Number Counts of WISE-2MASS Sources*, Mon. Not. R. Soc. **445**(2014)L60.

[14] Tiwari, P and Nusser, A.: *Revisiting the NVSS Number Count Dipole*, J. Cosmol. Astropart. Phys. **3**(2016)062.

[15] Řípa, J. and Shafieloo, A.: *Testing the Isotropic Universe using the Gamma-Ray Burst Data of Fermi/GBM*, Astrophys. J. **851**(2017)15.

[16] Migkas, K. and Reiprich, T.H.: *Anisotropy of the Galaxy Cluster X-ray Luminosity-Temperature Relation*, Astron. Astrophys. **611**(2018)A50.

[17] Migkas, K. *et al.*: *Probing Cosmic Isotropy with a New X-ray Galaxy Cluster Sample through the LXT Scaling Relation*, Astron. Astrophys. **636**(2020)A15.

[18] Abbott, B.P. *et al.*: *Observation of Gravitational Waves from a Binary Black Hole Merger*, Phys. Rev. Lett. **116**(2016)061102.

[19] Schwarzschild, K.: *On the Gravitational Field of a Mass Point According to Einstein's Theory*, Math. Phys. **189**(1916).

[20] Ruffini, R. and Wheeler, J.: *Introducing the Black Hole*, Phys. Today **24**(1972)30.

[21] Hawking, S.W.: *Black Holes in General Relativity*, Commun. Math. Phys. **25**(1972)152.

[22] Hawking, S.W., Perry, M.J. and Strominger, A.: *Soft Hair on Black Holes*, Phys. Rev. Lett. **116**(2016)231301.

[23] Antoniou, G., Bakopoulos, A. and Kanti, P.: *Evasion of No-Hair Theorems and Novel Black-Hole Solutions in Gauss-Bonnet Theories*, Phys. Rev. Lett.

120(2018)131102; Grumiller, D. *et al.*: *Spacetime Structure near Generic Horizons and Soft Hair*, Phys. Rev. Lett. **124**(2020)041601.

[24] Ovalle, J.: *Searching Exact Solutions for Compact Stars in Braneworld: A Conjecture*, Mod. Phys. Lett. A **23**(2008)3247; *Decoupling Gravitational Sources in General Relativity: From Perfect to Anisotropic Fluids*, Phys. Rev. D **95**(2017)104019.

[25] Ovalle, J. *et al.*: *Anisotropic Solutions by Gravitational Decoupling*, Eur. Phys. J. C **78**(2018)122.

[26] Ovalle, J. *et al.*: *Black Holes by Gravitational Decoupling*, Eur. Phys. J. C **78**(2018)960.

[27] Estrada, M. and Tello-Ortiz, F.: *A New Family of Analytical Anisotropic Solutions by Gravitational Decoupling*, Eur. Phys. J. C **133**(2018)453.

[28] Sharif, M. and Sadiq, S.: *Gravitational Decoupled Charged Anisotropic Spherical Solutions*, Eur. Phys. J. C **78**(2018)410.

[29] Hensh, S. and Stuchlik, Z.: *Anisotropic Tolman VII Solution by Gravitational Decoupling*, Eur. Phys. J. C **79**(2019)834.

[30] Sharif, M. and Ama-Tul-Mughani, Q.: *Study of (1+2)-dimensional Charged String Cloud with Minimal Geometric Deformation*, Int. J. Geom. Methods Mod. Phys. **16**(2019)1950187; *Gravitational Decoupled Solutions of Axial String Cosmology*, Mod. Phys. Lett. A **35**(2020)2050091.

[31] Ovalle, J.: *Decoupling Gravitational Sources in General Relativity: The Extended Case*, Phys. Lett. B **788**(2019)213.

[32] Contreras, E. and Bargueño, P.: *Extended Gravitational Decoupling in 2+1 Dimensional Spacetimes*, Class. Quantum Grav. **36**(2019)215009.

[33] Sharif, M. and Ama-Tul-Mughani, Q.: *Anisotropic Spherical Solutions through Extended Gravitational Decoupling Approach*, Ann. Phys. **415**(2020)168122.

[34] Sharif, M. and Ama-Tul-Mughani, Q.: *Extended Gravitational Decoupled Charged Anisotropic Solutions*, Chin. J. Phys. **65**(2020)207.

[35] Ovalle, J. *et al.*: *Hairy Black Holes by Gravitational Decoupling*, Phys. Dark Universe **31**(2021)100744.

[36] Sharif, M. and Saba, S.: *Gravitational Decoupled Anisotropic Solutions in $f(\mathcal{G})$ Gravity*, Eur. Phys. J. C **78**(2018)921; Sharif, M. and Waseem, A.: *Anisotropic Spherical Solutions by Gravitational Decoupling in Gravity*, Ann. Phys. **405**(2019)14; Sharif, M. and Saba, S.: *Extended Gravitational Decoupling Approach in $f(\mathcal{G})$ Gravity*, Int. J. Mod. Phys. D **29**(2020)2050041.

[37] Bordbar, G.H. and Peivand, A.R.: *Computation of the Structure of a Magnetized Strange Quark Star*, Res. Astron. Astrophys. **11**(2011)851.

[38] Dirac, P.A.M: *The Cosmological Constants*, Nature **139**(1937)323; *A New Basis for Cosmology*, Proc. R. Soc. Lond. A **165**(1938)199.

[39] Brans, C. and Dicke, R.H.: *Machs Principle and a Relativistic Theory of Gravitation*, Phys. Rev. **124**(1961)3.

[40] Weinberg, E.J.: *Some Problems with Extended Inflation*, Phys. Rev. D **40**(1989)3950.

[41] Will, C.M.: *The Confrontation between General Relativity and Experiment*, Living Rev. Rel. **4**(2001)4.

[42] Khoury, J. and Weltman, A.: *Chameleon Cosmology*, Phys. Rev. D **69**(2004)044026.

[43] Perivolaropoulos, L.: *PPN Parameter γ and Solar System Constraints of Massive Brans-Dicke Theories*, Phys. Rev. D **81**(2010)047501.

[44] Santos, C. and Gregory, R.: *Cosmology in Brans-Dicke Theory with a Scalar Potential*, Ann. Phys. **258**(1997)111.

[45] Sen, A.A., Sen, S. and Sethi, S.: *Dissipative Fluid in Brans-Dicke Theory and Late Time Acceleration*, Phys. Rev. D **63**(2001)107501.

[46] Mak, M.K. and Harko, T.: *Brans-Dicke Cosmology with a Scalar Field Potential*, Europhys. Lett. **60**(2002)155.

[47] Chakraborty, W. and Debnath, U.: *Role of Brans-Dicke Theory with or without Self-Interacting Potential in Cosmic Acceleration*, Int. J. Theor. Phys. **48**(2009)232.

[48] Sharif, M. and Waheed, S.: *Cosmic Acceleration and Brans-Dicke Theory*, J. Exp. Theor. Phys. **115**(2012)599.

[49] Thorne, K.S. and Dykla, J.J.: *Black Holes in the Dicke-Brans Theory of Gravity*, Astrophys. J. **166**(1971)L35.

[50] Hawking, S.W.: *Black holes in the Brans-Dicke Theory of Gravitation*, Commun. Math. Phys. **25**(1972)167.

[51] Geroch, R.: *A Method for Generating Solutions of Einsteins Equations*, J. Math. Phys. **12**(1971)918.

[52] Sneddon, G.E. and McIntosh, C.B.G.: *Generation of Solutions of the Brans-Dicke Equations*, Aust. J. Phys. **27**(1974)411.

[53] Bruckman, W.F. and Kazes, E.: *Properties of the Solutions of Cold Ultradense Configurations in the Brans-Dicke Theory*, Phys. Rev. D **16**(1977)2.

[54] Riazi, N. and Askari, H.R.: *Spherically Symmetric, Static Solutions of the Brans-Dicke Field Equations in Vacuum,*, Mon. Not. R. Astron. Soc. **261**(1993)229.

[55] Campanelli, M. and Lousto, C.O.: *Are Black Holes in Brans-Dicke Theory precisely the same as in General Relativity?*, Int. J. Mod. Phys. **2**(1993)451.

[56] Sharif, M. and Manzoor, R.: *Structure Scalars and Anisotropic Spheres in Brans-Dicke Gravity*, Phys. Rev. D **91**(2015)024018.

[57] Sharif, M. and Manzoor, R.: *Structure Scalars and Cylindrical Systems in Brans-Dicke Gravity*, Astrophys. Space Sci. **359**(2015)17.

[58] Sharif, M. and Majid, A.: *Complexity Factors for Static Axial System in Self-interacting Brans-Dicke Gravity*, Int. J. Geom. Methods Mod. Phys. **16**(2019)1950174.

[59] Sharif, M. and Majid, A.: *Decoupled Anisotropic Spheres in Self-interacting Brans-Dicke Gravity*, Chin. J. Phys. **68**(2020)406; *Compact Stars with MIT Bag Model in Massive Brans-Dicke Gravity*, Astrophys. Space Sci. **366**(2020)54.

[60] Fujii, Y. and Maeda, K.: *The Scalar-Tensor Theory of Gravitation* (Cambridge University Press, 2003); Brans, C.H.: *The Roots of Scalar-Tensor Theory: An Approximate History*, arXiv:gr-qc/0506063.

[61] Bergmann, P.G.: *Comments on the Scalar-Tensor Theory*, Int. J. Theor. Phys. **1**(1968)25; Wagoner, R.V.: *Scalar-Tensor Theory and Gravitational Waves*, Phys. Rev. D **1**(1970)3209; Nordvedt, K.: *Post-Newtonian Metric for a General Class of Scalar-Tensor Gravitational Theories and Observational Consequences*, Astrophys. J. **161**(1970)1059.

[62] Reasenberg, R.D. et al.: *Viking Relativity Experiment-Verification of Signal Retardation by Solar Gravity*, Astrophys. J. **234**(1070)L219.

[63] Faraoni, V.: *Scalar Field Mass in Generalized Gravity*, Class. Quantum Grav. **26**(2009)145014; Yazadjiev, S.S., Doneva, D.D. and Popchev, D.: *Slowly Rotating Neutron Stars in Scalar-Tensor Theories with a Massive Scalar Field*, Phys. Rev. D **93**(2016)084038; Motahar, Z.A. et al.: *Scalarization of Neutron Stars with Realistic Equations of State*, Phys. Rev. D **96**(2017)064046; Staykov, K.V. et al.: *Static and Slowly Rotating Neutron Stars in Scalar-Tensor Theory with Self-interacting Massive Scalar Field*, Eur. Phys. J. C **78**(2018)586; Fattoyev, F.J.: *Neutron Stars in General Relativity and Scalar-Tensor Theory of Gravity*, Arab. J. Math. **8**(2019)293; Danchev, V.I. and Doneva, D.D.: *Constraining the Equation of State in Modified Gravity via Universal Relations*, Phys. Rev. D **103**(2021)024049.

[64] Quiros, I.: *Selected Topics in Scalar-Tensor Theories and Beyond*, Int. J. Mod. Phys. D **28**(2019)7.

[65] Kase, R. and Tsujikawa, S.: *Neutron Stars in f(R) Gravity and Scalar-Tensor Theories*, J. Cosmol. Astropart. Phys. **09**(2019)054; Doneva, D.D. and Yazadjiev, S.S.:*Rapidly Rotating Neutron Stars with a Massive Scalar Field-Structure and Universal Relations*, J. Cosmol. Astropart. Phys. **11**(2016)019; Yazadjiev, S.S., Doneva, D.D. and Kokkotas, K.D.; *Oscillation Modes of Rapidly Rotating Neutron Stars in Scalar-Tensor Theories of Gravity*, Phys. Rev. D **96**(2017)064002; Maurya, S.K. et al.: *Charged Anisotropic Strange Stars in Brans-Dicke Gravity with a Massive Scalar Field through Embedding Approach* , arXiv:2008.10600.

[66] Misner, C.W. and Sharp, D.H.: *Relativistic Equations for Adiabatic, Spherically Symmetric Gravitational Collapse*, Phys. Rev. **136**(1964)B571.

[67] Tolman, R.: *On the Use of the Energy-Momentum Principle in General Relativity*, Phys. Rev. **35**(1930)875.

[68] Wilson, J.: *A Numerical Study of Gravitational Stellar Collapse*, Astrophys. J. **163**(1971)209; Bruenn, S.: *Stellar Core Collapse-Numerical Model and Infall Epoch*, Astrophys. J. **58**(1985)771; Adams, R., Cary, B. and Cohen, J.: *A Simple Model of a Supernova*, Astrophys. Space Sci. **155**(1989)271.

[69] Perlmutter, S. et al.: *Measurements of* Ω *and* Λ *from 42 High-Redshift Supernovae*, Astrophys. J. **517**(1999)565; Riess, A.G. et al.: *Observational Evidence from Supernovae for an Accelerating Universe and a Cosmological Constant*, Astron. J. **116**(1998)1009.

[70] Allen, S.W. et al.: *A Preference for a Non-zero Neutrino Mass from Cosmological Data*, Mon. Not. R. Astron. Soc. **346**(2003)78.

[71] Bennett, C.L. et al.: *First Year Wilkinson Microwave Anisotropy Probe (WMAP) Observations: Preliminary Maps and Basic Results*, Astrophys. J. Suppl. **148**(2003)1.

[72] Plebanski, J. and Krainski, A.: *An Introduction to General Relativity and Cosmology* (Cambridge University Press, 2006).

[73] Ruderman, A.: *Pulsars: Structure and Dynamics*, Annu. Rev. Astron. Astrophys. **10**(1972)427.

[74] Sawyer, R.F.: Phys. Rev. Lett.: *Condensed π^--Phase in Neutron-Star Matter*, **29**(1972)382.

[75] Sokolov, A.I.: *Phase Transitions in a Superfluid Neutron Liquid*, J. Exp. Theor. Phys. **79**(1980)1137.

[76] Kippenhahm, R.K. and Weigert, A.: *Stellar Structure and Evolution* (Springer, 1990).

[77] Shapiro, S.L. and Teukolsky, S.A.: *Black Holes, White Dwarfs and Neutron Stars: The Physics of Compact Objects* (John Wiley and Sons, 1983).

[78] Chandrasekhar, S.: *The Maximum Mass of Ideal White Dwarfs*, Astrophys. J. **305**(1931)81.

[79] Bombaci, I.: *The Maximum Mass of a Neutron Star*, **305**(1996)871.

[80] Baade, W. and Zwicky, F.: *Remarks on Supernovae and Cosmic Rays*, Phys. Rev. **46**(1934)76.

[81] Hewish, A. et al.: *Observation of a Rapidly Pulsating Radio Source*, Nature **217**(1968)709.

[82] Witten, E.: *Cosmic Separation of Phases*, Phys. Rev. D **30**(1984)272.

[83] Ofek, E.O.P. et al.: *SN 2006gy: An Extremely Luminous Supernova in the Galaxy NGC 1260*, Astrophys. J. **659**(2007)L13; Ouyed, R., Leahy, D. and Jaikumar, P.: *Predictions for Signatures of the Quark-nova in Superluminous Supernovae*, arXiv:0911.5424.

[84] Darmois, G.: *The Equations of Einsteinian Gravitation*, Mémorial des sciences mathématiques **25**(1927)58.

[85] O'Brien, S. and Synge, J.L.: *Jump Conditions at Discontinuities in General Relativity*, Commun. Dublin Inst. Adv. Stud. A **9**(1952).

[86] Kippenhahn, R. and Weigert, A.: *Stellar Structure and Evolution* (Springer-Verlag, 1990)

[87] Alcock, C. and Olinto, A.V.: *Exotic Phases of Hadronic Matter and their Astrophysical Application*, Annu. Rev. Nucl. Part. Sci. **38**(1988)161; Madsen, J.: *Physics and Astrophysics of Strange Quark Matter*, Lect. Notes Phys. **516**(1999)162.

[88] Bordbar, G.H. and Peivand, A.R.: *Computation of the Structure of a Magnetized Strange Quark Star*, Res. Astron. Astrophys. **11**(2011)851.

[89] Abbott, B.P. et al.: *GW170817: Observation of Gravitational Waves from a Binary Neutron Star Inspiral*, Phys. Rev. Lett. **119**(2017)161101.

[90] The LIGO Scientific Collaboration, the Virgo Collaboration, Abbott, B.P. et al: *GW190425: Observation of a Compact Binary Coalescence with Total Mass*$\sim 3.4M_{bigodot}$, Astrophys. J. Lett. **892**(2020)L3.

[91] Chodos, A. et al.: *New Extended Model of Hadrons*, Phys. Rev. D **9**(1974)3471.

[92] Farhi, E. and Jaffe, R.L.: *Strange Matter*, Phys. Rev. D **30**(1984)2379.

[93] Stergioulas, N.: *Rotating Stars in Relativity*, Living Rev. Relativ. **6**(2003)3.

[94] Haensel, P., Zdunik, J.L. and Schaffer, R.: *Strange Quark Stars*, Astron. Astrophys. **160**(1986)121; Cheng, K.S., Dai, Z.G. and Lu, T.: *Strange Stars and Related Astrophysical Phenomena*, Int. J. Mod. Phys. D **7**(1998)139; Harko, T. and Mak, M.K.: *An Exact Anisotropic Quark Star Model*, Chin. J. Astron. Astrophys. **2**(2002)248.

[95] Lopez-Ruiz, R., Mancini, H.L. and Calbet, X.: *A Statistical Measure of Complexity*, Phys. Lett. A **209**(1995)321; Calbet, X. and Lopez-Ruiz, R.: *Tendency Towards Maximum Complexity in a Nonequilibrium Isolated System*, Phys. Rev. E **63**(2001)066116; Catalan, R.G., Garay, J. and Lopez-Ruiz, R.: *Features of the Extension of a Statistical Measure of Complexity to Continuous Systems*, Phys. Rev. E **66**(2002)011102; Sañudo, J. and Lopez-Ruiz, R.: *Statistical Complexity and Fisher-Shannon Information in the H-atom*, Phys. Lett. A **372**(2008)5283.

[96] Herrera, L. et al.: *Structure and Evolution of Self-gravitating Objects and the Orthogonal Splitting of the Riemann Tensor*, Phys. Rev. D **79**(2009)064025.

[97] Casadio, R. et al.: *Isotropization and Change of Complexity by Gravitational Decoupling*, Eur. Phys. J. C **79**(2019)826.

[98] Karmarkar, K.R.: *Gravitational Metrics Of Sphierical Symmetry and Class-One*, Proc. Ind. Acad. Sci. A **27**)(1948)56.

[99] Eisenhart, L.P.: *Riemannian Geometry* (Princeton University Press, 1926).

[100] Herrera, L. and Santos, N.O.: *Local Anisotropy in Self-gravitating Systems*, Phys. Rep. **286**(1997)53.

[101] Abreu, H., Hernandez, H. and Nunez, L.A.: *Sound Speeds, Cracking and the Stability of Self-gravitating Anisotropic Compact Objects*, Class. Quantum Gravit. **24**(2007)4631.

[102] Chandrasekhar, S.: *The Dynamical Instability of Gaseous Masses Approaching the Schwarzschild Limit in General Relativity*, Astrophys. J. **140**(1964)417.

[103] Heintzmann, H. and Hillebrandt, W.: *Neutron Stars with an Anisotropic Equation of State: Mass, Redshift and Stability*, Astron. Astrophys. **24**(1975)51.

[104] Sharif, M. and Majid, A.: *Complexity Factor for Static Sphere in Self-interacting Brans-Dicke Gravity*, Chin. J. Phys. **6**(2019)38.

[105] Sharif, M. and Majid, A.: *Complexity of Dynamical Sphere in Self-interacting Brans-Dicke Gravity*, Eur. Phys. J. C **80**(2020)1185.

[106] Herrera, L. et al.: *On the Role of Density Inhomogeneity and Local Anisotrpy in the Fate of Spherical Collapse*, Phys. Lett. A **237**(1998)113.

[107] Gokhroo, M.K. and Mehra, A.L.: *Anisotropic Spheres with Variable Energy Density in General Relativity*, Gen. Relativ. Gravit. **26**(1994)75.

[108] Nutku, Y.: *The Post-Newtonian Equations of Hydrodynamics in the Brans-Dicke Theory*, Astrophys. J. **155**(1969)999.

[109] Schwarzschild, M.: *Structure and Evolution of the Stars* (Dover, 1958); Hansen, C. and Kawaler, S.: *Stellar Interiors: Physical Principles, Structure and Evolution* (Springer-Verlag, 1994).

[110] Sharif, M. and Majid, A.: *Cosmological Solutions through Gravitational Decoupling in Self-interacting Brans-Dicke Gravity*, Phys. Scr. **96**(2021)045003.

[111] Sen, S. and Seshadri, T.R.: *Self-interacting Brans-Dicke Cosmology and Quintessence*, Int. J. Mod. Phys. **12**(2003)445.

[112] Perlmutter, S. et al.: *Discovery of a Supernove Explosion at Half the Age of the Universe*, Nature **391**(1998)51.

[113] Sharif, M. and Majid, A.: *Extended Gravitational Decoupled Solutions in Self-interacting Brans-Dicke Gravity*, Phys. Dark Universe **30**(2020)100610.

[114] Sharif, M. and Majid, A.: *Extended Black Hole Solutions in Self-interacting Brans-Dicke Gravity*, Phys. Scr. **96**(2021)035002.

[115] Tolman, R.C.: *Static Solutions of Einstein's Field Equations for Spheres of Fluid*, Phys. Rev. **55**(1939)364.

[116] Delgaty, M.S.R. and Lake, K.: *Physical Acceptability of Isolated, Static, Spherically Symmetric, Perfect Fluid Solutions of Einstein's Field Equations*, Comput. Phys. Commun. **115**(1998)395.

[117] Bhar, P., Singh, K.N. and Manna, T.: *Anisotropic Compact Star with Tolman IV Gravitational Potential*, Astrophys. Space Sci. **361**(2016)284; Banerjee, S.: *Strange Quark Star with Tolman IV Background*, Pramana-J. Phys. **91**(2018)27.

[118] Krori, K.D. and Barua, J.: *A Singularity-free Solution for a Charged Fluid Sphere in General Relativity*, J. Phys. A: Math. Gen. **8**(1975)4.

[119] Zubair, M. and Abbas, G.: *Some Interior Models of Compact Stars in $f(\mathcal{R})$ Gravity*, Astrophys. Space Sci. **361**(2016)342.

[120] Buchdahl, H.A.: *General Relativistic Fluid Spheres*, Phys. Rev. D **116**(1959)1027.

[121] Ivanov, B.V.: *Static Charged Perfect Fluid in General Relativity*, Phys. Rev. D **65**(2002)104011.

[122] Burrows, A. and Lattimer, J.M.: *The Birth of Neutron Stars*, Astrophys. J. **307**(1986)178; Lattimer, J.M. and Yahil, A.: *Analysis of the Neutrino Events from Supernova 1987A*, Astrophys. J. **340**(1989)426.

[123] Timmes, F.X., Woosley,, S.E. and Weaver, T.A.: *The Neutron Star and Black Hole Initial Mass Function*, Astrophys. J. **457**(1996)834.

[124] Bowers, R. and Liang, E.: *Anisotropic Spheres in General Relativity*, Astrophys. J. **188**(1974)657.

[125] Cosenza, M. et al.: *Some Models of Anisotropic Spheres in General Relativity*, J. of Math. Phys. **22**(1981)118.

[126] Abellán, G. et al.: *Regularity Condition on the Anisotropy Induced by Gravitational Decoupling in the Framework of MGD*, Eur. Phys. J. C **80**(2020)177.

[127] Contreras, E., Tello-Ortz, F. and Maurya, S.K.: *Regular Decoupling Sector and Exterior Solutions in the Context of MGD*, Class. Quantum Grav. **37**(2020)155002.

[128] Martinez, C., Troncoso, R. and Zanelli, J.: *Exact Black Hole Solution with a Minimally Coupled Scalar Field*, Phys. Rev. D **70**(2004)084035; Herdeiro, C.A. and Radu, E.: *Asymptotically Flat Black Holes with Scalar Hair: A Review*, Int. J. Mod. Phys. D **24**(2015)1542014.

[129] Sharif, M. and Majid, A.: *Anisotropic Strange Stars through Embedding Technique in Massive Brans-Dicke Gravity*, Eur. Phys. J. Plus **135**(2020)558.

[130] Maurya, S.K. et al.: *A New Model for Spherically Symmetric Anisotropic Compact Star*, Eur. Phys. J. C **76**(2016)266.

[131] Rahaman, F. et al.: *A New Deterministic Model of Strange Stars*, Eur. Phys. J. C **74**(2014)3126.

[132] Rawls, M.L. et al.: *Refined Neutron Star Mass Determinations for Six Eclipsing X-ray Pulsar Binaries*, Astrophys. J. **730**(2011)25.

[133] Lake, K.: *All Static Spherically Symmetric Perfect-Fluid Solutions of Einstein's Equations*, Phys. Rev. D **67**(2003)104015.

[134] Sharif, M. and Majid, A.: *Anisotropic Compact Stars in Self-interacting Brans-Dicke Gravity*, Astrophys. Space Sci. **365**(2020)42.